WISSENSCHAFTLICHE ARBEITEN DER FACHRICHTUNG
GEODÄSIE UND GEOINFORMATIK DER LEIBNIZ UNIVERSITÄT HANNOVER
ISSN 0174-1454

Nr. 289

Seyed Mohammad Tavakkoli Sabour

Multi-Temporal Classification of Crops Using ENVISAT ASAR Data

HANNOVER 2011

WISSENSCHAFTLICHE ARBEITEN DER FACHRICHTUNG
GEODÄSIE UND GEOINFORMATIK DER LEIBNIZ UNIVERSITÄT HANNOVER
ISSN 0174-1454

Nr. 289

Multi-Temporal Classification of Crops Using ENVISAT ASAR Data

Von der Fakultät für Bauingenieurwesen und Geodäsie
Der Universität Hannover
zur Erlangung des Grades

DOKTOR - INGENIEUR

genehmigte Dissertation
von
M.sc. Seyed Mohammad Tavakkoli Sabour

HANNOVER 2011

Referent:	Univ.-Prof. Dr.-Ing. habil. Christian Heipke
Korreferentinen:	Prof. Dr.-Ing. Uwe Sörgel
	Prof. Dr.-Ing. habil. Uwe Stilla
	Prof. Dr.-Ing. habil. Monika Sester

Tag der mündlichen Prüfung: 24.09.2010

Zusammenfassung

Eine Vielzahl landwirtschaftlicher Anbauverfahren wirken sich auf das menschliche Leben und die Umwelt aus. Traditionelle lokale Messungen sind teuer und zeitaufwendig. Probedaten gelten ausschließlich für die punktuelle Messlage. Im Rahmen eines ESA-Pilotprojekts (AO335), wurden Methoden untersucht, um eine zuverlässige, kosteneffiziente und ständige Überwachung der Anbauverfahren zu ermöglichen. Ein landwirtschaftliches Gebiet im Bereich "Fuhrberger Feld", nahe Hannover (Deutschland) wurde als Untersuchungsgebiet ausgewählt.

ENVISAT ASAR Amplitudenbilder mit VV/VH Polarisation wurden in dieser Arbeit verwendet. Darüber hinaus wurden Probedaten durch Feldbesichtigungen gesammelt. Diese dienten sowohl als Trainingsdaten als auch als Referenz für die Genauigkeitsabschätzung. Die verfügbaren Daten deckten die landwirtschaftliche Saison 2004 ab. Umfangreiche Feldbesichtigungen fanden auf mehr als 50 Feldern statt. Diese erfolgten zeitgleich zu den Bildaufnahmen mittels ENVISAT. Die Testfelder umfassten die typischen Arten der verschiedenen Pflanzen der Region.

Der methodische Ansatz für das Monitoring besteht in der überwachten Klassifizierung von multitemporalen ASAR ENVISAT Daten.

In dieser Arbeit wurden Klassifikationsgenauigkeiten verschiedener Kombinationen von Vorverarbeitung, Datenkombination und Klassifikatoren getestet. Einfluss von Speckelunterdrückung und Kalibrierung auf die Klassifikation wurden ebenfalls getestet. Die Anpassung der Daten auf einen Anbaukalender in Verbindung mit zwei Klassifikatoren Maximum Likelihood (MLC) und Support Vector Machines (SVM) wurde untersucht.

Die Auswertung der Klassifikationsmethoden basiert auf Fehlermatrizen und Kappa Statistiken. Die Ergebnise zeigen, dass die auf den Anbaukalender angepassten Daten und zusammengefügten Signaturen, basierend auf Kulturen, die Genauigkeit der MLC Klassifikation eine allgemeine Genauigkeit von über 80% erreichen. Eine Anpassung auf den Anbaukalender verbessert die Genauigkeit der SVM-Klassifikation nicht. Diese Methode benötigt eine gesonderte Berechnung der Klassifikationen für die verschiedenen Kulturarten. Damit werden unabhängige Ergebnise für jede Klasse generiert. Es können sich dabei in einigen Gebieten Konflikte aus den unterschiedlichen Klassifizierungen ergeben. Eine Methode zur Kombination der Ergebnisse wurde entwickelt, welche basierend auf die Abschätzungsmethode des Klassifizierungsprozesses die Konflikte löst. Die

Kombinationsmethode zeigte gute Ergebnisse, dabei wurde die Genauigkeit der Klassifikation für einzelne Klassen konstant gehalten. Es konnte zudem gezeigt werden, dass Spekel-Filter und der verwendete Klassifikator unterschiedliche Effekte auf das Ergebnis des Verfahrens zur Klassifizierung haben.

Schlagwörter: Multitemporal, Klassifikation, SAR

Summary

Cultivation activities cause many effects on human life and the environment. Traditional in situ measurements are expensive, time consuming and sample data is for the probed location only. In the framework of an ESA pilot project (AO335), remote sensing methods are investigated aiming of reliable, cost efficient, and continuous monitoring of cultivation activities.

Within the “Fuhrberger feld”, close to Hannover, Germany, a test site was established. ENVISAT ASAR amplitude images with VV/VH polarization are used for the analysis. In addition, ground truth data was gathered by field acquisitions. The latter serves both to define training areas and also to give a reference for accuracy assessment. The available data covers the agricultural season of 2004.

Extensive Field acquisitions have been carried out on more than 50 fields close to the time, when the images have been taken. The test fields cover the typical different crop types of the region, whose areas have been chosen large enough to ensure sound assessment of the results.

The methodological approach for the monitoring task consists of supervised classification of multi-temporal ASAR ENVISAT data.

Different options in relation to multi-temporal classification of ASAR data, like selection of speckle filters, calibration, signature combinations and classification rules are investigated. In this thesis comparisons between different combinations of pre-processing, input data sets and classification rules are tested, like: classification of raw data or filtered (by speckle filters) data, calibration, matching to crop calendar i.e. usage of different sets of images from different acquisition times for different crop types, taking into account the respective phenological period of the crops, maximum likelihood classifier (MLC) versus support vector machines (SVM) classifiers, the evaluation of classification methods is based on error matrices and kappa statistics.

The results show that matching despeckled data to crop calendar and signatures merged based on crop types improves classification accuracy of MLC and results in an overall accuracy higher than 80%. Matching to crop calendar does not improve the accuracy of SVM classification. Matching to crop calendar requires the computation of separate classifications for different crop types, giving independent results for each type. Therefore, in some areas conflicts may arise from the different classifications. A rule was generated which is based on distance files obtained from classification processes, which showed good results and kept the achieved accuracy. It could be shown also that the proper selection of speckle filter and the used classification rule improve the result of the classification procedure.

Keywords: Multi-temporal, Classification, SAR

Chapter 1

1 Introduction

1.1 Motivation

Agriculture can be considered as a tie point between nature and mankind. It is influenced by human demands and decisions, technology, natural resources, and natural hazards. Additionally, agricultural products are the most important source of food for human populations. Cultivation activities impair natural resources, and cause pollution, erosion, deforestation and desertification in many regions of the world. Therefore, careful management of agricultural activities is necessary for adequate and sustainable provision of food, and minimization of impacts on natural resources. For this purpose, information on agricultural areas and products is needed. Due to global population growth, the economic development and limited natural resources, this demand is increasing. The cultivated crops differ from one year or season to another in many agricultural areas. Consequently, continuous monitoring of agricultural activities often becomes necessary.

Mapping agricultural fields is an effective method to provide information on crops and cultivation activities. The spatial distribution of features can be illustrated in a map. Furthermore, maps can be linked to other data and information in a GIS for decision support.

Remote sensing data is widely used for mapping agricultural areas. It offers cost effective and multifaceted data, usually in form of images. An image carries spatial data and therefore can be effectively used for mapping purposes. Various remote sensing products are provided over a wide range of the electromagnetic spectrum. Modern sensors are capable of acquiring data from the ultra violet spectrum to the microwave domain. Data from the various parts of the electromagnetic spectrum offer special advantages, they usually are adapted to particular applications, but have limitations, too.

Imaging radar sensors take images in the microwave domain. They are called active sensors since they actively transmit microwave signal that is then backscattered from the ground and finally received by the sensor. Microwave signals pass through clouds and reach the earth's surface also on cloudy days. Hence, radar imagery can be acquired almost independently of weather conditions and natural illumination.

The backscattering of radar signals is affected by physical characteristics of the target. A horizontal, flat (relatively to the wavelength) and hard surface acts as a mirror and results in a dark (low backscattering) area in a radar image. In contrast to a flat bare land, plants on a field tend to scatter microwave signals in any direction. Backscattered signal toward the sensor results bright areas on a radar image. In addition, the dielectric constant and the physical density of the target are essential factors for the penetration, reflection, or backscattering of the microwave signals (Henderson and Lewis 1998).

It is known, that space borne data can be provided at lower costs, if available (Redslob 2000). Global coverage, low costs, and independence from weather conditions of space borne radar data facilitate continuous monitoring over most regions of the earth. Continuous multi-temporal data reflects temporal changes of agricultural fields. In a multi-temporal approach, the influence of growth phases of plants on the radar backscattering characteristics can be exploited. Hence, multi-temporal approaches are considered to deliver higher classification accuracy than single date acquisitions (e.g. Hochschild et al. 2005, Tröltzsch 2002). But a multi-temporal analysis faces some complications that are explained under section "problem

definition". Subject of this study is to evaluate methods for multi-temporal crop classification using space borne SAR data.

1.2 Problem Definition

Agricultural monitoring using radar imagery is a solution for land related studies in many agricultural areas with frequent cloud cover, such as Northern Europe, but some problems complicate utilization of radar data for crop classification.

Radar data is usually taken in one channel, but acquisition in two or more polarizations is possible. Hence, spectral bands of optical (Visible-Infrared) data can be replaced by multi-polarized radar data in a classification process. Only few polarizations of space borne radar data are available (usually two), which impedes precise classification of radar data for agricultural crops. For instance, only about 35% to 45% of the training areas were correctly classified for most crops in a test of a single date space borne radar data set with two polarizations (VV/VH) and 30 meters spatial resolution (Lohmann et al. 2005).

The speckle effect, inherent in SAR data, results in a high interior variance of pixel values in each class and low separability between different classes in the feature space. Speckle can be reduced by various techniques to decrease the interior variance of each class and increase separability between classes. However, despeckling methods reduce the speckle effect at the cost of spatial information. In addition, the speckle effect in SAR images depends on surface properties and should not be considered as random noise. Therefore, it should be investigated if applying speckle filters is helpful for a specific study. In case the application of speckle filters improves the results of the desired process, it must be considered that different speckle filters affect pixel values in different ways. Therefore, it must be investigated, which filter is more useful for a desired purpose.

Another approach for improving the classification accuracy is to enlarge the feature space by means of more independent images. One possibility would be to extend the feature space by using fully polarimetric data (HH, VV, and cross polarizations). However, fully polarimetric data from space borne SAR systems usually is not available.

On the other hand, considering the independence from weather conditions and the relatively low cost of space borne radar data, the acquisition and classification of multi-temporal SAR data seem to be feasible. Seasonal variations can be considered as a specific signature of each crop. Therefore, multi-temporal data is especially beneficial for crop monitoring, which is the goal of this thesis. Each plant has a specific phenological period and characteristics, such as geometry, biomass, and water content that vary during the growth period. These changes in the course of time can be utilized as a temporal signature of one crop, if they can be observed on SAR images.

Apart from the high potential of multi-temporal SAR data for vegetation studies, there are some difficulties related to the application of the data for agricultural monitoring purposes. Plants of a cultivated crop on a field are expected to be observed during the vegetation period. Beyond this period, the field may stay as bare land, be cultivated with other crops, or be covered by rest of vegetation or wild plants. Therefore, using images of a complete year for classification of all crops may introduce some errors. This is due to the inclusion of irrelevant information in the classification, since any image that is not taken in the phenological period of a crop is irrelevant for training the classifier for that crop. But the same image may be useful for the recognition of another crop. Therefore, it may be important to choose a suitable set of images for each class. In this case, each class is classified by a set of images which may not be the same data set used for classification of other crops.

On the other hand, representation of all classes on a map is usually required. Thus, results for crops can be in conflict with each other. This happens if one area is classified as more than one crop. The combination of the results for crops classified by different sets of images is a challenging problem.

Multi-temporal classification of crops deals with growth phases of plants. It becomes possible if a crop has a fixed and known appearance period.

Another issue concerns a suitable classification method. Different classification methods (for example parametric methods such as maximum likelihood, non-parametric methods such as support vector machines (SVM)) may be applied, which can potentially yield different results. The Bayesian classification with maximum likelihood estimation is a well known parametric classifier, which has been vastly used for classification of remote sensing data. This method is

referred as maximum likelihood classification or classifier in most pattern recognition and remote sensing references (Duda et al. 2000, Richards and JIA Xiuping 1999, Jensen 1996). It considers a distribution of pixel values in each class for classifying data. On the other hand, SVM are non-parametric classifiers which use vectors of marginal objects of each class to form a hyperplane as a border between two classes. SVM as non-parametric classifiers are considered to be insensitive to diverse measurement scales in multi source data, to perform well with high dimensional data, and as not needing a feature selection (Tso and Mather 2001, Watanachaturaporn et al. 2004, Brenning et al. 2006).

This study aims at proper identification of agricultural activities by means of classification of radar images. Solutions for the problems, discussed above are sought in relation to classification of a multi-temporal set of space borne images. Preprocessing methods such as speckle filters are evaluated. Different classification methods and sets of images affect the results and are tested in order to find the proper combination of data and methods for monitoring agricultural activities in the study area. The purpose of this study is to indicate the required data and suitable classification methods for the development of a continuous monitoring system using space borne radar data.

Each crop has its individual characteristics such as growth behavior as well as forms of management during a year and surface textures. Phenological structures can be assumed from the temporal variability of plants. These phenological structures should reflect the specific growth behavior of arable crops regarding structure and are the basis for the development of a new hierarchical, multi-temporal classification strategy.

1.3 Contents of this Thesis

This study is built on previous studies in the field of agricultural monitoring using remote sensing data. As described in the previous section, a variety of preprocessing, data combination and classification methods are conceivable. Some methods are investigated and presented in this study, which seem to lack in literature. The aim is to improve accuracy of classification through new methods. Results of different methods are compared and evaluated.

Chapter 2 describes the theoretic basics of the study in two sections. The first section contains a brief introduction to radar remote sensing principles and a presentation of natural features in radar data. Since the applied methods are based on amplitude images, it is necessary to consider the appearance of land cover in radar amplitude images.

The next section explains classification techniques. The concept of classification is briefly explained and definitions of some classifiers are presented to be used as a reference in the following sections. Prerequisites, considerations, advantages and disadvantages of classifiers relating to radar data and multi-temporal classification are discussed and compared.

Chapter 3 contains the state of the art. Literature in the field of agricultural monitoring using radar images and applied methods especially in the field of multi-temporal radar data is inspected. The aim of this chapter is to identify open research questions.

Chapter 4 introduces the data and methods used for this study and its specifications. ENVISAT ASAR images, field visits, orthophotos and maps are used in this study. Acquisitions, description of SAR images, data collected by field visits, and target classes are explained in this Chapter.

The method and test design are illustrated. First, temporal changes of agricultural fields and the impact on the backscattering of SAR signals are investigated. Furthermore, data preparation methods, applied preprocessing and tested classification methods are explained. Following, test design and evaluation method for applied processes are proposed.

In chapter 5 results of the methods and tests introduced in Chapter 4 are presented, discussed and compared with theoretic considerations and previous works.

Chapter 6, conclusions, reviews the results of the study, open problems, and outlook for new research ideas.

Chapter 2

2 Basics

Data acquisition without physical contact with targets is known as remote sensing. Electromagnetic (EM) energy is the actual medium for remote sensing. A range of electromagnetic wavelengths from nanometer to meter is used for data acquisition of the earth's surface as well as atmosphere and other planets. Optical sensors provide panchromatic, multispectral, and hyperspectral data in the ultra violet, the visible and the near infrared domain. Optical data is influenced by chemical and physical properties of targets.

Data gathered in wavelengths between 3 and 50 micrometers from the earth's surface is mainly influenced by temperature and emissivity of the target. This type of data is widely used for surface temperature measurements.

Microwave measurements in wavelengths from 1 to 100 centimeter are mainly influenced by the shape, material, and conductivity (dielectric constant) of the target. EM energy in longer wavelengths is less affected by clouds and rainfall. Wavelengths longer than 5cm are almost not affected by weather conditions. A drawback of the use of longer wavelengths is that the spatial resolution decreases and penetration increases providing less information from the surface of the target.

Sensors are often distinguished into active and passive based on the source of the measured EM energy. If the EM energy originates from a natural or artificial source aside the sensor, the sensor is a passive sensor. Otherwise, if the measured EM energy is transmitted by the sensor, the sensor is known as active. Active sensors are independent from natural illumination and therefore can operate at night as well as in the daytime with almost no difference. Radar sensors and laser scanners are two widely used active systems of remote sensing.

Radar data is used in this study and classification methods are applied for information extraction from radar data. Therefore, basics of radar remote sensing and classification in remote sensing are presented in this Chapter.

2.1 Radar Imaging

Radar systems as active sensors emit electromagnetic radiation in the microwave domain and record the backscattered radiation. Imaging radar forms an image of the observed scene and is used for observation of the earth and its atmosphere. Principles of radar and characteristics of the side looking radar are introduced as basis of imaging radar. In sequence, SAR as an improved imaging radar system is described. Finally, the influence of target parameters on radar signals and imaged scenes is investigated.

2.1.1 Principle of Radar

Radar systems use electromagnetic waves to identify the range, altitude, direction, or speed of both moving and fixed objects such as aircrafts, ships, motor vehicles, weather formations, and terrain. The term RADAR was coined in 1941 as an acronym for Radio Detection and Ranging (Henderson and Lewis 1998)[1].

A radar system has a transmitter that emits electromagnetic energy which is scattered by the target and detected by a receiver. A typical radar measures the strength and round-trip time of the signals that are emitted by a radar antenna and scattered by a distant surface or object.

[1] This is the important reference for information of section 2.1, where no other reference is cited.

Radar is used in many contexts including meteorological detection of precipitation, measuring ocean surface waves, air traffic control, police detection of speeding traffic, and by the military.

A mono static radar antenna alternately transmits and receives pulses at particular microwave wavelengths (in the range 1 cm to 1 m, which corresponds to a frequency range of about 30 GHz to 300 MHz) and polarizations (waves polarized in a single vertical or horizontal plane). At ever longer wavelengths the radiation is known as radio waves.

An active imaging system sends out radiation, some of which is scattered back to the receiver. The backscattering signal, which is influenced by the positions and shapes of target bodies and their properties (material, direction, etc), can be used to form kinds of images that superficially resemble those recorded by optic sensors.

2.1.2 Radar Equation

The fundamental relation between the characteristics of the radar, the target, and the received signal is described by the radar equation. It explains the power that is received (P_r) by the receiver as a function of the transmitted power (P_t), the distance to target (R), the gain of antenna (G), the wavelength (λ), and the radar cross section of the target (σ). σ depends on the target receiving area (A_s), the absorbed energy at target (α), and the gain of the target towards the receiver (g_s) as:

$$\sigma = A_s(1-\alpha)g_s \tag{2.1}$$

Since aerial remote sensing radars view the earth's surface and not an object source, P_r is related to the power returned from an illuminated area (A) defined by the resolution cell of the imaging system. Therefore, σ is redefined as radar scattering per unit area (σ^0) also known as radar backscattering coefficient.

The Radar equation can be written for a monostatic radar (same antenna used for transmit and receive) system as:

$$P_r = P_t.(\sigma^0 A).(\frac{G^2 \lambda^2}{(4\pi)^3 R^4}) \quad (2.2)$$

This shows that the received power declines as the fourth power of the range, which means that the received power from distant targets is very small.

In a real-world situation, path loss effects should also be considered. Path loss is the loss of power of an EM signal traveling (propagating) through space due to environment of the path.

2.1.3 Imaging Radar System

As described, a radar system emits EM pulses and observes scattered energy. Each pulse lasts only microseconds. An imaging radar sends narrow oblique pulses perpendicular to the flight direction. The pulse meets the earth's surface over a swath in different ranges from nadir. The look angle may expand up to more than 80 degrees. Airborne radar sensors can observe a relatively small area due to the low flight elevation. Therefore, airborne radar sensors have usually a wide span of look angles from less than 30° to 80° to cover a larger area. In contrast, space borne radar sensors operate in a much higher elevation. A pulse with 5° difference between minimum and maximum look angles, records a range between 5 to 50 kilometers on the earth.

A radar system measures its distance to a scatterer using the delay time of each echo (slant range). This distance is considered as approximately proportional to distance from Sensor on a two dimensional space (ground range). Some definitions relating to radar system are explained here.

Figure 2.1 shows how an imaging radar system works. The sensor moves forward at some altitude above the terrain in **azimuth** direction while the pulses spread outward in the **range** (look) direction, perpendicular to the flight line. Any line-of-sight from the radar to a ground point within the terrain strip defines the **slant range (** R_s **)** to that point.

Ground Range (R_g) is the distance between the aircraft nadir (directly below) and any ground target point on a plane (flat or an ellipsoid). The ground point closest to the aircraft flight trace, at which sensing begins, is the **near range** limit. The pulsed ground point at the greatest distance normal to the flight path fixes the **far range**. At the radar antenna, the angle between a horizontal plane and a given slant range direction is called the **depression angle (β)** for any point along that directional line. The complementary angle (measured from a vertical plane) is known as the **look angle (ϕ)**. The **incident angle (θ)** at any point within the range is the angle between the radar beam direction (of look) and local vertical with respect to the geoid. The **Local incident angle (θ_l)** is the angle between the radar beam direction and local vertical with respect to the terrain. The incident angle may be considered equal to look angle for an air borne sensor, but in the case of a space borne sensor, the incident angle is significantly larger than the look angle due to the curvature of the earth's surface. The look angle increases outward from near to far range and pulse travel times increase outward between these limits.

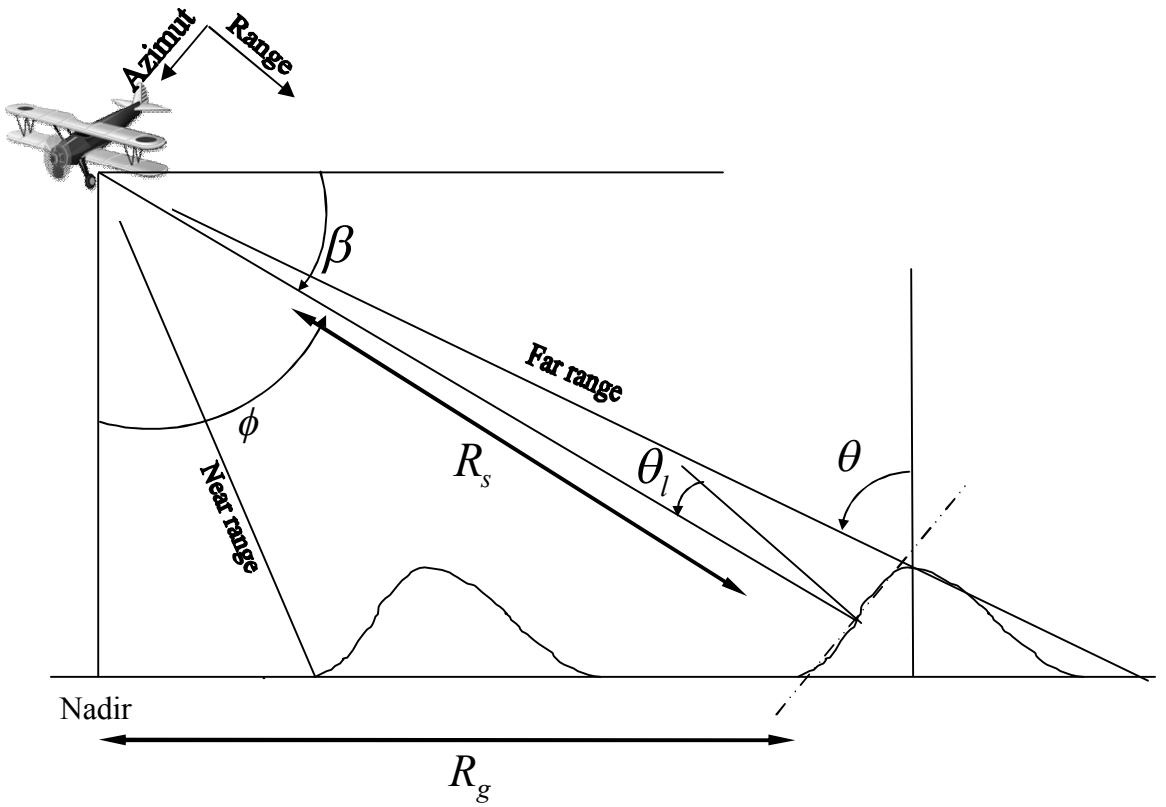

Figure 2.1. A schema of an imaging radar system, describing some definitions.

The relief influences the imaging geometry in radar images. Relief displacements are known from optical imagery, but relief displacements in radar images differ from that of optical images. This difference is due to the calculation of distance from signal travel time, and one operating antenna as illumination source and receiver (monostatic acquisition). Travel time for a pulse scattered by an elevated object such as a mountain top is shorter than for an object in the plain of the same ground range. Therefore, elevated objects tend to appear displaced towards sensor in the image. If the slant range to the top of an object is shorter than that to the bottom of the same object, such as the left mountain in Figure 2.2, the backscattered signal from the top is received before that from the bottom. Hence, the top is imaged closer to the sensor than the bottom in the image. This effect is known as **layover.** In case the slant range to the top is not shorter than to the near bottom, **foreshortening** happens (left bottom of right mountain in Figure 2.2).

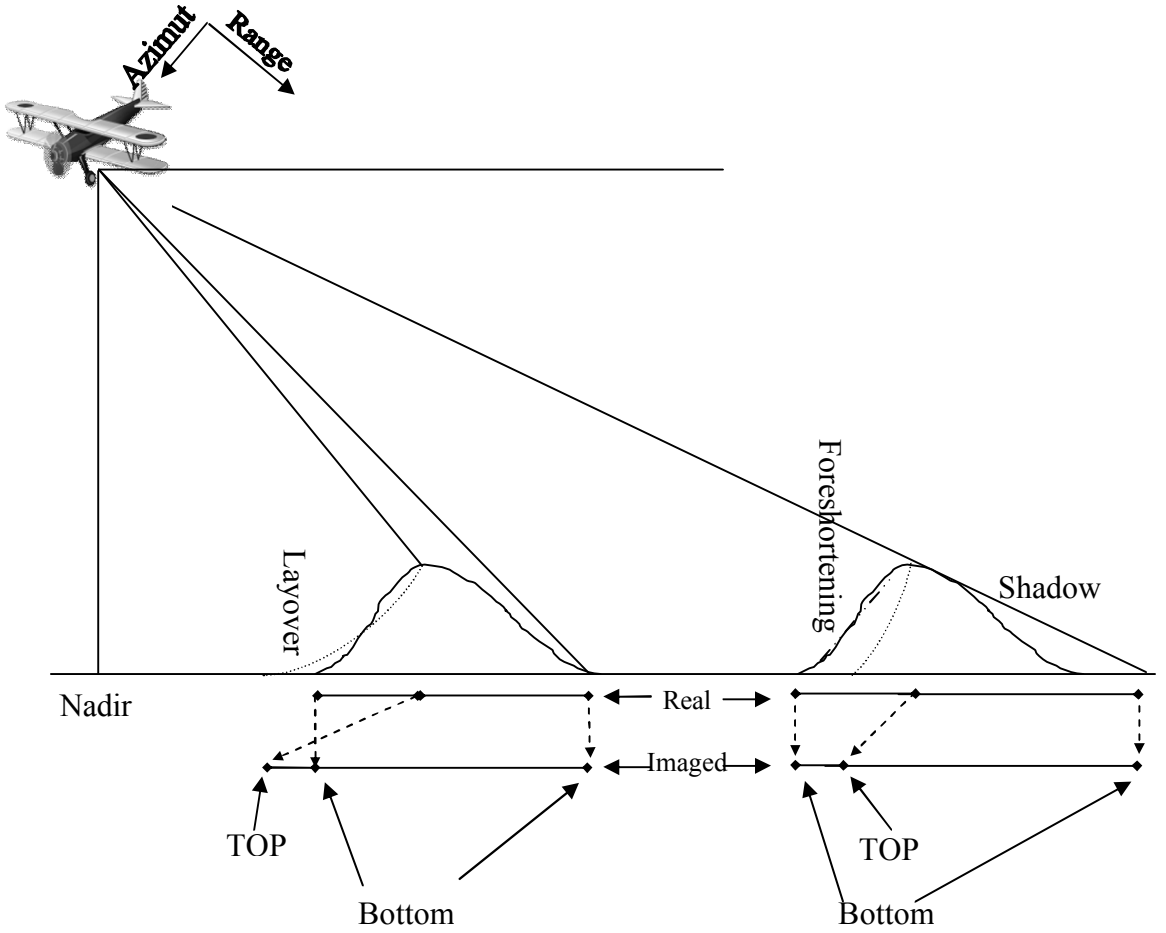

Figure 2.2. Influence of relieves on radar image.

Layover is more relevant for small look angles and foreshortening for large look angles. Due to layover and foreshortening, slopes facing the sensor are imaged shorter than their real length considering the scale of the image. In contrast, slopes facing away from sensor stretch over a larger area on the radar image, so that the imaged distance between the top and the bottom of the opposite slope of a mountain is longer than its real distance. If the depression angle becomes smaller than the opposite slope, as it is the case for the right mountain in Figure 2.2., the slope is not illuminated at all. Therefore, no signal is returned from the area behind the mountain resulting in a dark area called **shadow.** Otherwise, the opposite slope is illuminated and presented as a relatively dark area. This dark area spreads from far bottom (e.g., right bottoms on the Figure 2.2) to the imaged position of top, or to the near bottom (e.g., left bottom on the Figure 2.2) if layover occurred.

2.1.4 Resolution

Spatial resolution of an imaging system determines if it provides the necessary geometric detail for a known purpose. It indicates the minimum separating distance between two targets that is necessary to display them as two individual features. Resolution for imaging radar is defined in two directions: parallel (azimuth) and perpendicular (range) to the flight direction (Henderson and Lewis 1999).

The **range resolution** of a pulse is determined by the pulse length of the transmitted radar signal. The pulse length is calculated using the speed of light (c) and duration of transmission (τ). Since a radar pulse must travel to the target and back to the sensor, the pulse length is divided by 2 in order to determine the **slant range resolution** (S_r):

$$S_r = c\tau / 2 \tag{2.23}$$

Slant range resolution is constant across the entire range, however, the **ground range resolution** (G_r) is usually more important to the user. G_r is variable across the range and more complex to calculate. In order to calculate the ground range resolution (for flat terrain), the slant range resolution must be divided by cosine of the depression angle or sine of look angle.

$$G_r = c\tau / 2\sin\phi = c\tau / 2\cos\beta \tag{2.24}$$

Equation 2.24 indicates that ground range resolution improves from near to far range. It describes, too, why near nadir acquisition is not possible, where range resolution tends to infinity.

The **azimuth resolution** (A_r) is defined by the beam width (β_h) in radians and the distance in the range (R) as:

$$A_r = \beta_h R \tag{2.25}$$

The azimuth resolution improves as the beam width and/or distance in range decreases. The beam width is expressed in terms of the wavelength (λ) and the length of radar antenna (l) as:

$$\beta_h = \lambda / l \tag{2.26}$$

Therefore, the resolution can be improved by decreasing the wavelength and/or increasing the antenna length. Both possibilities have limitations. Lower wavelengths are affected by atmosphere and the length of the antenna is limited by platform capabilities.

2.1.5 Synthetic Aperture Radar

The definitions in the previous section explain "Real Aperture Radar" (RAR). As described, azimuth resolution of a RAR depends on range, length of antenna, and wavelength. Therefore, the larger the range is, the poorer is the resolution. Hence, a space borne RAR system would need a huge antenna of some kilometers length to provide a reasonable azimuth resolution which is not feasible.

A synthetic aperture radar (SAR) simulates a large antenna using more frequent pulses transmitted from a small antenna. One transmitted pulse of a space borne SAR meets the earth's surface over a wide area in azimuth direction. Since the illuminated area spreads some kilometers in azimuth direction, the received energy may experience Doppler shifts relating to the motion between radar and scatterer. Doppler shift is zero if the radial motion component between the sensor and the scatterer is zero. Zero motion (in illumination direction) happens for any scatterer located on the line of sight from radar perpendicular to flight direction. The further away a scatterer is situated from this line, the more Doppler frequency shift the pulse

experiences. Therefore, any value of Doppler shift represents an angle in azimuth direction between the line of sight perpendicular to the flight direction and the line of sight to the scatterer (Henderson and Lewis 1999).

Processing this information from thousands of pulses for each cell results in a higher azimuth resolution. The maximum attainable azimuth resolution of a SAR (A_s) system is calculated as:

$$A_s = l/2 \tag{2.27}$$

Equation 2.27 shows the most important advantage of SAR that the azimuth resolution is independent of range, which is a unique property of SAR amongst remote sensing sensors.

However, the coherent nature of the SAR signal results in speckle. A SAR system records both the amplitude and the phase of the back scattered signal. Each resolution cell of the system contains many scatterers. The phases of the return from these scatterers are distributed and speckle may be caused by phase interference. This gives a grainy look to the image. Speckle is not randomly distributed on the image because it depends on the target surface. Therefore, speckle carries information about the scene. On the other hand, speckle affects statistics of the image and fades patterns on the image resulting in difficulties for manual and machine interpretation of SAR images. Hence, it is useful for many applications to reduce the speckle effect.

Using a so called multi-look processing, speckle is minimized to improve image quality (radiometric resolution) at the expense of azimuth resolution. Each image is divided into sub beams as looks. All looks are averaged to produce an image with reduced speckle. The resolution is multiplied by the number of looks resulting in a reduced azimuth resolution. Therefore, a multi look depression of speckle reduces spatial resolution as well.

SAR products of ENVISAT are usually multi look processed before being delivered to the user. Furthermore, speckle filters can be applied by the user to reduce the speckle effect if necessary. For each purpose, it must be investigated if speckle suppression is necessary or information carried by speckle is useful.

2.1.6 Polarization

Polarization describes the orientation of oscillations of waves relating to magnetic field of the wave. A SAR sensor can measure the polarization state of the backscattered signal. Polarization of a backscattered signal depends on the polarization of the transmitted signal as well as on the scatterer. The polarization of wave may change due interaction with the scatterer object. This is known as depolarization. Depolarization of radar signals may occur due to the multiple reflections at the target. So part of the backscattered waves are depolarized. Therefore, the polarization of backscattered signal carries useful information on the scene. A SAR antenna must be able to send and transmit electromagnetic waves in more than one polarization, in order to produce multi-polarization data. If a scene is observed by a radar with two orthogonal polarizations in the transmitted signal (not simultaneous), and also two orthogonal polarizations in the received signal, a set of four estimates of the polarimetric reflectivity for each element in the scene is available.

Assuming that the wave is traveling in z direction of a rectangular 3D coordinate system, the wave field has only x and y components. The x component is usually referred as H (for horizontal) and y component as V (for vertical). The electric vector has two phase angles in x and y directions as ϕ_x and ϕ_y. The phase difference is defined as:

$$\phi = \phi_y - \phi_x \tag{2.3}$$

The polarization state of a wave may be described by the shape traced out in a fixed plane by the electric vector as such a plane wave passes over it.

Polarization becomes linear if

$$\phi = m\pi\,,\ m = 0,\pm 1,\pm 2,\ldots. \tag{2.4}$$

In this case, the tip of the vector traces out a single line in the plane, hence this special case is called **linear polarization**. The direction of this line depends on the relative amplitudes of the two components (H and V). If the amplitude of the H component is zero the wave is vertical polarized and if the amplitude of the V component is zero the wave is horizontally polarized.

The wave is **circular polarized** if the amplitudes of the two components of electric field are equal and if:

$$\phi = \pm\pi / 2 \tag{2.5}$$

In this case one component is zero when the other component is at maximum or minimum amplitude. If the component magnitudes are not equal and ϕ does note equal to $m\pi, m = 0,\pm1,\pm2,...$, or to $\pm\pi/2$, the electric vector traces out an ellipse in the plane and the wave is **elliptically polarized** (Henderson and Lewis 1998, Mott 1992).

2.1.6.1 Scattering Matrix

We consider an object illuminated by an electromagnetic plane wave[1] with incident electric field:

$$E^i = E_v^i V_i + E_h^i H_i \tag{2.6}$$

Where E^i is the incident electric field, E_v^i and E_h^i are the projections of E^i onto the unitary vectors V_i and H_i as a reference basis.

The wave is backscattered by the object. The scattered wave is an outgoing spherical wave, which can be locally considered as a plane wave over the area occupied by the receiving antenna. The electric field of the scattered wave can be described as:

$$E^s = E_v^s V_s + E_h^s H_s \tag{2.7}$$

The superscript s refers to the scattered wave and V_s and H_s are the unitary vectors as a reference basis for scattered wave.

It is useful to adopt the following matrix notation for the electric fields of incident and scattered wave:

$$E^i = \begin{bmatrix} E_v^i \\ E_h^i \end{bmatrix} \text{ and } E^s = \begin{bmatrix} E_v^s \\ E_h^s \end{bmatrix} \tag{2.8}$$

[1] Plane wave is a constant-frequency wave whose wave fronts (surfaces of constant phase) are infinite parallel planes of constant amplitude normal to the phase velocity vector.

Using this matrix notation, the components of E^i and E^s are related by a complex 2×2 matrix:

$$\begin{bmatrix} E_v^s \\ E_h^s \end{bmatrix} = \frac{e^{-jkr}}{r} \begin{bmatrix} S_{hh} & S_{hv} \\ S_{vh} & S_{vv} \end{bmatrix} \begin{bmatrix} E_v^i \\ E_h^i \end{bmatrix} \tag{2.9}$$

where r is the distance between scatterer and the antenna, and k is the wave number of illuminating field. The scatterer matrix S is defined as:

$$[S] = \begin{bmatrix} S_{hh} & S_{hv} \\ S_{vh} & S_{vv} \end{bmatrix} \tag{2.10}$$

The scattering matrix can directly be measured by the sensor using a sequence of four transmit and receive cycles at different polarizations. For example, S_{hh} can be measured by transmitting a horizontally polarized pulse and receiving only the horizontal component of the echo and other polarizations in similar way by choosing the appropriate combination of transmit and receive polarizations (Reigber 2001).

The two off-diagonal elements of [S] are identical for a monostatic radar system, in which the reciprocity property[1] holds for most targets (Boerner et al. 1998). Therefore, $S_{hv} = S_{vh}$ is valid for most natural scatterers and only three complete component of the scattering matrix are independent. Polarimetric scattering can be formulated as a target vector instead of a scattering matrix (Kostinski and Boerner 1986).

$$k = V([S]) = \frac{1}{2} trace([S]\psi) \tag{2.11}$$

where trace (.) is the sum of diagonal elements of the argument, and ψ is a set of 2×2 complex basis matrices which are orthogonal under hermitian inner product (Cloude 1986). Several basis sets have been used in the literature. Two examples are often used:

[1] the reciprocity theorem states that if an electromagnetic field E in one branch of a reciprocal network produces a current I in another, then if the electromagnetic field E is moved from the first to the second branch, it will cause the same current in the first branch, where the electromagnetic field has been replaced by a short circuit (Irwin 1987).

ψ_L corresponds to a straightforward ordering of elements of [S], and ψ_P uses the Pauli spin matrices $[\sigma_i]$. Their explicit expressions are (Sanchez 1999):

$$\psi_L = 2\left(\begin{bmatrix}1 & 0\\ 0 & 0\end{bmatrix},\begin{bmatrix}0 & 0\\ 1 & 0\end{bmatrix},\begin{bmatrix}0 & 1\\ 0 & 0\end{bmatrix},\begin{bmatrix}0 & 0\\ 0 & 1\end{bmatrix}\right) \tag{2.12}$$

and

$$\psi_P = \sqrt{2}\left\{\left[\sigma^i\right]\right\}, \qquad \mathrm{i} = 0,1,2,3 \tag{2.13}$$

where

$$\sigma^0 = \begin{bmatrix}1 & 0\\ 0 & 1\end{bmatrix}, \sigma^1 = \begin{bmatrix}1 & 0\\ 0 & -1\end{bmatrix}, \sigma^2 = \begin{bmatrix}0 & 1\\ 1 & 0\end{bmatrix}, \sigma^3 = \begin{bmatrix}0 & -j\\ j & 0\end{bmatrix} \tag{2.14}$$

Target vectors k become:

$$k_L = \begin{bmatrix}S_{vv}\\ S_{vh}\\ S_{hv}\\ S_{hh}\end{bmatrix} \quad \text{and} \quad k_P = \frac{1}{\sqrt{2}}\begin{bmatrix}S_{vv}+S_{hh}\\ S_{vv}-S_{hh}\\ S_{vh}+S_{hv}\\ j\left(S_{vh}-S_{hv}\right)\end{bmatrix} \tag{2.15}$$

For monostatic sensors and in the general case of backscattering reciprocal targets, one of the entries of the target vector is redundant, and three new component vectors are defined.

$$k_{3L} = \begin{bmatrix}S_{vv}\\ \sqrt{2}\times(S_{vh})\\ S_{hh}\end{bmatrix} \quad \text{and} \quad k_{3P} = \frac{1}{\sqrt{2}}\begin{bmatrix}S_{vv}+S_{hh}\\ S_{vv}-S_{hh}\\ 2S_{vh}\end{bmatrix} \tag{2.16}$$

The PAULI-basis has the advantage of the strong relationship between the elements of the scattering vector to three basic scattering mechanisms (Sanchez 1999, Cloude 1986).

The first Pauli matrix describes the component of isotropic odd-bounce scatterers, such as idealized flat surfaces or trihedral corner reflectors. The second Pauli matrix is related to isotropic even-bounce scattering, e.g., a double-bounce, and the last matrix corresponds to isotropic even-bounce scattering with an orientation rotated by $\pi/4$ like a double bounce target whose axis is rotated to the line-of-sight direction (e.g., dihedral corner reflectors with a rotation of 45 degrees). Also a significant contribution of the volume backscattering (e.g., from vegetation) is found in the third matrix.

A complex vector $\vec{\omega}$ can describe any idealized scattering mechanism (one single deterministic scatterer is present in each resolution cell) in the chosen basis. The projection of $\vec{\omega}$ onto $\vec{k}$ estimates the contribution of a certain scattering mechanism $\vec{\omega}$ to the measured vector $\vec{k}$.

$$\mu = \vec{\omega}^{\iota} . \vec{k} \tag{2.17}$$

Where ι indicates the adjoint (complex conjugate transpose) operation. The μ represents the complex scattering amplitude of the chosen scattering mechanism so the measured scattering matrix can be decomposed into contributions from any set of orthogonal scattering mechanisms (Sanchez 1999).

2.1.6.2 Scattering by Random Media: Partial Scatterer

The scattering matrix describes the scattering characteristics of a single deterministic scatterer, while the spatial unit in radar imaging systems is the resolution cell which may contain many small scatterers. This case can be described by another important class of scatterers known as distributed targets. Backscattering of each resolution cell results from the coherent superposition (the overlain backscattering of a wave by several scatterers) of several scattering processes whose locations are spatially distributed inside the resolution cell. Most natural terrain surfaces belong to this class. Each scatterer in the resolution cell is represented by its own scattering matrix. Hence, the measured total scattering matrix is a coherent superposition of all these individual scattering matrices (Cloude 1992).

One method to describe the polarimetric scattering process of distributed targets is the introduction of a covariance or coherency matrix. The covariance matrix for the reciprocal backscattering case (Cloude 1992):

$$[C_3] = \left\langle \vec{k}_{3L} \vec{k}_{3L}^{\,l} \right\rangle = \begin{bmatrix} \left\langle S_{hh} S_{hh}^* \right\rangle & \sqrt{2}\left\langle S_{hh} S_{hv}^* \right\rangle & \left\langle S_{hh} S_{vv}^* \right\rangle \\ \sqrt{2}\left\langle S_{hv} S_{hh}^* \right\rangle & 2\left\langle S_{hv} S_{hv}^* \right\rangle & \sqrt{2}\left\langle S_{hv} S_{vv}^* \right\rangle \\ \left\langle S_{vv} S_{hh}^* \right\rangle & \sqrt{2}\left\langle S_{vv} S_{hv}^* \right\rangle & \left\langle S_{vv} S_{vv}^* \right\rangle \end{bmatrix} \quad (2.18)$$

And the coherency matrix:

$$[T_3] = \left\langle \vec{k}_{3P} \vec{k}_{3P}^{\,l} \right\rangle \quad (2.19)$$

Where $\langle ... \rangle$ denotes spatial averaging. These matrices contain complete scattering information about distributed targets such as variance and correlation for elements of [S]. The eigenvector analysis of the coherency matrix $[T_3]$ acts as basis for another class of decomposition theorems, as proposed by Cloude and Pottier et al. (1995). One advantage of $[T_3]$ is that it is in general of full rank 3 due to the spatial averaging, while $\vec{k}$ spans one-dimensional subspace of the vector space defined by ψ. Therefore, $[T_3]$ is a hermitian positive semidefinite matrix, which can be diagonalized and possesses real eigenvalues. So, it can be written as a sum of three independent coherency matrices, each one spanned by one of the eigenvectors of $[T_3]$:

$$[T_3] = \sum_{i=1}^{3} [T_3]_i = \lambda_1 (e_1 e_1^t) + \lambda_2 (e_2 e_2^t) + \lambda_3 (e_{31} e_{13}^t) \quad (2.20)$$

Where λ_i are eigenvalues of $[T_3]$ and e_i its orthogonal eigenvectors. The eigenvalues can be interpreted as an amplitude of the scattering mechanism, described by the corresponding eigenvector. This results in the measurable polarimetric scattering entropy H_{pol} (Cloude and Pottier 1995):

$$H_{pol} = \sum_{i=1}^{3} - P_i \log_3 P_i \,, \qquad P_i = \frac{\lambda_i}{\sum_{j=1}^{3} \lambda_j} \tag{2.21}$$

Possible values for H_{pol} lie between 0 and 1. If only one significant eigenvalue exists, the entropy becomes 0. This happens for a deterministic scatterers, which can also be described by a single scattering matrix. An entropy close to 1 occurs in the case of three equal eigenvalues, indicating a superposition of several equally dominant scattering processes. Any unitary three dimensional vector, and so as well the eigenvectors of $[T_3]$, can be composed in terms of a set of 5 angles (Sommerfeld 1895):

$$\vec{e} = \begin{bmatrix} \cos\alpha \exp(i\phi_1) \\ \sin\alpha \cos\beta \exp(i\phi_2) \\ \sin\alpha \sin\beta \exp(i\phi_3) \end{bmatrix} \tag{2.22}$$

Also known as **point reduction theorem** equation (2.22) expresses that any scattering vector can be seen as resulting from the vector $[0,0,1]^T$ by a rotation about a first component (α), a rotation about a third component (β) and applying the scattering phase angles (ϕ) (Cloude and Pottier 1995). The angle β represents the orientation of the scatterer with respect to the radar line of sight orientation. For example, this can be used for the estimation of azimuthal terrain slopes (Lee et al. 1994). The other angle α is associated with a rotation of the two dimensional basis of the polarimetric signature of the scatterer and has values between 0 and 90 degree. α provides information on the type of scattering mechanism. $\alpha = 0^\circ$ corresponds to an isotropic flat surface ($S_{hh} = S_{vv}$) and $\alpha = 90^\circ$ to an isotropic dihedral or helix ($S_{hh} = -S_{vv}$). Values between 0 and 90 degree represent anisotropic scattering mechanisms ($S_{hh} \neq S_{vv}$) (Sanchez 1999, Reigber 2001). Higher values of α indicate larger difference between Backscattering in VV and HH polarizations.

Information of this section on polarization helps us to understand the influence of polarization of a radar signal on recorded data. A complex scene such as dense vegetation coverage contains many small scatterers per resolution cell so that multi-reflection of signals inside the vegetation

volume is expected, which increases the chance of depolarization. On the other hand, a simple homogenous target area scatters or reflects the signal with less depolarization. Therefore, cross-polarization data (data recorded in orthogonal polarization of emitted signal) provides useful information on the vegetation coverage. Another important issue is the fact that a vertically polarized wave is more than a horizontally polarized wave reflected by targets having strong vertical components such as wheat field. Vegetation of crop fields usually contains vertical components. Hence, vertical polarization is considered to be more suitable than horizontal polarization for investigation of most vegetation types. Considering this information and other experiments, VV/VH data outperforms HH/HV data of the ENVISAT SAR sensor for agricultural monitoring. Therefore, VV/VH data are used for agricultural monitoring in this study.

2.1.7 Target Scattering

Information extraction from SAR data is based on amplitude images in many studies. Tone and patterns of an image, aside from system parameters, depend on target parameters, too. On its way between the sensor and the target surface, the pulse may be reflected, scattered, or penetrate the surface. The specular surface **reflection** happens in the opposite direction of the pulse emission from a specular surface with the same local incident angle. Therefore, reflected energy is usually not received by the sensor with the exception if the local incident angle is zero and a specular surface is directed towards the sensor. Reflection of the pulse from the volume of a target in many directions is called **volume scattering**. The scattered part of EM energy towards the radar antenna is recorded by the sensor. The more energy is scattered towards sensor, the higher the intensity. A signal may also **penetrate** a target surface and be scattered inside the target. Reflection, scattering, and penetration of a pulse depend on frequency of pulse, local incident angle, and target parameters such as roughness, shape, orientation, structure, and material.

Roughness is one of the important parameters for tone in a radar image. Large scale roughness, larger than the cell size, determines slopes in the imaged area and is responsible for orientation of slopes affecting local incident angle. In general, smaller local incident angle results in brighter tone in the intensity image. In addition, large scale roughness causes anomalies in tone

like brighter areas which are due to layover or foreshortening and darker areas that appear behind elevated objects.

Roughness inside a cell determines the scattered part of the pulse. Hence, a rough surface is expected to be recorded brighter than a smooth surface of same physical properties. Roughness depends on the wavelength of the pulse (λ), the local incident angle (θ_l), and average height variations (h_{rms}) inside the cell. Peak and Oliver (1971) suggested the following categories of roughness:

A target is considered smooth if:

$$h_{rms} < \lambda / 25 \cos\phi \tag{2.28}$$

A target is considered rough if:

$$h_{rms} > \lambda / 4 \cos\phi \tag{2.29}$$

and any roughness between these values is considered to be intermediate. However, these hard separations only serve as explanation of the concept, in reality roughness is a continuous function of wavelength, local incident angle and height variations in one cell.

Shape, orientation, and texture of objects on the target surface affect the tone in radar images. Linear objects such as a line of trees and a bank of a river oriented parallel to the flight direction form dihedral reflectors and reflect a large part of the signal back to the sensor resulting in a bright area in the SAR image. Corner reflectors as trihedral reflectors facing towards the sensor are seen as very bright points.

Another important parameter determining the tone of a target in a radar image is the dielectric constant. The dielectric constant is a physical property of material relating to electrical conductivity. Natural dry materials have a dielectric constant between 3 and 8. This parameter is 80 for liquid water. Therefore, the dielectric property of targets is controlled by their water content. Higher dielectric values cause higher reflectivity and less penetration. Hence, two similar surfaces may be imaged diversely because of different water content (Henderson and Lewis 1999).

Signal penetration also depends strongly on the wavelength of the pulse. Longer wavelengths penetrate more into target material. Hence, the penetrating signal is scattered by the volume instead of the surface. Volume backscattering is more complex than a surface reflection. Vegetation is a good example for a volume scatterer. Pulses in longer wavelengths, e.g., L-band, may pass through vegetation and meet the earth's surface. In contrast, smaller wavelengths tend to be scattered by the canopy and do not penetrate into the vegetation volume. Hence, the signal is a combination of scattering from canopy, leaves, and the earth's surface having different shapes, sizes, orientations, and water content.

2.1.8 Operating Space Borne SAR Systems

Seasat, the first satellite with a SAR sensor, was launched on 26 June 1978 and operated for 105 days in L-band (23.5 cm). Characteristics of this satellite and other launched satellites with SAR sensors are presented in Table 2.1.

Satellite	Launched	Operated until	Acquisition band	Best Spatial Resolution
Seasat	26.06.1978	10.10.1978	L	25 m
Almaz-T#2, Resurs-R #2	25.07.1987	17.10.1992	S (10cm)	2.5 m
Almaz-T#3, Resurs-R #3	31.03.1991	Operating	S (10cm)	2.5 m
ERS 1	17.07.1991	10.03.2000	C	30 m
JERS-1	11.02.1992	1998	L	18 m
ERS-2	21.04.1995	Operating	C	30 m
RADARSAT-1	04.11.1995	Operating	C	10 m
ENVISAT	01.03.2002	Operating	C	30 m
ALOS	24.01.2006	Operating	L	10 m
TerraSAR-X	15.06.2007	Operating	X	1 m
RADARSAT-2	14.12.2007	Operating	C	10 m
Tandem-X	21.06.2010	Operating	X	1 m

Table 2.1. some important remote sensing satellites carrying SAR sensors.

It is known that C-band signals are scattered by vegetation volume. L-band signals pass mainly through vegetation and therefore are influenced by the earth's surface more than vegetation. Hence, C-band data was the proper choice for this study at the start (2003). ASAR ENVISAT data is provided free of charge by ESA for this research project.

2.2 Classification

Remote sensing data is usually provided as images formed by many pixels, each one representing an area of the observed scene. Each pixel of an image is usually associated with a digital number (DN) representing a measurement from the area covered by the pixel. DNs are usually coded as values such that the measured parameter is properly presented. Range and statistical distribution of DNs of different images are variable depending on sensor, coding system, and scene. Coding of remotely sensed data is often done by up to 16 bit per pixel representing up to more than 65,000 energy levels. Although, coding by more than 16 bits per pixel is possible it is usually not necessary.

An image can also represent spatial information which is provided from other data sources or by interpretation of remote sensing data. Some examples are digital elevation models (DEM), thematic maps, and the normalized difference vegetation index (NDVI).

A combination of multi-source, and/or multi-temporal data is sometimes needed for information extraction from remote sensing data. Such complex multi-dimensional (of many sources, bands, polarizations, channels, dates, etc.) data is usually difficult to be directly used as information for decision support. Classifying a study area in desired categories based on patterns of the complex data set is a solution for many applications.

DNs can be translated to brightness, so the data can be interpreted by humans. However, human interpretation has its limitations. We can analyze only three images presented as color components of one image at a time. The human visual system can recognize a limited number of gray levels and even less levels of color brightness. Therefore, simultaneous visual interpretation of a complex data set from many sources is difficult or even impossible for a human interpreter.

Pattern classification or pattern recognition as a main sub-topic of machine learning deals with this problem. Classification techniques are developed to categorize complex data sets of many measurements according to their statistics and/or relationships. In the case of complex spatial data the aim is to classify the geographical space (pixels) for a limited number of manageable classes. In order to do this, pixel vectors as patterns contain DNs as components. Any pixel vector has one component per feature (e.g., a spectral band) and any feature constructs a dimension of a multi dimensional space called feature space. A feature space provides a room for the representation of a statistical distribution of pixels independent of their spatial distribution. In a classification, a classifier separates the feature space between desired classes, so that any pixel can be labeled according to its location in the feature space (Duda et. al 2000, Bishop 2007).

There are two broad classes of classification procedures according to the learning phase of the classifier. In a supervised classification a classifier is trained by ground truth, so each pixel is assigned to a known class by the classifier. An unsupervised classification tries to group pixel vectors based on their distribution in feature space without any ground truth. In an unsupervised classification, pixels are categorized in clusters which are purely symbolic and not related to land cover yet. Following, clusters can be related to land cover types by visual interpretation, maps, field visits and other data sources. An unsupervised classification can be applied as a fast strategy for emergent conditions (floods, earth quakes, …) or if no prior information is available (inaccessible areas, historical images, …). In addition, it can be used as a base for feature selection, and as a sampling strategy for a supervised classification as well as a support for visual interpretation.

In another categorization, classifiers are known as parametric or non-parametric. A parametric classifier uses statistics of populations (pixels) under the assumption that the distribution of a population fits to a known parameterized distribution (e.g., normal distribution). Non-parametric classifiers do not rely on the assumption that the data is drawn from a given probability distribution.

In case the assumptions of a parametric classification are satisfied, parametric classifiers perform well. However, the accuracy of the classification decreases if the assumptions are violated. Non-parametric classifiers are independent of statistical distributions of the populations. Therefore, they perform well if classes have clear borders independent of the

statistical distribution of the data. In addition, non-parametric methods are not affected by differences in scale of multi-source data. Another advantage of non-parametric classification methods compared to parametric methods is their lower sensitivity to a lack of training samples compared to the size of feature space and number of classes, while performance of parametric methods depends strongly on sample size. For a parametric classifier, training samples should represent the distribution of the population in a multi- or hyper-dimensional feature space. The larger the feature space becomes, the more samples are needed. Non-parametric classifiers try to find borders between classes and if samples are enough to represent borders, any more samples that do not significantly change borders are not necessary (Watanachaturaporn et. al 2008).

In this study, a maximum likelihood classifier (MLC) as a parametric classifier and support vector machines (SVM) as a non-parametric classifier are used for classification and compared to each other. The maximum likelihood classifier is widely used for classification of remote sensing data and can be considered as a standard method in remote sensing. SVM is a relatively new classifier in the field of remote sensing. It has been increasingly used for classification of remote sensing data in the last years due to its good performance for classifying hyper-dimensional, multi-source, and multi-scale data with a small sample size.

Following, definitions and considerations of MLC and SVM are explained.

2.2.1 Bayesian Classification

Bayes' theorem relates the conditional and marginal probabilities of two random events. The two events in classification of remote sensing data are classes (ω_i) and pixel vectors (x) (Richards and JIA Xiuping 1999).

Let M be the number of classes for an image represented by:

$$\omega_i, i = 1,...,M$$

To determine the class to which a pixel at a location x belongs, conditional probability of

$$p(\omega_i \mid x), i = 1,...M$$

are of interest. The position vector x is a column vector of values for the pixel. It describes the pixel as a point in multidimensional feature space with coordinates defined by the values of the pixel in the image. The probability $p(\omega_i \mid x)$ gives the conditional probability that the correct class is ω_i for a pixel at position x. Classification is performed according to:

$$x \in \omega_i \text{ if } p(\omega_i \mid x) > p(\omega_j \mid x) \text{ for all } j \neq i \tag{2.30}$$

A Bayesian classifier needs a parameter estimation for classification. In many applications Maximum Likelihood Estimation (MLE) is used as parameter estimation for the Bayesian classifier. The MLE is a statistical method used to fit a mathematical model to some data. It considers a distribution for a population to estimate probabilities.

The probability of ω_i given x ($p(\omega_i \mid x)$) is defined as:

$$p(\omega_i \mid x) = p(x \mid \omega_i) \times p(\omega_i) / p(x) \tag{2.31}$$

where $p(\omega_i)$ is the probability that class ω_i occurs in the image. The $p(\omega_i)$ are called à priori or prior probabilities and $p(\omega_i \mid x)$ are posterior probabilities. $p(x)$ is the probability of finding a pixel from any class at location x. Since $p(x)$ is equal for any class ω_i, the classification rule (2.30) becomes:

$$x \in \omega_i \text{ if } p(x \mid \omega_i) p(\omega_i) > p(x \mid \omega_j) p(\omega_j) \text{ for all } j \neq i \tag{2.32}$$

$p(x \mid \omega_i)$ are known from training data and $p(\omega_i)$ can be estimated from the analyst's knowledge. Discriminate functions ($g_i(x)$) are defined from equation 2.32 as:

$$g_i(x) = \ln\{p(x \mid \omega_i) p(\omega_i)\} = \ln p(x \mid \omega_i) + \ln p(\omega_i) \tag{2.33}$$

In the case that prior probabilities are unknown, the prior probability of all classes may be considered as equal. Hence, the discriminate function depends only on $p(x \mid \omega_i)$. The vector x belongs then to the class ω_i, where $p(x \mid \omega_i)$ is higher than for any other class.

A special case of Bayesian classification that uses Maximum Likelihood estimation with Gaussian distribution is referred as Maximum Likelihood classifier (MLC) by some authors in the field of pattern classification and remote sensing (Duda et al. 2000, Richards and JIA Xiuping 1999).

2.2.1.1 Normal Class Models

The normal distribution, also known as Gaussian distribution, is one of the most used statistical distribution models by parametric classifications.

In this case MLE considers the distribution of the investigated population (e.g., pixels of an image) as normal distributed and calculates $p(x \mid \omega_i)$ for each pixel vector of an image.

The class conditional property $p(x \mid \omega_i)$ in the case of a one dimensional feature space is described by:

$$p(x \mid \omega_i) = (2\pi)^{-1/2} \sigma_i^{-1} \exp\left\{ -\frac{1}{2}(x - m_i)^2 / \sigma_i^2 \right\} \tag{2.34}$$

In which x is a single dimensional variable, and m_i and σ_i are expectation value and standard deviation of class ω_i. σ_i^2, called variance of the distribution, is described by:

$$\sigma_i^2 = \frac{1}{q_i - 1} \sum_{j=1}^{q_i} (x_j - m_i)^2 \tag{2.35}$$

Where q_i is the number of pixels in class ω_i. If the feature space is multi-dimensional, x and m_i are vectors and the variance is replaced by the covariance matrix $\sum_i$ taking into account not only multi-dimensionality of feature space but also the effect of correlation between features. The covariance matrix is defined by:

$$\sum_i = \frac{1}{q_i - 1} \sum_{j=1}^{q_i} \left\{ (x_j - m_i)(x_j - m_i)^t \right\} \tag{2.36}$$

Where x_j is the jth sample, m_i mean vector of population, and superscript "t" is the vector transpose operation. All vectors x_j and m_i have one element for each feature of the multi-dimensional feature space. Equation 2.34. can be recast as:

$$p(x \mid \omega_i) = (2\pi)^{-N/2} \mid \sum_i \mid^{-1/2} \exp\left\{ -\frac{1}{2}(x - m_i)^t \sum_i^{-1} (x - m_i) \right\} \quad (2.37)$$

Where x is the pixel vector, $|\sum_i|$ is the determinant of the covariance matrix, and N is the number of dimensions in feature space. The term $(2\pi)^{-N/2}$ is common to all $g_i(x)$ and can be ignored in the discriminant function for Maximum Likelihood.

$$g_i(x) = \ln p(\omega_i) - \frac{1}{2} \ln \mid \sum_i \mid - \frac{1}{2}(x - m_i)^t \sum_i^{-1} (x - m_i) \quad (2.38)$$

2.2.2 Support Vector Machines (SVM)

Support vector machines (SVM) are a set of related supervised learning methods used for classification. A special property of SVM is that they simultaneously minimize the classification error and maximize the margin between classes.

SVM are binary classifiers which construct one linear hyperplane supported by marginal data vectors for each class such that the hyperplanes of two classes are parallel. A separating hyperplane between two marginal hyperplanes divides the data into two classes. Classes are often too complex to be separated by a linear hyperplane in feature space. Hence, input vectors are mapped to a higher dimensional space where a maximal separating hyperplane is constructed. The separating hyperplane is the hyperplane that maximizes the distance between the two marginal hyperplanes. An assumption is made that the larger the margin or distance between these parallel hyperplanes becomes, the better the generalization error of the classifier will be. Although, SVM were first investigated in the late seventies (Vapnik 1979), they have been receiving increasing attention in remote sensing since the late nineties (Burges 1998, Waske and Schiefer 2006).

SVM as a new classifier in the field of remote sensing is investigated in this study for classification of multi-temporal SAR data. Hence, the definition of SVM is discussed in this

section. Following, parts of the article of Cortes and Vapnik (1995) are used with a little change to explain SVM classification basics.

2.2.2.1 Optimal Hyperplanes

In this section, we review the method of optimal hyperplanes (Vapnik, 1982) for separation of training data without errors. In the next section we introduce a notion of soft margins, which will allow for an analytic treatment of learning with errors on the training set.

The set of labeled training patterns

$$(y_1, x_1), \ldots, (y_\ell, x_\ell), \qquad y_i \in \{-1, +1\} \tag{2.39}$$

is said to be linearly separable if there exists a vector w and a scalar b such that the inequalities

$$w.x_i + b \geq 1 \quad \text{if} \quad y_i = 1$$

$$w.x_i + b \leq -1 \quad \text{if} \quad y_i = -1 \tag{2.40}$$

are valid for all elements of the training set (2.39). Below we write the inequalities (2.40) in the form:

$$y_i.(w.x_i + b) \geq 1 \qquad i = 1, \ldots, \ell \tag{2.41}$$

The optimal hyperplane

$$w_0.x + b_0 = 0 \tag{2.42}$$

is the unique one which separates the training data with a maximal margin: it determines the direction w/|w| where the distance between the projections of the training vectors of two different classes is maximal, this distance $\rho(w,b)$ is given by:

$$\rho(w,b) = \min_{\{x:y=1\}} \frac{x.w+b}{|w|} - \max_{\{x:y=-1\}} \frac{x.w+b}{|w|} \tag{2.43}$$

The terms: $\min_{\{x:y=1\}} x.w+b = 1$ and $\max_{\{x:y=-1\}} x.w+b = -1$ are the results of (2.41) for support vectors of the classes $y_i = +1$ and $y_i = -1$. The scalar b can be eliminated in (2.43).

The optimal hyperplane (w_0, b_0) is the argument that maximizes the distance (2.43). It follows from (2.43) and (2.41) that:

$$\rho(w_0, b_0) = \frac{2}{|w_0|} = \frac{2}{\sqrt{w_0.w_0}} \tag{2.44}$$

This means that the optimal hyperplane is the unique one that minimizes w.w under the constraints (2.41).

Vectors x_i for which $y_i.(w.x_i + b) = 1$ will be termed **support vectors**. We show that the vector w_0 that determines the optimal hyperplane can be written as a linear combination of training vectors:

$$w_0 = \sum_{1}^{l} y_i.\alpha_i^0 x_i \tag{2.45}$$

where $\alpha_i^0 \geq 0$.

We construct a Lagrangian

$$L(w,b,\Lambda) = \frac{1}{2} w.w - \sum_{i=1}^{l} \left(\alpha_i^0.[y_i(x_i.w+b) - 1]\right), \tag{2.46}$$

where $\Lambda^t = (\alpha_1,...,\alpha_l)$ is the vector of non-negative Lagrange multipliers corresponding to the constraints (2.41).

At the point of the minimum (with respect to w and b) one obtains:

$$\left.\frac{\partial L(w,b,\Lambda)}{\partial w}\right|_{w=w_0} = \left(w_0 - \sum_{i=1}^{l} \alpha_i^0 . y_i . x_i \right) = 0 , \tag{2.47}$$

$$\left.\frac{\partial L(w,b,\Lambda)}{\partial b}\right|_{b=b_0} = \begin{pmatrix} \sum \alpha_i^0 . y_i \\ \alpha_l \end{pmatrix} = 0 , \tag{2.48}$$

From equality (2.47) we derive:

$$w_0 = \sum_{i=1}^{\ell} \alpha_i^0 . y_i . x_i , \tag{2.49}$$

which expresses, that the optimal hyperplane solution can be written as a linear combination of training vectors. Note, that only training vectors x_i, with $\alpha_i > 0$ have an effective contribution to the sum (2.49). Hence, $\alpha_i > 0$ for support vectors.

We also show that to find the vector of parameters α_i:

$$\Lambda_0^T = (\alpha_1^0, ..., \alpha_\ell^0), \tag{2.50}$$

one has to solve the following quadratic programming problem:

$$W(\Lambda) = \Lambda^T \mathrm{I} - \frac{1}{2} \Lambda^T D \Lambda \tag{2.51}$$

with respect to $\Lambda_0^T = (\alpha_1^0, ..., \alpha_\ell^0),$ subject to the constraints:

$$\begin{aligned} &\Lambda \geq 0, \\ &\Lambda^T Y = 0, \end{aligned} \tag{2.52}$$

where $I^T = (1,...,1)$ is an $\ell-$dimensional unit vector, $Y^T = (y_1,...,y_\ell)$ is the $\ell-$dimensional vector of labels, and D is a symmetric $\ell \times \ell-$matrix with elements

$$D_{ij} = y_i y_j x_i . x_j, \qquad i, j = 1,..., l \tag{2.53}$$

The inequality of (2.52) describes the nonnegative quadrant ($\Lambda \geq 0$). We therefore have to maximize the quadratic form (2.51) in the nonnegative quadrant, subject to the constraints (2.52).

When the training data (2.39) can be separated without errors, the maximum of the functional (2.51) is related to the pair (Λ_0, b_0), and the maximal margin ρ_0 from (2.44):

$$W(\Lambda_0) = \frac{2}{\rho_0^2}, \tag{2.54}$$

If for some Λ_* and large constant W_0 the inequality

$$W(\Lambda_*) > W_0 \tag{2.55}$$

is valid, one can accordingly assert that all hyperplanes that separate the training data (2.39) have a margin

$$\rho < \sqrt{\frac{2}{W_0}} \tag{2.56}$$

If the training set (2.39) cannot be separated by a hyperplane, the margin between patterns of the two classes becomes arbitrarily small, resulting in the value of the functional $W(\Lambda)$ turning arbitrary large. Maximizing the functional (2.51) under constraints (2.52) one therefore reaches a maximum (in this case one has constructed the hyperplane with the maximal margin ρ_0), or one finds that the maximum exceeds some given large constant W_0 (in which case a separation of the training data with a margin larger than $\sqrt{2/W_0}$ is impossible).

2.2.2.2 The Soft Margin Hyperplane

Consider the case where the training data cannot be separated without errors. In this case one may want to separate the training set with a minimal number of errors. To express this formally let us introduce some non-negative variables $\xi_i \geq 0,\ i = 1,...,l$.

We can now minimize the functional

$$\phi(\xi) = \sum_{i=1}^{\ell} \xi_i^{\sigma} \tag{2.57}$$

for small $\sigma > 0$, subject to the constraints

$$y_i (w.x_i + b) \geq 1 - \xi_i , \qquad i = 1,..., \ell ,$$

$$\xi_i \geq 0 , \qquad i = 1,..., \ell , \tag{2.58}$$

For sufficiently small σ , the functional (2.57) describes the number of the training errors. Minimizing (2.57) one finds some minimal subset of training errors:

$$(y_{i_1}, x_{i_1}),...,(y_{i_k}, x_{i_k}) .$$

If this data is excluded from the training set one can separate the remaining part of the training set without errors. To separate the training part of the training data one can construct an optimal separating hyperplane.

This idea can be expressed formally as: minimize the functional

$$\frac{1}{2} w^2 + CF\left(\sum_{i=1}^{\ell} \xi_i^{\sigma} \right) \tag{2.59}$$

subject to constraints (2.58), where $F(u)$ is a monotonic convex function and C is a constant.

For sufficiently large C and sufficiently small σ, the vector w_0 and constant b_0, that minimize the functional (2.59) under constraints (2.58), determine the hyperplane that minimizes the number of errors on the training set and separate the rest of the elements with maximal margin.

Note, however, that the problem of constructing a hyperplane which minimizes the number of errors on the training set is in general NP-complete (NP = nondeterministic polynomial time, a problem that needs an unreasonable amount of process time to be solved). To avoid NP-completeness of our problem we will consider the case $\sigma = 1$ (the smallest value of σ for which the optimization problem (2.51) has a unique solution). In this case the functional (2.59) describes (for sufficiently large C) the problem of constructing a separating hyperplane which minimizes the sum of deviations, ξ, of training errors and maximizes the margin for the correctly classified vectors. If the training data can be separated without errors the constructed hyperplane coincides with the optimal margin hyperplane.

In contrast to the case with $\sigma < 1$ there exists an efficient method for finding the solution of (2.59) in the case of $\sigma = 1$. Let us call this solution **the soft margin hyperplane**.

Therefore, we consider the problem of minimizing the functional

$$\frac{1}{2}w^2 + CF\left(\sum_{i=1}^{\ell}\xi_i\right) \tag{2.60}$$

subject to the constraints (2.58), where $F(u)$ is a monotonic convex function with $F(0) = 0$. To simplify the formulas we only describe the case of $F(u) = u^2$ in this section. For this function the optimization problem remains a quadratic programming problem.

We showed that the vector w, can be written as a linear combination of support vectors x_i:

$$w_0 = \sum_{i=1}^{\ell}\alpha_i^0 . y_i . x_i \ .$$

To find the vector $\Lambda^T = (\alpha_1, ..., \alpha_\ell)$ one has to solve the dual quadratic programming problem of maximizing

$$W(\Lambda,\delta) = \Lambda^T \mathrm{I} - \frac{1}{2}\left[\Lambda^T D\Lambda + \frac{\delta^2}{C}\right] \tag{2.61}$$

Subject to constraints

$$\begin{aligned} &\Lambda^T Y = 0, \\ &\delta \geq 0, \\ &0 \leq \Lambda \leq \delta \mathrm{I}, \end{aligned} \tag{2.62}$$

where I, Λ, Y, and D are the same elements as used in the optimization problem for constructing an optimal hyperplane, δ is scalar, and (2.62) describes coordinate-wise inequalities.

Note, that (2.62) implies that the smallest admissible value δ in functional (2.61) is

$$\delta = \alpha_{\max} = \max(\alpha_1,...,\alpha_\ell).$$

Therefore, to find a soft margin classifier one has to find a vector Λ that maximizes

$$W(\Lambda) = \Lambda^T \mathrm{I} - \frac{1}{2}\left[\Lambda^T D\Lambda + \frac{\alpha_{\max}^2}{C}\right] \tag{2.63}$$

under the constraints $\Lambda \geq 0$ and $\Lambda^T Y = 0$. This problem differs from the problem of constructing an optimal margin classifier only by the additional term with $\alpha_{\max}$ in the functional (2.63). Due to this term the solution to the problem of constructing the soft margin classifier is unique and exists for any data set.

The functional (2.63) is not quadratic because of the term with $\alpha_{\max}$. Maximizing (2.63) subject to the constraints $\Lambda \geq 0$ and $\Lambda^T Y = 0$ belongs to the group of so-called convex programming problems. Therefore, to construct a soft margin classifier one can either solve the convex programming problem in the ℓ-dimensional space of parameters Λ, or one can solve the quadratic programming problem in the dual $\ell+1$ space of the parameters Λ and δ.

2.2.2.3 The Method of Convolution of the Dot-Product in Feature Space

The algorithms described in the previous sections construct hyperplanes in the input space. To construct a hyperplane in a feature space one first has to transform the n-dimensional input vector x into an N-dimensional feature vector through a choice of an N-dimensional vector function ϕ:

$$\phi : \Re^n \rightarrow \Re^N$$

An N-dimensional linear separator w and a bias b is then constructed for the set of transformed vectors

$$\phi(x_i) = \phi_i(x_i), \phi_2(x_i), ..., \phi_N(x_i), \qquad i = 1, ..., \ell$$

Classification of an unknown vector x is done by first transforming the vector to the separating space $(x \mapsto \phi(x))$ and then taking the sign of the function

$$f(x) = w.\phi(x) + b \,. \tag{2.64}$$

According to the properties of the soft margin classifier method the vector w can be written as a linear combination of support vectors (in the feature space). That means

$$w = \sum_{i=1}^{\ell} y_i \alpha_i \phi(x_i) \tag{2.65}$$

The linearity of the dot-product implies, that the classification function f in (2.64) for an unknown vector x only depends on the dot-products:

$$f(x) = \phi(x).w + b = \sum_{i=1}^{l} y_i \alpha_i \phi(x).\phi(x_i) + b \tag{2.66}$$

The idea of constructing support vector networks comes from considering general forms of the dot-product in a Hilbert space (Anderson, Bahadur 1966):

$$\phi(u).\phi(v) \equiv K(u,v) \tag{2.67}$$

According to the Hilbert-Schmidt theory (Courant, Hilbert 1953) any symmetric function $K(u,v)$, with $K(u,v) \in L_2$, can be expanded in the form

$$K(u,v) = \sum_{i=1}^{\infty} \lambda_i \phi_i(u).\phi_i(v) \tag{2.68}$$

where $\lambda_i \in \Re$ and ϕ_i are eigenvalues and eigenfunctions

$$\int K(u,v)\phi_i(u)d(u) = \lambda_i \phi_i(v)$$

of the integral operator defined by the kernel K(u, v). A sufficient condition to ensure that (2.67) defines a dot-product in a feature space is that all the eigenvalues in the expansion (2.68) are positive. To guarantee that these coefficients are positive, it is necessary and sufficient (Mercer's theorem[1]) that the condition

$$\iint K(u,v)g(u)g(v)dudv > 0$$

is satisfied for all g such that

$$\int g^2(u)du < \infty \,. \tag{2.69}$$

Functions that satisfy Mercer's theorem can therefore be used as dot-products. Aizerman et al (1964) consider a convolution of the dot-product in the feature space given by a function of the form

$$K(u,v) = \exp\left(-\frac{|u-v|}{\sigma}\right), \tag{2.70}$$

which they call Potential functions.

However, the convolution of the dot-product in feature space can be given by any function satisfying Mercer's condition; in particular, to construct a polynomial classifier of degree d in n-dimensional input space one can use the following function.

[1] In mathematics, specifically functional analysis, Mercer's theorem is a representation of a symmetric positive-definite function on a square as a sum of a convergent sequence of product functions (Mercer 1909)

$$K(u,v) = (u.v + 1)^d . \qquad (2.71)$$

Using different dot-products K(u, v) one can construct different learning machines with arbitrary types of decision surfaces (Boser 1992). The decision surface of these machines has a form

$$f(x) = \sum_{i=1}^{\ell} y_i \alpha_i K(x, x_i),$$

where x_i is the image of a support vector in input space and α_i is the weight of a support vector in the feature space.

To find the vectors x_i and weights α_i one follows the same solution scheme as for the original optimal margin classifier or soft margin classifier. The only difference is that instead of matrix D (determined by (2.53)) one uses the matrix

$$D_{i,j} = y_i y_j K(x_i, x_j), \qquad i, j = 1,...,l.$$

The function K is called kernel function.

Some well-known kernel functions are listed in Table 2.1.

Kernel function	Definition	Parameters
Linear	$x.x_i$	
Polynomial	$(x.x_i + 1)^d$	d is polynomial degree positive integer
Radial Basis	$\exp\left(-\gamma . \| x - x_i \|^2\right)$	γ is the spread of Gausian kernel
Sigmoid	$\tanh(\kappa(x.x_i) + r)$	κ and r are user defined values

Table 2.1. Some well known kernel functions.

2.2.2.4 SVM Parameters

SVM are binary classifiers, developed to perform binary classification. However, multiclass classification is more important in remote sensing. A number of methods have been proposed to create multiclass SVM from binary counterparts. Two popular simple methods are one against all (OAA) and one against one (OAO).

The OAA strategy classifies each class against all other classes. For an M class classification, M binary SVM classifiers are created. Each class is trained to discriminate one class from the remaining classes.

The OAO strategy creates SVM classifiers for all possible pairs of classes. For an M class classification, M(M-1)/2 binary classifiers are created. Each classifier labels data as two classes. Finally, the class label that occurs most frequently is assigned to that data. A tie-breaking strategy is needed in case of a tie. Random selection of one of the tied classes is a common solution.

SVM includes a penalty parameter (C) that allows a certain degree of misclassification which is particularly important for non-separable training sets. The penalty parameter controls the trade-off between allowing training errors and forcing rigid margins. It creates a soft margin that permits some misclassifications, such that it allows some training points on the wrong side of the hyperplane. Increasing the value of the penalty parameter increases the cost of misclassifying points and forces the creation of a more accurate model that may not generalize well. A lower penalty parameter allows more misclassification of the training data and results in a smoother hyperplane. Since the accuracy of the classification is usually evaluated using control samples which are not included in the training phase, the penalty parameter must be set so that the misclassification of control samples is minimized. A large value of c might cause an overfitting to the training data.

All kernel types except linear kernels have user defined parameters which influence the hardness of the separating hyperplane. The softer the hyperplane, the better the hyperplane is fitted to the training data. A too soft hyperplane may cause overfitting to training data and poor generalization.

Hence, an optimal trade-off between generalization and error minimization maximizes the accuracy of classification using a kernel function. This optimal trade-off should usually be

found by trying different values. Some softwares include a 2-dimentional grid search that optimizes generalization and penalty parameters.

2.3 Summary

Basic information that is necessary for the implementation and understanding of the study and the investigations of this thesis is provided in this chapter. The subchapter radar imaging starts from the general function of radar systems and continues explaining side looking radar. A radar imaging system emits narrow pulses perpendicular to the flight direction of the platform and receives the backscattered signals. The delay time of backscatters is transformed to the distance from the sensor. The intensity of backscatters depends on the target object and the local incident angle. Synthetic aperture radar is an advanced imaging radar system that simulates each pulse of a huge antenna by thousands of pulses of a small antenna. It enables imaging space borne radar remote sensing.

Following, classification of remotely sensed data is discussed. A classifier categorizes the data (e.g., pixels of an image) into a few classes that are easier to understand and to present. Classifiers are usually categorized as parametric or non-parametric. Parametric classifiers use statistics of data and fit it to a known distribution (e.g., normal distribution) for classification. In contrast, non-parametric classifiers are related to non-parametric statistics, whose interpretation does not depend on the population fitting of any parameterized distributions.

The Maximum likelihood classifier (MLC) that is vastly used for classification of remotely sensed data has been explained in this Chapter. MLC fits the data to a normal distribution using mean and covariance matrices of classes from training data. Despite this simple concept MLC performed very well for classification of remotely sensed data. Thus, it is often accepted as a standard method to be compared with other classifiers as well as for the production of land cover maps.

Support vector machines (SVM) are non parametric classifiers. The concept was proposed in the 1970s. It has gained increasing attention in the field of remote sensing over the last 10 years. Some researchers reported that SVM outperform other classifiers especially if a large

number of variables (e.g., bands of hyperspectral data or dates of multi-temporal data) is available. SVM are used in this study to investigate their performance for classification of multi temporal radar data.

Chapter 3

3 State of the Art in Classification of Multi-temporal SAR Data

This Chapter reviews the research that has taken place in the field of agricultural monitoring using radar data. This review is based on published literature and tries to explain the up-to-date state of technique in this field and related fields of the study.

Since the successful launch of the European remote sensing satellites ERS-1, ERS-2 and ENVISAT, SAR images of the earth's surface are regularly acquired. Also the Canadian satellites Radarsat and the German satellites TerraSAR-X and TanDEM-X provide SAR data. In the framework of the IACS (integrated administrative and control system) initiated by the European Union, apart from optical satellite data, radar data are increasingly used for monitoring in member countries. Beside visual interpretations of multi-temporal SAR images, this data represents the basis of various application-oriented researchers in the field of the agricultural monitoring with SAR.

An approach for radar data classification procedures is the so-called “optical way of the classification“. It means that classification procedures, which were applied to images of optical

sensors, are applied to radar images. The multi-spectral channels are replaced by different polarisations, channels, and/or multi-temporal SAR data.

In the following, techniques that have been applied in the field of agricultural monitoring using SAR data are reviewed.

3.1 Observation of Temporal Changes on Radar data

The well-known effect of plants on radar signals is visible on SAR images especially in C- and X- bands (Figure 3.1). Backscattering of plants depends strongly on their physical properties. Density, height, water content, shape, direction of components (leaves and branches), and direction of plantation define how the plants influence backscattering of the SAR signal from a field. These characteristics (except direction of plantation) change in the course of time due to the growth phases of plants and cultivation activities. Therefore, the appearance of the field on SAR images changes as the plants grow, dry or are harvested. These variations are periodical and predictable for many crops if natural phenomena or farmers' decisions do not change them.

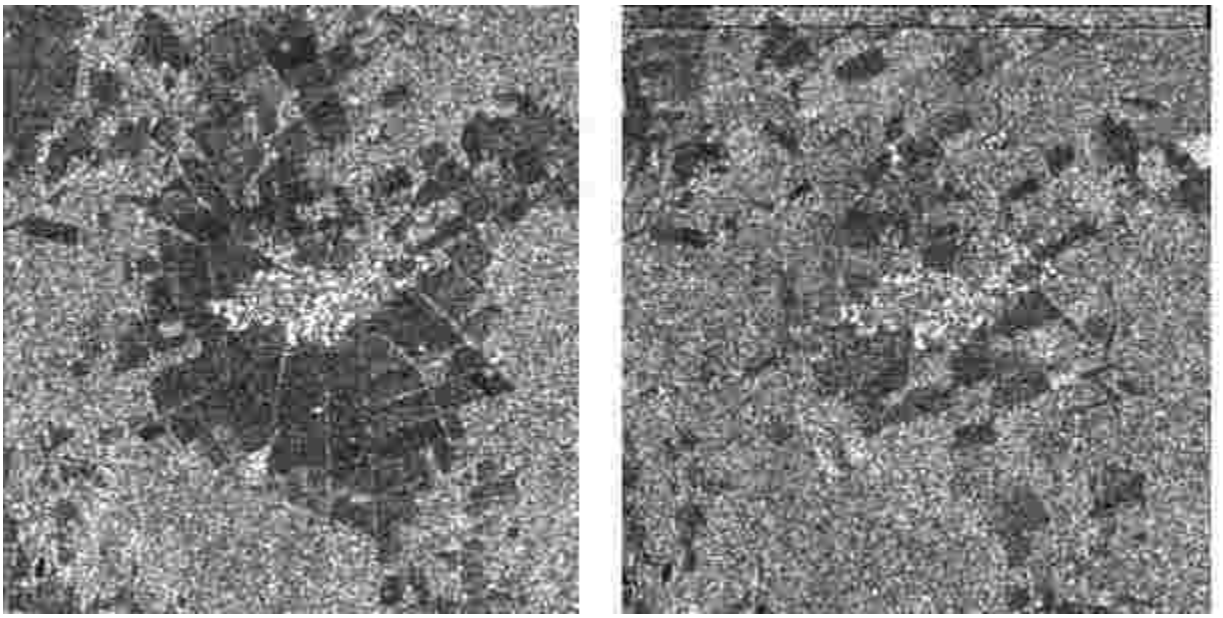

a b

Figure 3.1. ASAR ENVISAT images taken in March (a) and June (b) 2004 from the town Fuhrberg and surrounding agricultural area.

Different plants differ in their structure (surface properties) and in their growth process (phenology) which is recorded in SAR images. This is the basis of distinction of the types of crops in a multi-temporal classification (Del Frate et al. 2003, Hochschild et al. 2005, Tavakkoli Sabour et al. 2007, Karjalainen et al. 2008).

An experiment (Lohmann et al. 2005) indicated that only about 35% to 45% of training samples are correctly classified for crops if two SAR images acquired simultaneously of different polarizations (VV and VH) are classified. Accuracy of classification using single date images showed a high dependency on the acquisition date. Each crop can be classified pretty accurately at specific dates, like rape in April, peas and strawberries in May, weeds in September, and sugar beets in October. This indicates that the success of a classification for each class depends on the season, when the image has been taken. This is due to the known fact of plant phenology (Schneider 1994), which is highly seasonal dependent. In the same test (Lohmann et al. 2005) almost 100% of the same training samples are correctly classified as 24 multi-temporal images from 12 dates (one VV and one VH each date) are used. This comparison (among others) states the potential of multi-temporal SAR data versus single acquisitions for crop monitoring. In another attempt, Bruzzone et al. (2004) extracted two features from multi-temporal SAR images. These two features were “temporal variability of backscattering” and “long-term coherence”. It is shown that classification of these two extracted features was more accurate than classification of original raw data between four classes (forest, urban, water, agricultural fields). The experience of Seynat and Hobbs (1998) with a similar technique confirms these results.

These samples, among others, show the benefit of temporal changes of plants for crop classification, which is due to the growth and cultivation activities and influences SAR images.

3.2 Feature Selection According to the Date of Data Acquisition

A wide range of data sources are available for geospatial analysis. Maps, statistics, elevation models, and especially remote sensing data from different sensors and platforms can be often acquired. This large variety of data sources provides solutions for many problems.

Therefore, a feature selection strategy is required to find the optimal data combination for a problem. Many combinations of SAR and optical data have been tested for classification of agricultural fields. Considering the approach of this thesis, we focus on feature selection for multi-temporal data.

The choice of suitable images used for crop discrimination depends on the dates of image acquisition because the growing phase at which crop types could be identified were found to be crop dependent (Schotten et al., 1995). Most crop types were mixed up before August and the largest separability was observed between mid-May and mid-July using ERS data over the Flevoland site, while most crops grew. In western Canada, images acquired in July were superior to the other acquisition dates in correctly classifying the crop types in both the optical and microwave regions (Brisco and Brown 1995). Moreover, only one optical image combined with multi-temporal SAR data provided acceptable accuracies for the classification of 4 different crop types. Based on a single TM scene acquired in May and combined with 6-m resolution airborne radar images acquired on 4 different dates, an overall accuracy of 87% correct classification was achieved. By selecting the most appropriate ERS images observing temporal profiles of 5 crop types, Ban and Howarth (1999) could achieve an accuracy of 88.5% by a sequential masking method (Blaes et al. 2005).

Another test on the Flevoland test site using 70 ERS SAR images showed the capability of multi-temporal SAR data for crop classification. It is also shown that rainfall and frost affect SAR images and classification (Saich and Borgeaud 1999). Freezing conditions diminished the amount of power scattered back to the radar by about 7dB. This is because of decrease in dielectric constant as the soil freezes. On the other hand, rainfall increases the brightness on some dates but has no or little effect on some other dates. Since a fraction of the rain will be intercepted by the vegetation canopy and the remainder passes through to the ground surface, the influence of rainfall on radar image depends on the relative importance of vegetation and soil in determining the total backscattered power.

Yakam-Simen et al. (1998) used time-series of RADARSAT to recognize crops in fall and winter, when the croplands are without vegetation. The aim is successfully reached using a time-series approach, but there are limitations for spring-summer crops.

Hochschild et al. (2005) classified crops using multi-source-multi-temporal data. IRS-Pan, ETM+, and ASAR ESA and ENVIAST were used. Grain types could not be separated in a pixel based classification.

Karjalainen et al. (2008) used 12 calibrated multi-temporal ENVISAT SAR images (VV, VH) for supervised classification of crops in a relatively large area in Finland and could classify crops successfully. A classification using multi regression of local parameters and backscattering coefficient was too inaccurate, but it could be shown that more complex models become slightly more accurate.

3.3 Classifiers

A classifier is required for pattern classification as a sub-topic of machine learning. Different classifiers handle the data in diverse manners. Based on data distribution, size of feature space, sample size, and target classes, one or more classifiers are usually suitable. Many researchers compared classifiers for classification of remote sensing data for crop monitoring.

Bruzzone et al. (2004) compared two classifiers: a hierarchical thresholding and a neural network classifier. It is shown that the neural network classifier performed better than the hierarchical thresholding classifier if temporal variability of backscattering and long-term coherence of multi-temporal SAR data are classified. Hierarchical thresholding was more accurate with raw data. The best results were achieved using neural network and the two extracted temporal components, since the progressive changes of vegetation is exaggerated and irrelevant data suppressed.

Brenning et al. (2006) compared six non-parametric classifiers for multi-temporal classification of SAR data: support vector machines (SVM), stabilized linear discriminant analysis (SLDA), logistic discrimination, Bagging, double Bagging, and K-nearest neighbor (KNN) (k=1, 9, 25). All classifiers except logistic discrimination yield similar results with about 80% accuracy in the field level classification. Logistic discrimination classifier classified only about 70% of fields correctly. SVM performed best on pixel level and SLDA classifier on field level.

Camps-Valls et al. (2008) have introduced a general methodological framework based on composite kernels for multi-temporal classification of remote sensing images that simultaneously takes the spectral, spatial, and multi-sensor information into account. They reported that the method provides an alternative to stacking features for exploiting heterogeneous data sources and treats the nonlinear relationship among pixels (and among features) at different time instants with tunable flexibility.

These reports among others confirm that performance of different classifiers depends on the data, classes and strategy of classification. Therefore, selection of the proper classifier is an essential duty for classification of a multi-temporal data set.

3.4 Influence of Polarization, Frequency, and Resolution on classification

Limitations of using single polarization (VV) and single frequency (C-band) SAR data for crop identification were mentioned by Ferrazzoli et al. (1999). As possible solution, two test sites characterized by very large fields were studied by multi-polarimetric and multi-frequency data. For these classifications, 9 classes were defined on the basis of geometrical differences among crop types, leading to different polarimetric signatures. It was demonstrated that, for each class, there were some combinations of frequencies and polarizations that produced significant separability between classes. This approach obtained a high accuracy level of 90% for airborne SAR data. For landscapes with large crop fields, the classification accuracy was improved from 55% to 85% based on 7 crop classes using images in VV, HH and HV instead of the single VV polarization (Del Frate et al. 2003). Using a single dual polarized image, the classification accuracy was also quite high at 86%. These Alternating Polarization (AP) images provided by the ASAR sensor with high temporal revisiting capability should improve the classification performance. Finally, several experiments have shown that the low spatial resolution of a SAR based approach is a limiting factor for crop discrimination (Bouman and Uenk 1992) and the single band imagery is another limitation (Foody et al. 1994).

3.5 Combination of Results

Sometimes, different classes can be classified by diverse data sets. For example, each crop can be classified best using images that are taken in its growth period. Therefore, different classes are classified by independent classifications of separate data sets. In order to represent results as a map, a decision rule is needed if a pixel is classified as different classes by independent classifications. A parameter is usually used as discriminant parameter. Chen (2008) decided based on confidence of each pixel in different classification procedures. This approach examines the posterior probability of the maximum-Likelihood classifier or inverse-distance weight for the distance based classifier for each pixel.

3.6 Summary

Multi-temporal classification of SAR data is investigated by researchers from different aspects. Temporal feature selection proper to the plants phenology is known to be the most important issue in the field of multi-temporal classification. Different classifiers are used for classification of multi-temporal data. Accuracy of classification depends usually not on only one factor. A proper combination of data set, classifier and data representation is often more important than a single factor such as classifier or feature selection. For example, one classifier performs well in pixel based classification another one with segment based classification of the same data. Some classifiers are improved by proper feature selection, whereas others are not significantly influenced by feature selection.

It can be said, that the results of investigations represent the factors of classification for the used data, in desired area and classes. Therefore, investigations are necessary for other areas, data and target classes.

Chapter 4

4 Data, Method, and Evaluation

This Chapter introduces the data sets, processing methods, and test design of this study. The data consists of SAR images, orthophotos, maps, and ground truth. Data sources and properties are described in the subchapter “Data”. Agricultural classes that exist in the study area and target classes that must be classified are explained. Following thereafter, data analyses which are used to prepare data for multi-temporal classification are explained.

The section test design represents discrimination parameters and sample sizes for the evaluation of the applied classification methods. An evaluation parameter should be able to compare results of different methods and help to decide if two methods differ from each other and if one outperforms the other. The training sample size is important for classification accuracy: a larger sample size results usually in higher accuracy. Also, a minimum number of samples is required for a reliable accuracy assessment. On the other hand, acquisition of samples is often expensive so it must be minimized to reduce the costs.

4.1 Data

This subchapter is partitioned under titles: images, and ground truth to describe the utilized data. ENVISAT SAR images are classified for crop monitoring. Orthophotos, available as digital images, serve as geometric reference and for field mapping as a starting point for the sample acquisition strategy. Ground truth is necessary for training and quality assessment.

4.1.1 Images

Available images consist of orthophotos and ENVISAT ASAR images. Orthophotos are orthorectified airborne true-color photos from the year 2003 provided by LGN (Landesvermessung + Geobasisinformation Niedersachsen). The pixel size of the orthophotos is 40 cm that is reduced to one meter in order to decrease computational load. Orthophotos are used as geometric reference in this study.

Image Swath	Swath With (km)	Distance from Nadir (km)	Incidence Angle Range (°)
IS1	104.8	187.2 - 292.0	15.0 - 22.9
IS2	104.8	242.0 - 346.9	19.2 - 26.7
IS3	81.5	337.2 - 418.7	26.0 - 31.4
IS4	88.1	412.0 - 500.1	31.0 - 36.3
IS5	64.2	490.4 - 554.6	35.8 - 39.4
IS6	70.1	549.7 - 619.8	39.1 - 42.8
IS7	56.5	614.7 - 671.1	42.5 - 45.2

Table 4.1 Specifications for ASAR image mode swath (for satellite altitude of 786.18 km) (ESA 1998).

ASAR images are APP (alternating polarization mode precision image) level 1 of ENVISAT. This is a multi-look, ground-range, digital image of level 0 AP product and the most up to date auxiliary information available at the time of processing (ESA 2002). Engineering corrections

and relative calibration (antenna elevation gain, range spreading loss) are applied. The data of each acquisition contains two co-registered images of polarization combination VV and VH. In addition, absolute (external) calibration parameters are provided in the product annotation. Data acquisition in APP mode is possible in seven swaths. Table 4.1 represents the specifications of the seven swaths. Images of swaths IS5, IS6, and IS7 are used in this study. These swaths have the largest incidence angle; hence the signal travels longer through plants. Therefore, data of swaths with larger incident angle are expected to be more influenced by vegetation.

The coverage of each image of this study is 100 km in along track and 56.5 to 64.2 km in across track. Geometric resolution is about 25-28 meters in range and azimuth whereas the pixel size is 12.5×12.5 meters (ESA 2002).

Images were provided free of charge by ESA within an ENVISAT pilot project “AO335”. 22 images taken on 11 dates between December 2003 and November 2004 were utilized. All the images were acquired in descending direction at approximately 9:30 local time. These images are processed to recognize crop types cultivated in the year 2004 (see Table 4.2).

Nr.	Image Date	Inspection Date	Swath
1	17.11.2003	26.11.2003	IS6
2	17.03.2004	19.03.2004	IS 7
3	05.04.2004	05.04.2004	IS 6
4	21.04.2004	21.04.2004	IS 7
5	10.05.2004	10.05.2004	IS 6
6	26.05.2004	10.05.2004	IS 7
7	30.06.2004	14.06.2004	IS 7
8	07.08.2004	07.08.2004	IS 5
9	11.09.2004	08.09.2004	IS 5
10	13.10.2004	13.10.2004	IS 7
11	01.11.2004	01.11.2004	IS 6

Table 4.2 Data takes of ENVISAT ASAR APP images, polarization VV/VH in the study area

4.1.2 Ground Truth

Within the study area a total of about 50 fields around the village Brelingen and the town Fuhrberg were selected as ground truth samples. The location of these fields is shown in Figure 4.1. Each sample field should be large enough in any direction, that it can contain some pure pixels that are not affected by neighboring fields. Therefore, only fields were selected with an area of at least 100 x 100 meters.

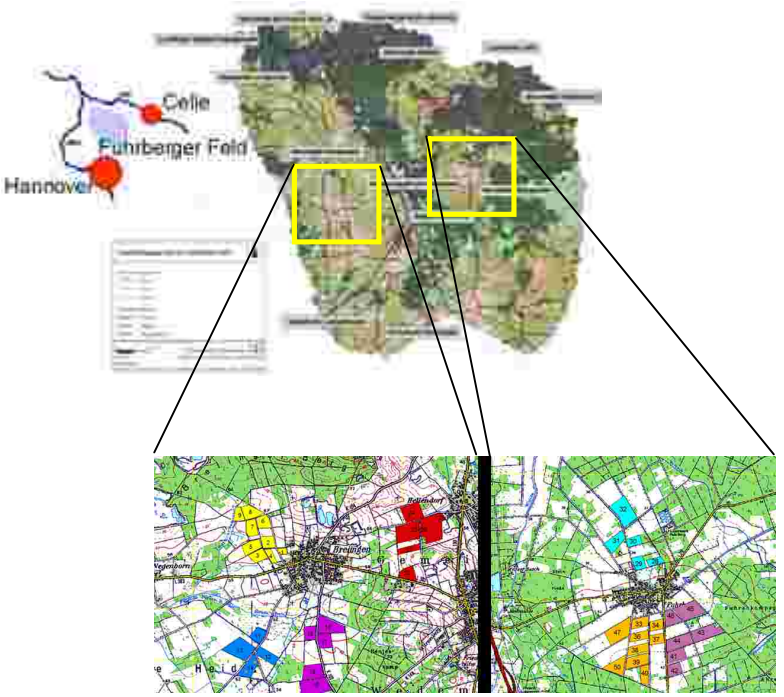

Figure 4.1 Study area and sample fields.

The fields were inspected close to the time of each image acquisition. Dates of field visits are listed in Table 4.2; during each field visit, the field geometry was updated if boundaries between crop fields had changed. Sometimes fields had to be excluded if they had become too small.

Ground truth consisted of sampling general information like crop type. Additionally, information on the kind of mechanical treatment of the soil and the plants, vegetation coverage,

vegetation condition, observable fertilizers, and irrigation were sampled. In addition, digital ground photographs were taken.

Altogether, 18 different types of fields are observed in the study area:

lea, fallow, peas, strawberry, willow, potato, rape, phacelia, summer barley, summer rye, asparagus, pasture, wild grain, winter barley, winter rye, winter wheat, sugar beet, and bare land. For some classes, only a single field was available as sample. Hence, an accuracy assessment for these classes was not possible. Accuracy of classification could be evaluated for the seven classes: potato, summer barley, asparagus, pasture, winter barley, winter rye, and sugar beets. These crops are **target classes** in this study. Accuracy of classification for the rest of the classes cannot be evaluated due to the lack of control fields. These classes are labeled "others" in this thesis. Although, an accuracy assessment for others is not possible, they participate in the training phase of classification because they exist in the study area and the effect of their inclusion in classification was to be considered. If these other classes are not contained in training, their extent is misclassified as one of the target crops while this misclassification is not considered in the accuracy assessment of target classes.

4.2 Data Preparation

Data is usually pre-processed before beginning the main analysis. Images must often be georeferenced or reprojected to the proper coordinate system. In addition, some image processing may be needed and ground truth must be properly organized.

4.2.1 Preprocessing of SAR Images

Spatial data, which is used in a study, must be geometrically related to each other. A simple transformation to the desired coordinate system is often enough for maps or rectified images, but remote sensing data contain systematic and non-systematic distortions because of sensor system, motions, and relief. Therefore, raw images must usually be rectified using sensor information, elevation models, and ground control points.

The study area of this thesis has a flat terrain; all the agricultural fields around Fuhrberg and Brelingen lie in elevations between 40 and 60 meters above sea level. Hence, the effect of relief on the geometry of agricultural fields is ignored in this study. The received images were georeferenced by ESA based on sensor parameters. Therefore, a rectification by ground control points was enough to register the images.

4.2.2 Speckle Suppression

As explained in Chapter 2, the speckle effect depends on target surface properties. It means that speckle carries information about the target, which may be useful for interpretation of SAR images.

On the other hand, speckle affects statistics and distribution of pixel values in feature space in a manner that variance in each class and covariance between classes increases. This effect reduces separability of classes from each other and may increase the classification error.

In this study, SAR images are filtered by some conventional filters to test the influence of speckle filters on the classification results. Tested filters are: median, mean, Lee (Lee 1980), Frost (Frost et al. 1982), gamma map (Touzi et al. 1988), local region (Durand et al. 1987), and Lee-sigma (Lee 1983).

4.2.3 Sample Grouping

More than one sample field per class is available for the target classes. The samples of a class from different fields can be used separately in training the classifier. Each sample field represents a sub-class.

If signatures of each class are used separately, small sub-class variations in classes (species of a crop, different soil types, etc.) are considered in the classification. On the other hand, there is the risk that each signature is too specialized and the feature space occupied by separate signatures of a class does not encapsulate gaps between samples of a class so some areas belonging to the class may be misclassified. Figure 4.2 illustrates the condition in a 2-dimensional space.

Another approach is to merge sample fields of a class in order to train the classifier once per class using pixel vectors of all samples of the class. A training sample of a class occupies an

area of feature space that contains all sample fields of a class. Sub-classes are ignored and no merging of sub-classes after classification is necessary.

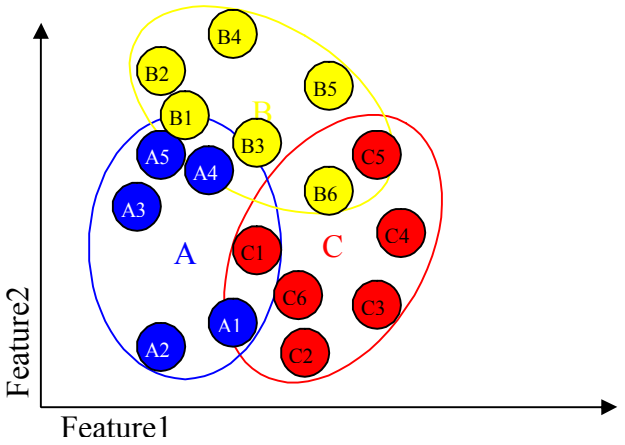

Figure 4.2 Merging signatures can change the results. Small circles are training samples of three classes A, B, and C. Large ellipses indicate borders of classes in the feature space after merging signatures of classes.

If samples of a class differ from each other so that parts of the samples of another class are inserted between them, merging of the sample fields causes an unwanted mixture between two classes. This may happen, for example, if sub-variants of a crop are present, which affect samples of the crop. Some samples such B6, C5, C1, and A1 may partly or completely be misclassified if samples of each class are merged before classification (see Figure 4.2). Classification using separated samples may prevent this problem, but large areas of feature space in the middle of samples classes A and C may be misclassified depending on the applied classification method. This happens because the classification model is fitted to single samples and the space between sample fields is excluded from the class. If this exclusion corresponds to the reality, the classification will be more accurate with separated sample fields, otherwise, merged sample fields result in more accurate classification.

In general, classification using separated sample fields results in a high interior accuracy (correctly classified area of training samples) but classification accuracy of areas aside the training samples is often more interesting, because the user wants to know the accuracy of

classification in unknown regions aside from samples areas. This can be measured using control samples that are excluded from the training phase and are spatially independent from the training samples. The expression “classification accuracy” generally indicates the accuracy calculated using control samples.

Since the result of sample grouping depends on the distribution of classes in the feature space, its influence on the accuracy of classification must be investigated for each class separately. This investigation may lead to a formation of sub-classes.

4.2.4 Calibration of SAR Images

Available SAR products are the amplitude images derived from measured intensity of backscattered signal. As described in Chapter 2, the backscattering coefficient (σ^0) of the target is one of the parameters that influence the recorded intensity. Since other parameters are usually constant for a space borne sensor, σ^0 can be calculated from the amplitude image pixel digital number (DN) and the local incident angle (α). The relationship between DN and σ^0 can be written as:

$$DN^2 = K.\frac{\sigma^0}{\sin(\alpha)} \tag{4.1}$$

K is an absolute calibration constant. σ^0 for ground range corrected products (see Chapter 2) can be derived as:

$$\sigma^0_{i,j} = \frac{DN^2_{i,j}}{K}\sin(\alpha_{i,j}) \text{ for i=1…L and j=1…M} \tag{4.2}$$

Where L and M are number of image lines and columns, respectively, and $\alpha_{i,j}$ is the local incident angle at image line and column (Rosich et al. 2004).

Since K is sensor, processor, and product-type dependent, calibration of image pixels to σ^0 is necessary if SAR images from different sensors or product types are processed together.

In this study, all SAR images originate from three swathes of ENVISAT. Each swath of ENVISAT has its own absolute calibration constant. Therefore, the influence of calibration on

the maximum likelihood classification as a standard parametric classifier is tested and reported in Chapter 5. Non-parametric classifiers are known to be less affected by multi-source data having diverse ranges and distributions (Watanachaturaporn et al. 2004 and 2008). As a consequence, the test is ignored for SVM.

4.2.5 Crop Calendar

A crop calendar for the study area is established based on the information from field visits. Table 4.3 represents planted crops on some of the fields. Each crop has its own phenological period, and its temporal appearance may differ slightly on different fields.

Image date	17.11	17.03	05.04	21.04	26.05 10.05	30.06	07.08	11.09	13.10	01.11
Visited	26.11	19.03	05.04	21.04	10.05	14.06	07.08	08.09	13.10	01.11
Field 11	Pasture	Pasture	Pasture	Pasture	Pasture	Pasture	Pasture	Pasture	Pasture	Pasture
Field 21	Winter Barley	Winter Barley	Winter Barley	Winter Barley	Winter Barley	Winter Barley	Rest	Wild Grain	Fallow	Rape
Field 3	Winter Rye	Winter Rye	Winter Rye	Winter Rye	Winter Rye	Winter Rye	Rest	Wild Grain	Winter Grain	Winter Grain
Field 5	Winter Barley	Winter Barley	Winter Barley	Winter Barley	Winter Barley	Winter Barley	Winter Barley	Rape	None	Winter Grain
Field 6	Winter Barley	Winter Barley	Winter Barley	Winter Barley	Winter Barley	Winter Barley	Rest	Rape	Rape	Rape
Field 8	None	None	None	Sugar Beet	Sugar Beet	Sugar Beet	Sugar Beet	Sugar Beet	Sugar Beet	Sugar Beet
Field 9	Fallow	Fallow	Fallow	Fallow	Fallow	Fallow	Fallow	Fallow	Fallow	Fallow
Field 18	Winter Wheat	Winter Wheat	Winter Wheat	Winter Wheat	Winter Wheat	Winter Wheat	Winter Wheat	Wild Grain	None	Winter Grain
Field 19	Rape	Rape	Rape	Rape	Rape	Rape	Rest	Rape	Winter Grain	Winter Grain
Field 16	Winter Rye	Winter Rye	Winter Rye	Winter Rye	Winter Rye	Winter Rye	Rest	Rest	Rest	Winter Grain
Field 28	Asparagus	Asparagus	Asparagus	Asparagus	Asparagus	Asparagus	Asparagus	Asparagus	Asparagus	Asparagus
Field 29	Fallow	None	Summer Barley	Summer Barley	Summer Barley	Summer Barley	Summer Barley	Phacelia	Phacelia	Phacelia
Field 30	Rape	None	Summer Barley	Summer Barley	Summer Barley	Summer Barley	None	Rape	Rape	Rape
Field 42	Rape	Rape	Rest	None	Sugar Beet	Sugar Beet	Sugar Beet	Sugar Beet	Rest	Rest

Table 4.3 Crops planted on some fields at different dates, and related images

This information on temporal progression of crop fields is used for explanation of the results of classification tests. It is also used for a classification according to the cultivation period of crops.

4.3 Multi-Temporal Classification

The method of agricultural monitoring in this study is classification of ASAR multi-temporal images. Images that are chronologically relevant to the growth period of a crop are used in a multi-temporal classification matched to the crop calendar. If multi-temporal data without matching to the crop calendar (all available data) is classified, irrelevant temporal data distort statistics of classes and reduce the accuracy of classification. This is especially important for parametric classifiers such as maximum likelihood. As mentioned in previous Chapters, non-parametric classifiers (for example, SVM) are less affected by irrelevant data. Therefore, improvement in accuracy of classification using data matched to the crop calendar is expected for classification by maximum likelihood and not by SVM.

A classification matched to the crop calendar can be optimized for one crop or one group of crops having similar phenological periods. Hence, more than one classification process is necessary for classification of crops having different phenological periods. Each crop is classified using the data set that corresponds to the temporal appearance of the crop. It is possible in some areas and for some crops that more than one main crop is cultivated on a field. However, this is not the case in our study area. Each field is cultivated by one main crop and possibly intermediate crops (see Table 4.3). Intermediate crops are cultivated or allowed to grow as wild after harvest of main crops and before seeding the field for the next agricultural season. Intermediate crops are often not harvested or are used as animal food. The appearance time of these crops follows the calendar of the last and the next main crop. Thus, no fixed and known cultivation period can be considered for them. Since a multi-temporal classification is based on the temporal progress of crops, it is not possible for crops without fixed and known phenological periods such as intermediate crops. Therefore, intermediate crops are ignored in multi-temporal classification and only one crop per field for one year is considered as the main

crop. However, some areas may be classified as more than one crop by a multi-temporal classification matched to the crop calendar, which contradicts previous considerations. In this case, the result of one classification can be correct and others must be rejected as misclassification.

A solution of this conflict is to use the estimation factor of the classifier. Each classifier calculates one or more estimation factors to assign pixel vectors to classes. For example, maximum likelihood estimation calculates a probability per class for each pixel. These values are used to solve the conflict problem. Estimation factors of conflicting classes for the same pixel are compared and the pixel is assigned to the most probable (according to the estimation factor) class. It must be considered that the calculated factor may be affected by the dimensionality of feature space. Hence, estimation factors of two classification processes can be compared if two feature spaces have the same number of dimensions or the factors are normalized.

Probability values of maximum likelihood and distance values to the separating hyperplanes of SVM are used to solve the conflict problem in this thesis.

4.4 Evaluation Method

The evaluation method of this study is explained in this section. It consists of evaluation parameters and sample size. Evaluation parameters are quantities that should represent the suitability of applied methods for the desired aim and facilitate reliable comparison between different methods. Training and evaluation of a classification is based on samples. A too small training sample size makes a classification too inaccurate and results may not fulfill the desired purpose. On the other hand, a very large sample size may become too expensive. Congalton and Green (1999) is the main reference of this section.

4.4.1 Evaluation Parameters

As the aim of this study is the investigation of methods to improve the accuracy of multi-temporal classification of SAR data, parameters are needed to evaluate classification accuracy.

Calculating an error matrix is a standard method for accuracy assessment of a classification. An error matrix is a two-dimensional array of numbers that indicates the number of sample units assigned to a particular category in a classification in comparison with reference data. Reference data is usually considered as correct and may be provided from maps, remote sensing data, field visits, videos, etc. A pixel is considered as sample unit in many studies. The columns of an error matrix usually represent reference data while the rows show classification results (inverse order is present, too). Any error in a classification is an omission from a correct category and a commission to an incorrect category.

Overall accuracy, producer's accuracy, and user's accuracy are three accuracy measures that can be calculated using an error matrix. Overall accuracy is the sum of correctly classified pixels divided by the number of all sample pixels. It is a well-known accuracy measure that represents quality of a classification as a single value. It indicates how accurate the classification result is all together but no more information is provided in detail. For example, two classification methods, each with 80% overall accuracy for the same data set, may be evaluated as equal. However, the methods may not be equally reliable: for example one method classifies all the classes at 80% correctness, another classifies one class very poorly, and the others slightly more accurately than 80%. An error matrix represents more information than a single accuracy value.

As Table 4.4 shows, n samples are distributed into k^2 cells. Each sample is assigned to one of k classified and one of k reference classes. Three accuracy measures can be calculated as:

$$\text{Overall accuracy} = \frac{\sum_{i=1}^{k} n_{ii}}{n}$$

$$\text{Producer's accuracy of } j = \frac{n_{jj}}{n_{+j}}$$

$$\text{User's accuracy of } i = \frac{n_{ii}}{n_{i+}} \tag{4.3}$$

where k is number of classes, n is total number of sample pixels, n_{ii} and n_{jj} are the number of correctly classified pixels of classes i and j.

Producer's accuracy, also known as completeness, indicates the proportion of correctly classified samples of a class relating to the total samples of that class. Producer's accuracy reflects the misclassification of the class as other classes (omission error).

	Reference data (j)					
Classified data (i)		1	2	k	Row sum n_{i+}	User's accuracy
	1	n_{11}	n_{12}	n_{1k}	n_{1+}	n_{11}/n_{1+}
	2	n_{21}	n_{22}	n_{2k}	n_{2+}	n_{22}/n_{2+}
	K	n_{k1}	n_{k2}	n_{kk}	n_{k+}	n_{kk}/n_{k+}
	Column sum n_{+j}	n_{+1}	n_{+2}	n_{+k}	n	
Producer's accuracy		n_{11}/n_{+1}	n_{22}/n_{+2}	n_{kk}/n_{+k}		$(n_{11}+n_{22}+n_{kk})/n$

Table 4.4 Mathematic scheme of an error matrix.

User's accuracy, also known as correctness, indicates the proportion of correctly classified samples of a class in relation to the all samples classified as that class. Hence, user's accuracy of a class i describes the probability that a pixel classified as class i belongs to the class i in fact. User's accuracy reflects the misclassification of other classes as the desired class (commission error).

4.4.1.1 Kappa

Overall accuracy only indicates the agreement between classified and reference data. It does not provide any information about its confidence level, which is the extent of the agreement between repeated measurements. In addition, a significance test of the difference between two error matrices is often demanded. Kappa statistics solve these problems. It is a discrete multivariate technique for statistically determining if one error matrix significantly differs from another one. The result of performing a Kappa analysis is known as KHAT ($\hat{k}$), which is based on the overall accuracy and the chance agreement. $\hat{k}$ can be thought of as the chance-corrected overall accuracy, and possible values range from +1 (perfect agreement) via 0 (no agreement) to -1 (complete disagreement).

In order to calculate KHAT the following equations are needed:

Let

$$p_{ij} = n_{ij} / n \tag{4.4}$$

$$p_{i+} = \sum_{j=1}^{k} p_{ij} \quad \text{and} \quad p_{+j} = \sum_{i=1}^{k} p_{ij} \tag{4.5}$$

$$p_0 = \sum_{i=1}^{k} p_{ii} \text{ is overall accuracy} \tag{4.6}$$

$$p_c = \sum_{i=1}^{k} p_{i+} p_{+j} \text{ is the chance agreement.} \tag{4.7}$$

The maximum likelihood of Kappa is given by:

$$\hat{k} = \frac{p_0 - p_c}{1 - p_c} \tag{4.8}$$

A KHAT value can be calculated for each error matrix. It measures how well the classified data agrees with the reference data. Since $\hat{k}$ is asymptotically normal distributed, the significance of

$\hat{k}$ for a single error matrix can be tested to determine if the agreement between classified data and reference data is significantly better than a random classification.

Furthermore, KHAT facilitates a comparison between two independent error matrices with $\hat{k}_1$ and $\hat{k}_2$ in order to indicate if one method or data set is significantly more accurate than the other one.

The significance of a single error matrix can be calculated by:

$$Z = \frac{\left|\hat{k}_1\right|}{\sqrt{\hat{\mathrm{var}}(\hat{k}_1)}} \tag{4.9}$$

where $\hat{\mathrm{var}}(\hat{k}_1)$ is computed as:

$$\hat{\mathrm{var}}(\hat{k}) = \frac{1}{n}.\left\{\frac{\theta_1(1-\theta_1)}{(1-\theta_2)^2} + \frac{2(1-\theta_1).(2\theta_1\theta_2-\theta_3)}{(1-\theta_2)^3} + \frac{(1-\theta_1)^2.(\theta_4-4\theta_2^2}{(1-\theta_2)^4}\right\}$$

where

$$\theta_1 = \frac{1}{n}\sum_{i=1}^{k} n_{ii} \,,$$

$$\theta_2 = \frac{1}{n^2}\sum_{i=1}^{k} n_{i+}n_{+i} \,,$$

$$\theta_3 = \frac{1}{n^2}\sum_{i=1}^{k} n_{ii}(n_{i+}+n_{+i}) \,,$$

$$\theta_4 = \frac{1}{n^3}\sum_{i=1}^{k}\sum_{j=1}^{k} n_{ij}(n_{j+}+n_{+i})^2$$

The agreement will be higher than a random agreement if $Z \geq Z_{\alpha/2}$ where α is the confidence level of the two-tailed Z test[5].

To test if two different error matrices are significantly different Z is calculated by:

$$Z = \frac{\left|\hat{k}_1 - \hat{k}_2\right|}{\sqrt{\hat{\text{var}}\left(\hat{k}_1\right) + \hat{\text{var}}\left(\hat{k}_2\right)}} \tag{4.10}$$

If $Z \geq Z_{\alpha/2}$ the two error matrices are significantly different in the considered confidence level.

Error matrices and the significant tests of implemented classification methods are presented in Chapter 5 of this thesis.

4.4.2 Sample Size

Sample data is necessary for two phases of any supervised classification: 1) training 2) evaluation. In the first phase, samples are used as a representative pattern for training of the classifier. Samples represent the distribution of categories in feature space so that the data can be classified based on this representation.

Accuracy of classification is evaluated in the next phase using samples that are not included in the training phase. These samples are referred to as control samples. Control samples must be independent of training samples in order to evaluate classification accuracy for the areas aside of training samples, which is often interesting in accuracy assessment of classification.

Size of training and control samples directly influences the accuracy of the classification and the reliability of the accuracy assessment. Hence, the theme sample size is discussed in this section.

This theme is important for the current study to determine the reliability of the results provided by implemented methods. In addition, changes in sample size and classified data affect the classification results. The knowledge about available sample size and its difference from

[5] Any statistical test for which the distribution of the test statistic under the null hypothesis can be approximated by a normal distribution (Sprinthall 2003).

recommended or standard sample size clarifies the potential for improvement of classification accuracy by sampling method, sample size and additional data.

4.4.2.1 Training Samples

Some classifiers need a minimum number of training samples to work. For example, n+1 samples are required for an n dimensional feature space to avoid the covariance matrix to become singular. The inverse of a singular matrix in discriminant function expressions cannot be found. Therefore, at least n + 1 samples are necessary for classification using MLC. This minimum determines only a precondition of a classifier so that the classifier can be applied. More interesting is the minimum number of samples that result in an accurate classification.

The Hughes phenomenon (Hughes 1968) relates accuracy of classification with measurement complexity and sample size. Measurement complexity or the total discrete values of observed data for an image is the number of all possible values in each band of the image. Bands of images may be spectral bands, channels or polarizations of radar data, dates of multi-temporal data, as well as quantitive spatial data represented as an image. If all dimensions of the feature (bands of an image) space have the same number of discrete values, the total number of discrete values is the product of the number of dimensions and the number of discrete values in each dimension.

The Hughes phenomenon (Figure 4.3) indicates that more samples (mathematically expected) result in more accurate classification. Measurement complexity may improve classification accuracy if enough samples are available. More complex measurement results (mathematically expected) in higher accuracy if an infinite training sample size is available. A maximum of measurement complexity can be calculated for a finite number of samples and target classes so that any more- or less-complex measurement decreases accuracy of classification.

Spatial distribution of samples and extent of the study area influence accuracy of a classification by remote sensing data. For example, classification in a large area with a small sample size that covers only 1% of the study area is not as accurate as a classification in a small area with the same sample size covering 50% of the small study area. In a large area, more variability in land cover, soil types, plant species, soil moisture, and elevation is expected than in a small area. Therefore, more samples are necessary in a larger area to achieve the same

accuracy of the small area. No recommendation about the sample size according to the study area is found in the literature, although, up to 10% of study areas are often sampled in different studies.

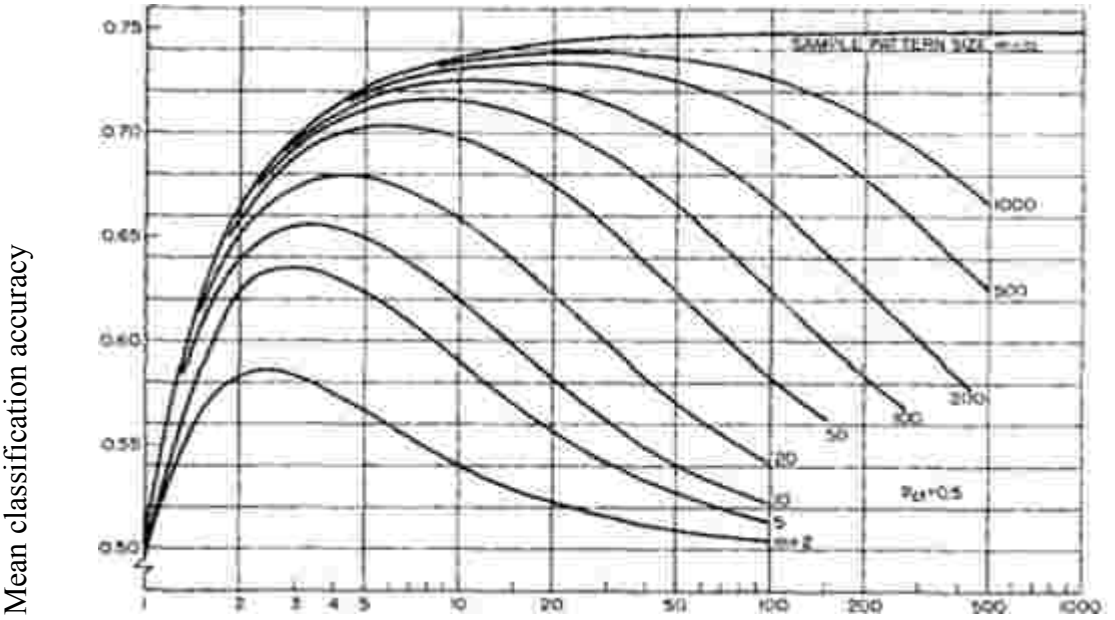

Figure 4.3 Accuracy of a binary classification with different number of samples size (m) and measurement complexity. Apriori probability of classes is considered equal ($P_{c1} = P_{c2} = 0.5$) (Hughes 1968).

On the one hand, as many samples as possible should be provided to improve classification accuracy: on the other hand, sample acquisition is limited by many factors, most of them can be calculated as costs. Misclassification results in costs, too. A trade-off between sampling costs and misclassification costs is often an optimal solution in a commercial project.

Swain and Davis (1978) recommend 10N (N is number of features) as an experimental minimum and 100N as highly desirable number of samples for training of a classifier.

Barrett and Curtis (1992) recommend training sample size as $100 * (CV)^2$ per class where CV is the coefficient of variation (standard deviation divided by mean). This method does not consider the complexity of measurement: it recommends 16 samples per class for very homogenous areas and up to 70 samples per class for complex areas.

4.4.2.2 Control Samples

Tortora (1978) represented the procedure for calculating the appropriate sample size of an error matrix. Let $\Pi_i, i = 1,...,k$, be the proportion of the population in the *i*th category of k categories, then the minimum number of control samples (n) at a desired confidence level $(1-\alpha)$ and precision (b_i) can be calculated by:

$$n = B\Pi_i(1-\Pi_i)/b_i^2 \tag{4.11}$$

where B is the upper $(\alpha/k)\times 100th$ percentile of the χ^2 distribution with 1 degree of freedom.

This method for calculating the minimum sample size of an error matrix is used and recommended by many researchers (Story and Congalton 1986). This method provides information about minimum control sample size of error matrices in the current study.

4.4.2.3 Available Ground Truth

53 agricultural fields within two agricultural areas Fuhrberg and Brelingen were visited close to the image-acquisition time. The extent of all sample fields is about 3.7 square kilometers corresponding to about 14% of all agricultural fields in the two study areas. Considering the 30-meter spatial resolution of ENVISAT data and possible geometric inaccuracy of images, a 30-meter wide buffer from the border of each field is ignored in order to avoid mixed pixels in the training and control phases. Hence, the area of samples is reduced to about 2.6 square kilometers. Statistics of available sample fields are presented in Table 4.5. Some crops (e.g., phacelia) that were not cultivated as the main crop of any field are not included in Table 4.5. Only one sample field is available in the case of some rare crops. Since pixels within a field are often correlated, the accuracy of classification cannot be reliably evaluated for these rare crops. Therefore, no control sample of rare crops was incorporated in the accuracy assessment, although the samples are used during the training phase in order to consider the error accrued by rare crops. There are two fields for willow available, but the fields were cultivated in different seasons. In addition, the two fields have diverse phenological periods, and hence willow cannot be classified and evaluated in a multi-temporal classification either. Hence, this class is excluded from accuracy assessment.

4 to 11 sample fields are available for target classes asparagus, potato, summer barley, winter barley, pasture, winter rye, and sugar beets.

Training samples: VV and VH polarizations of the 11 acquisition dates are used for multi-temporal classification. Hence, the feature space has 22 dimensions. All classes have more than n+1=23 sample pixels, thus the covariance matrix does not become singular for any class. However, the provided ground truth should be divided between training and control samples such that the training sample size becomes smaller than the values represented in Table 4.5.

Class	Sample pixels	Number of fields containing samples	Proportion of class to the whole sample area in percent %
Lea	304	1	02.1
Fallow	126	1	00.9
Peas	79	1	00.6
Strawberry	122	1	00.9
Bare land	163	1	01.1
Rape	521	1	03.6
Summer rye	96	1	00.7
Winter wheat	125	1	00.9
Willow	281	2	02.0
Asparagus	847	4	05.9
Potato	3022	5	21.0
Summer barley	1420	5	09.9
Winter barley	1380	5	09.6
Pasture	1080	6	07.5
Winter rye	1786	7	12.4
Sugar beets	3020	11	21.0

Table 4.5 Geometric statistics of sample fields. Classes over the thick line are not included in accuracy assessment.

Control samples: Considering the recommendation of Tortora (1978) as the required number of control samples per class, we need the proportion of each class in the study area. Since the samples are chosen randomly, the proportion of samples of each class to all samples may be considered as an approximation for proportion of classes to all crops in the study area.

Control sample selection: as mentioned, pixels of a field are expected to have some degree of correlation. Therefore, control samples must originate from fields, from which no pixel was incorporated into the training phase. In this way, the accuracy is evaluated for areas, which, geometrically do not overlap training fields. Hence, sample fields (not sample pixels) are randomly used as training and control samples.

Only one sample field per class can be considered as control sample. Considering more control fields per class reduces training sample size so that the training sample of some classes becomes too small for classification. The calculated accuracy via one control field may not be representative of the classification accuracy for many fields of a class. Hence, each test is repeated three times (Table 4.7). Each time one sample field per class is excluded from the training and used as control sample. Therefore, the accuracy assessment is implemented using a larger control sample (three control fields per class instead of one) which increases confidence of accuracy assessment.

Class	Confidence level 95%	Confidence level 99%
Asparagus	179	244
Potato	535	731
Summer barley	287	392
Winter barley	280	382
Pasture	224	306
Winter rye	350	479
Sugar beets	535	730

Table 4.6 Required number of control samples for each class at 95% and 99% confidence levels (according to the recommendation of Tortora (1978)).

Table 4.7 represents the number of training and control sample pixels in each test. If the recommendation of Swain and Davis (1978) is accepted as minimum and desirable limits, samples of rare classes do not fulfill the minimum limit of 10N. More than the desirable limit of 100N sample pixels are available for potato and sugar beets. The sample size of asparagus, summer barley, winter barley, pasture, and winter rye lies between the minimum and desirable limits. Hence, more than the minimum number of samples is available for classes that are incorporated in the accuracy assessment. Table 4.8 indicates the confidence level of individual and the sum of control sample per class. Many sample fields are too small to serve as control sample of their class. The whole control samples of the three tests fulfill the required sample size at 99% confidence level for all crops.

	Test1		Test2		Test 3		Sum of control pixels
	Training pixels	Control pixels	Training pixels	Control pixels	Training pixels	Control pixels	
Asparagus	481	365	597	249	736	110	725
Potato	2428	594	2211	811	2352	670	2075
Summer barley	1084	336	1021	399	1041	379	1114
Winter barley	1120	260	899	481	1119	261	1002
Pasture	850	230	877	203	1034	46	479
Winter rye	1580	206	1515	271	1546	240	717
Sugar beets	2897	123	2961	59	2514	506	688

Table 4.7 Number of training and control pixels used for each test.

	Test1		Test2		Test 3		Sum	
Confidence level	95%	99%	95%	95%	99%	99%	95%	99%
Asparagus	1	1	1	0	0	1	1	1
Potato	1	0	1	1	0	1	1	1
Summer barley	1	0	1	1	0	1	1	1
Winter barley	0	0	1	0	0	1	1	1
Pasture	1	0	0	0	0	0	1	1
Winter rye	0	0	0	0	0	0	1	1
Sugar beets	0	0	0	0	0	0	1	1

Table 4.8 Confidence evaluation of control samples for individual tests and classes at confidence levels 95% and 99%. 1 = the precondition of the confidence level is fulfilled. 0 = control sample is too small for desired confidence level.

4.5 Summary

Data, method and test design of the thesis has been discussed in this Chapter. The data consists of ENVISAT ASAR images from the year 2004 and ground truth gathered from about 50 agricultural fields in two areas around the town Fuhrberg and the village Brelingen. Data preparation methods that are used in this study are explained and their necessity is discussed. Multi-temporal classification is introduced as the method for monitoring of agricultural activities. Furthermore, methods for classification that are applied in this study are discussed. Data sets and classification methods are evaluated using error matrices which are constructed based on control samples. An error matrix provides useful information about omission and commission errors. Kappa statistics of an error matrix indicate if the calculated accuracy is significantly higher than a random agreement. In addition, it can be used for comparison of two independent error matrices.

Sample size is another important issue in accuracy assessment. Larger training samples result in higher accuracy at higher costs. No global lower or upper limit for training sample size is defined. Only some experimental recommendations are available that can be used as guide lines. More training samples are necessary for classification of high-dimensional data than of low-dimensional data, in order to achieve equal or higher accuracy by high-dimensional data.

A solution for sample size is a trade-off between costs of sampling and costs of misclassification so that the total costs are kept minimal.

On the other hand, clear relations between control sample size and reliability of tests are defined by statistics. The number of control samples of a class required to achieve a desired confidence level can be calculated in an accuracy assessment.

Figure 4.4 represents the sequence of a multi-temporal classification and its accuracy assessment. Results and evaluation of implemented methods are represented in Chapter 5.

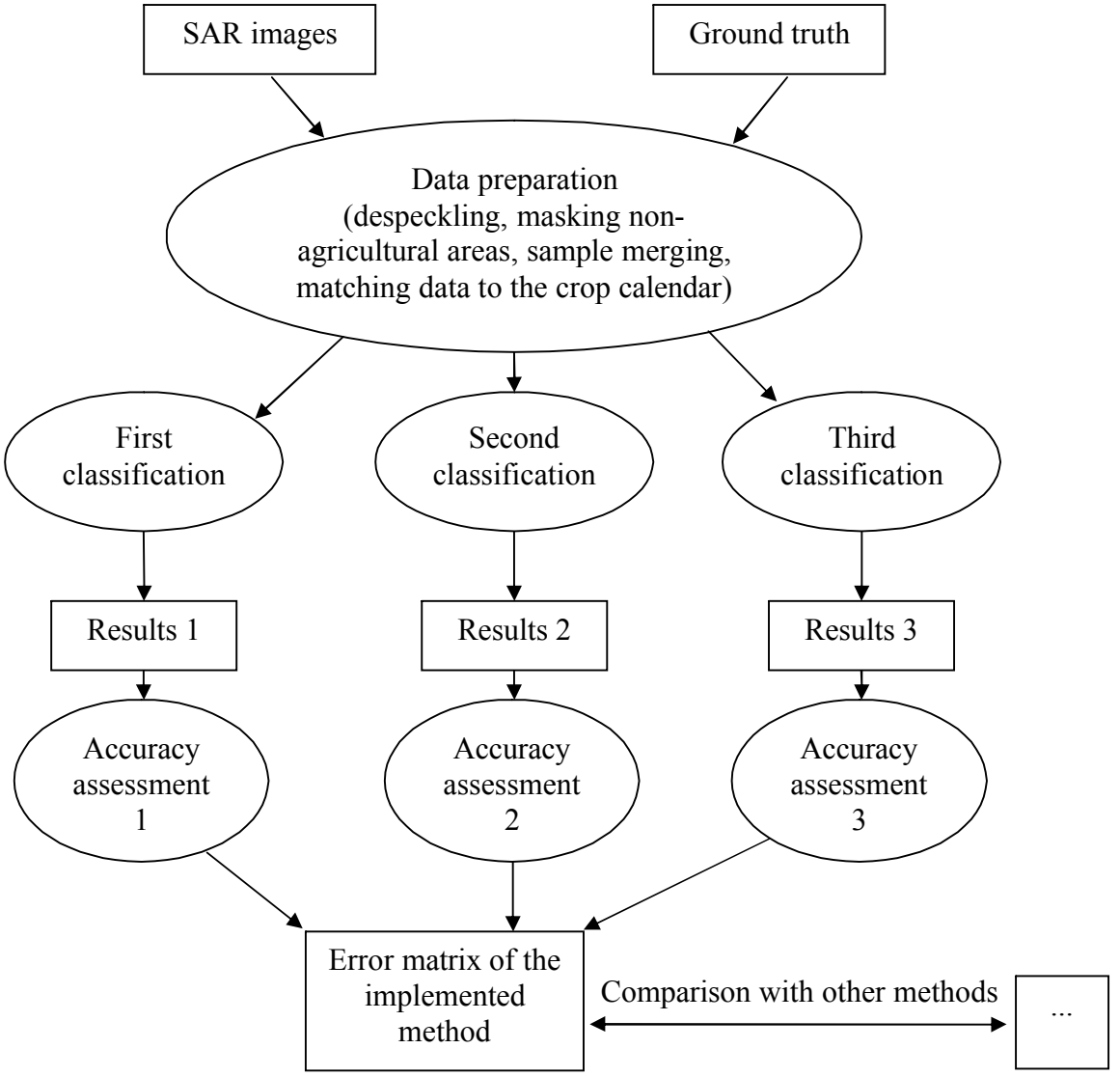

Figure 4.4 sequence of a multi-temporal classification and its accuracy assessment for an implemented method.

Chapter 5

5 Results and Discussion

This Chapter presents results of the investigated methods for monitoring agricultural fields using SAR data. The methods introduced in Chapter 4 are implemented and presented in this Chapter. Backscattering statistics of some samples of the study area are discussed. Furthermore, pre-processing methods are tested and evaluated for multi-temporal SAR data.

Finally, results of multi-temporal classification for crops using the introduced methods, data combination, and classifiers are presented and discussed. It could be shown that MLC and SVM classifiers can classify the crops at about 80% overall accuracy. Performance of SVM depends strongly on the feature selection, whereas, SVM is less influenced by feature selection of multi-temporal data.

5.1 Backscattering of Crop Fields

As explained in Chapter 2, the intensity of the backscattered signal depends on the distance between sensor and target, the dielectric constant, shape, orientation, and material of the target (soil and vegetation).

5.1.1 Backscattering of Crop Fields in the Study Area

Backscattering of some example sample crop fields in the study area is investigated and related to sensor and local parameters. This discussion explains multi-temporal signatures of six sample fields for multi-temporal classification and investigates the influence of vegetation growth on SAR images in the study area. The main crops of the sample fields were winter barley (field 23), winter ray (field 50), rape (field 19), sugar beet (field 36), potato (field 44), and pasture (field 14). In addition, a sample of forest and one sample of a settlement area are investigated together with the agricultural samples. Forest and settlement areas are stable land cover types that are rarely changed within one year at the scale of ENVISAT data. These samples serve as stable bases to describe the influence of agricultural activities and vegetation growth on backscattering of SAR signals.

Table 5.1 presents information on images, observed moisture condition, and regional precipitation of the last day before the SAR acquisition. Unfortunately, observed surface moisture is not available for all image-acquisition dates. Moreover, the two categories of dry and wet are too coarse for describing the moisture condition. Hence, the regional precipitation data (last line of Table 5.1) was taken from the free archive of www.wetterzentrale.de.

Imaged	17.11	17.3	5.4	21.4	10.5	26.5	30.6	7.8	11.9	13.10	1.11
Visited	26.11	19.3	5.4	21.4	10.5	-	14.6	7.8	8.9	13.10	1.11
Swath	IS6	IS7	IS6	IS7	IS6	IS7	IS7	IS5	IS5	IS7	IS6
Surface moisture	?	?	Wet	Dry	Wet	?	?	Dry	?	Dry	Wet
Rained in last 24h (mm)	15	0	2	0	1	0	1	0	11	0	1

Table 5.1 Information on used images and dates from 17.11.2003 until 01.11.2004.

Sensor and local parameters together with land cover data of the fields (Tables 5.2) are used to describe the backscattering of the sample areas (Figures 5.1 and 5.2).

Field		Image dates										
		17.11	17.3	5.4	21.4	10.5	26.5	30.6	7.8	11.9	13.10	1.11
23	Crop Type	Winter Barley							Bare Land	Rape		
	Canopy coverage (%)	>75	>75	>75	>75	>75	>75	>75	<12.5	>75	>75	>75
	Vegetation height (cm)	12	15	15	40	70	80	90	0	12	50	50
50	Crop Type	Winter Rye								Wild Grain	Bare Land	Winter Grain
	Canopy coverage (%)	?	50-75	>75	>75	>75	>75	>75	>75	<12.5	<12.5	<12.5
	Vegetation height (cm)	?	8	8	25	60	80	100	100	0	0	6
19	Crop Type	Rape							Rest	Wild Rape	Winter Grain	
	Canopy coverage (%)	50-75	50-75	50-75	>75	>75	>75	>75	>75	<12.5	<12.5	12.5–25
	Vegetation height (cm)	8	10	25	60	100	115	130	50	10	10	10
36	Crop Type	Fallow	Bare Land			Sugar Beet						Bare Land
	Canopy coverage (%)	>75	<12.5	<12.5	<12.5	<12.5	12.5-25	50-75	>75	>75	>75	<12.5
	Vegetation height (cm)	10	0	0	0	5	20	35	50	50	50	0
44	Crop Type	Bare Land		Potato							Winter Barley	
	Canopy coverage (%)	<12.5	<12.5	<12.5	<12.5	<12.5	25-50	>75	>75	12.5-25	<12.5	<12.5
	Vegetation height (cm)	0	0	0	0	3	25	45	50	50	6	10
14	Crop Type	Pasture										
	Canopy coverage (%)	>75	>75	>75	>75	>75	>75	>75	>75	>75	>75	>75
	Vegetation height (cm)	15	10	10	10	10	12	15	20	10	10	15

Tables 5.2 Land cover data of six sample fields. For each field, cultivated crops in the year 2004 are presented. Canopy coverage and vegetation height are presented for each date separately.

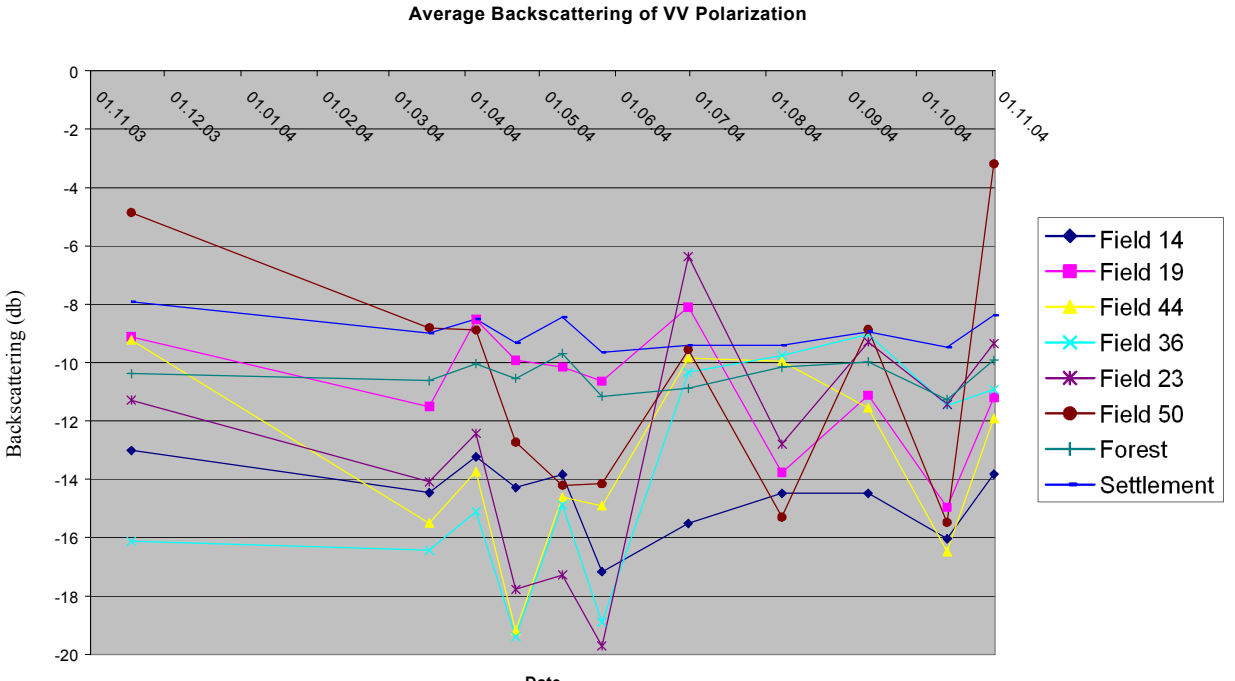

Figure 5.1 Average backscattering of sample areas in VV polarization of ENVISAT SAR

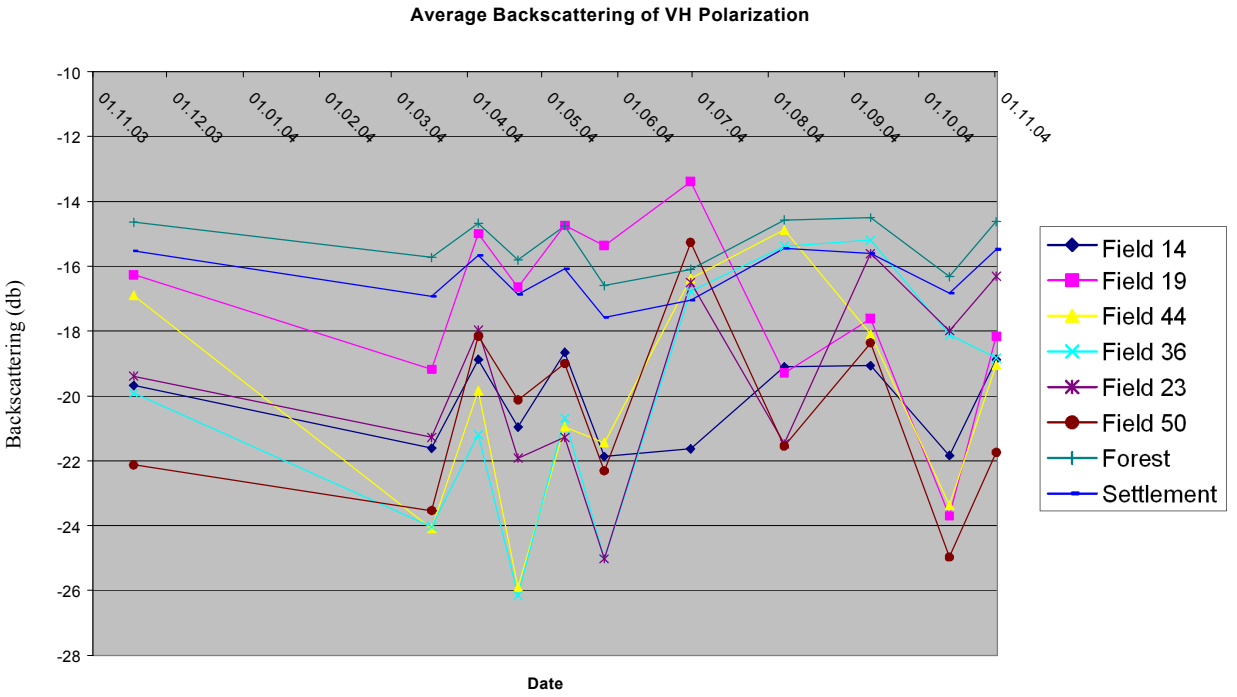

Figure 5.2 Average backscattering of sample areas in VH polarization of ENVISAT SAR

Settlement areas show a relatively high backscattering in both VV and VH polarizations because of many corner reflectors and depolarization by multiple reflections before

backscattering. As a consequence of the stable condition of the settlement area, the mean backscattering varies within only 2db at different dates. The observed variation of backscattering is mainly due to the moisture of the target surface on rainy days. The backscattering drops slightly on dry days of 17.03, 21.04, 26.05, 07.08, and 13.10 compared to the other dates. A comparison between four acquisitions from 26.05 until 11.09 of swaths IS5 and IS7 does not indicate any effect of incident angle on backscattering of settlement area. The little increase in VV backscattering of swath IS5 on 11.09 is probably due to rainfall. Temporal progress of VH backscattering in the settlement area follows the VV backscattering before May and after October. VH backscattering increases between June and September because of vegetation growth in the town.

Average backscattering of the forest area is fairly correlated with that of the settlement area. VV backscattering of the settlement area is always about 1 to 2 db higher than for forest whereas the VH backscattering is about 1db less than for forest on all dates.

Pastures are relatively stable areas that experience little changes in the course of time (Tables 5.2, field 14). Backscattering of the pasture sample (field 14) tends to follow the temporal trend of the settlement and the forest with higher temporal variation at lower backscattering. The lower backscattering is due to the absence of corner reflectors (compared with settlement and forest). Lack of corner reflectors lets other factors (plants, moisture and look angle) dominate the backscattering of pasture. Hence, more temporal change in backscattering of pasture is observed due to the change in moisture and incident angle. In contrast to forest and settlement areas, VV backscattering of pasture in August and September (swath IS5) was obviously higher than in May and June (swath IS7).

Field number 23 was cultivated by winter barley in autumn 2003. Winter barley was harvested in July 2004 and replaced by rape in August. VV backscattering of the field decreases from November 2003 to May 2004 as the moisture decreased. This trend is not observable for VH backscattering, which is mainly controlled by depolarization of the signal by plants. VV and VH backscattering of the field reached a minimum on 26.05.2004 and a maximum on 30.06.2004. Acquisitions of both dates were in swath IS7 so the difference in backscattering cannot relate to the difference in look angle. One millimeter of rainfall is recorded in the night before 30.06.2004 at regional scale. Unfortunately, the field was not visited on these two dates. However, the information of the visit on 14.06.2004 indicates that corn appeared in June 2004

and the structure of plants changed from spread leaves to the vertically standing plants (Figure 5.3). The high backscattering of 30.06.2004 is probably due to moisture, vertical structure of plants (especially important for vertical polarization with large look angle), and presence of the corn. Backscattering drops in August as the field is left without vegetation. VV and VH backscattering increase when the rape appears on the field. Backscattering of rape in October is lower than acquisitions before and after it. This can be explained by the low moisture on 13.10.2004 and the large look angle (IS7) of the sensor.

a b c

Figure 5.3 Images of field number 23. a: 10.05.2004, b: 14.06.2004, c: 07.08.2004

Field number 50 was cultivated by winter rye in autumn 2003. The field was harvested in August and the rest of plants was left in the field in September together with some wild plants. The field was planted by grains but no plants were visible in October. Small new grains rose before the last acquisition in November.

The temporal progress of backscattering of rye is somewhat similar to that of barley, but the backscattering and the variations differ from barley. In winter, when backscattering of the soil dominates, field 50 has a very high backscattering in VV polarization and very low backscattering in VH polarization. Similar conditions could be observed in November 2004, too. VV backscattering of field 50 decreased from November 2003 till May 2004 parallel to field 23 but at about 4 to 7 db higher backscattering. Rye had low backscattering in May and high backscattering in June similar to barley, although these values were not absolute minimum and maximum backscattering of field 50. In contrast to barley, rye was harvested later than

07.08.2004, but the plants were dry so that VV backscattering was lower than for field 23 and VH backscattering was close to it in August, whereas field 23 was harvested before that date.

a b c

Figure 5.4 Images of field number 50. a: 14.06.2004, b: 07.08.2004, c: 08.09.2004

VH backscattering of rye was slightly higher than barley, when the plants rose over 15cm between April and July. After harvesting, wet rests of plants caused an increase in VV and VH backscattering in September. VV and VH backscattering decreased to a minimum on the dry day of 13.10.2004 when no plants were visible in the field. VV backscattering reached a maximum in November 2004 like it did in November 2003. This high VV backscattering in winter was probably due to the water content of the soil, which dominated the backscattering in the absence of plants. VH backscattering of the field remained low on the last acquisition similar to the previous winter because a flat field with small plants does not depolarize the radar signal.

Field 19 was mainly cultivated by rape in the year 2004. Rape was planted in autumn and continued to the end of June (probably harvested in July). After harvesting, the rests were left on 07.08.2004 and wild rape (not planted) rose in September. Later, winter grains were planted on field 19.

Backscattering of field 19 dropped from November 2003 to March 2004 such as other fields. The field was covered by small plants of rape with about 50% canopy coverage in November and March. Hence, backscattering was dominated by soil for the two first acquisitions. The decrease in backscattering, which was observable for all fields and in both polarizations, can be explained by look angle (IS6 vs. IS7) and/or moisture. The well-known high backscattering of

rape occurred from April till June, when the plants were higher than 25cm. The backscattering in both polarizations increased as the plants grew, the maximum backscattering occurred at the last phase of growth. Backscattering (VV and VH) decreased in August when rape was harvested and only the rests covered the field. Wild rape increased the backscattering in September whereas backscattering fell in October when the small plants of grains covered the field and hence soil controlled the backscattering. The increased backscattering in November was probably because of high moisture and small look angle.

Field 36 was a fallow field in November 2003 with 100% canopy coverage of spread leaves grass. The field had no vegetation coverage in March and April 2004. Sugar beet plants rose in May and lasted until October when they were harvested. The field was bare land in November 2004.

Despite of the high canopy coverage by green plants in November 2003, VV backscattering of the field was as low as in the March 2004, when no plants were visible and the field was dryer than the previous November. The effect of plants can be observed on VH backscattering in November. VH backscattering of field 36 decreased from November to March more than other fields due to the presence of plants in November and lack of them in March. Backscattering of the field does not seem to be effected by plants before June when plants rose about 35cm high and canopy coverage was over 50%. Backscattering of sugar beet (VV and VH) increased as the plants grew until September. Similar to other samples, VV and VH backscattering of sugar beet were slightly reduced in October due to the less moisture and larger look angle, although, the plants do not change. Despite the higher moisture and smaller look angle in November, little increment can be seen in VV backscattering, and VH backscattering is decreased because of plants removal, whereas VV and VH backscattering of all other samples were meaningfully increased in November in comparison with October.

Field 44 was not covered by plants before May 2004, although, typical cultivation rows of potato were observable in March. Plants appeared in May and potatoes were harvested in August, but rests covered the field in September. New grains rose in October and November up to 10cm.

Temporal changes of backscattering for potato were somewhat similar to sugar beet especially until May with the exception that backscattering of field 44 (bare land) in November 2003 was

much higher than field 36 (was covered by grass). VV and VH backscattering of potato remained on 26.05 as high as 10.05 due to the growth of plants, whereas backscattering of other fields (except VV backscattering of rye) decreased on 26.05 due to the less moisture and larger look angle. Backscattering of potato field rose close to the backscattering of sugar beet in June and August. VV and VH backscattering of potato field decreased in September after harvesting and continued to decrease in October because of less vegetation coverage, less moisture and larger look angle. Backscattering of field 44 increased again in November such as other samples.

This discussion explained the influence of changes in vegetation coverage on the radar backscattering. The comparison between stable areas (settlement, forest, and pasture) and agricultural fields indicate that the backscattering of agricultural fields strongly varies due to the cultivation, growing, and harvest. This effect of agricultural fields on backscattering can be used as a chronological signature of agricultural fields in a multi-temporal classification.

5.2 Multi-Temporal Classification

This section reports and discusses the results of multi-temporal classification with different settings of pre-processing, time series, and classifiers. The advantage of speckle suppression for classification is evaluated for some conventional speckle filters. Furthermore, signature merging and matching to the crop calendar for crop classification are investigated. Maximum likelihood and SVM classifiers are compared for multi-temporal classification of crops. A combination method is introduced and applied in order to integrate results of different crops with diverse phenological periods (see Chapter 4).

All tests of this section (except for despeckling) are made using the same images, training, and control samples (Figure 4.4).

5.2.1 Despeckling

Speckle of SAR images increases interior variance inside each class (crop type) and decreases separability between different classes resulting in low accuracy of classification due to the mixture between classes. However, speckle depends strongly on surface properties and is no noise. The speckle in SAR data carries information on the target, which may be useful to distinguish classes. Some conventional speckle filters have been tested to investigate how despeckling and the type of filter affect the multi-temporal classification accuracy of ASAR images. The overall accuracy (correctly classified area of control fields of all classes) of classification computed using five control fields per crop are presented in Table 5.3. The influence of some speckle filters and median filter on the accuracy of multi-temporal classification using the maximum likelihood classifier is shown and compared with classification of raw images.

Filter	Overall Accuracy (%)
None	70
Lee (Lee 1980)	86
Frost (Frost et al. 1982)	82
Gamma Map (Lopes et al. 1990)	84
Local Region (Alparone 1992)	75
Lee-Sigma (Lee 1983)	85
Median	86

Table 5.3. Accuracy of multi-temporal classification of data filtered by some conventional speckle filters (decimals are rounded). Data is matched to crop calendar.

Overall accuracy of classification using images filtered by Gamma Map, Lee-Sigma, Lee and Median filters varies between 84% and 86%, which shows besides a good accuracy also little variation between the four filters. Images filtered by median and Lee filter gave the best value of accuracy (86%). Median filter has the disadvantage that it displaces borders of fields. Our test does not reflect the misclassification due to this displacement because a border of 30

meters of each field is ignored in this study. Hence, it must be considered that the median filter may introduce errors due to border displacement and affect accuracy of classification. Therefore, the Lee filter is chosen to reduce the speckle effect of ASAR images in this study.

5.2.2 Multi-Temporal Classification Using Per Class Merged Samples Versus Separate Samples

This test investigates results of the multi-temporal classification by maximum likelihood classifier using per class merged and separate samples. The method is explained in Chapter 4 of this thesis. Multi-temporal data is matched to the crop calendar before classification in this test (Table 5.4). Error matrices of two classifications using merged and separate samples are provided (Tables 5.5 and 5.6). The class "others" includes rare crops that have no control samples (see Chapter 4).

Acquisition date	Potato	Summer barley	Asparagus	Pasture	Winter barley	Winter rye	Sugar beets
17.11.2003				×	×	×	
17.03.2004		×	×	×	×	×	
05.04.2004	×	×	×	×	×	×	×
21.04.2004	×	×	×	×	×	×	×
10.05.2004	×	×	×	×	×	×	×
26.05.2004	×	×	×	×	×	×	×
30.06.2004	×	×	×	×	×	×	×
07.08.2004	×		×	×			×
11.09.2004	×			×			×
13.10.2004				×			
01.11.2004				×			

Table 5.4 Images that are classified for crops types. Applied images for each class are marked by a ×.

		Reference Data (Pixel)									
	Class names	Others	Potato	Summer Barley	Asparagus	Pasture	Winter Barley	Winter Rye	Sugar beets	Sum	User's accuracy %
Classified Data (Pixel)	Others	-	45	156	0	32	0	61	68	362	-
	Potato	0	1390	0	20	0	0	0	185	1595	87
	Summer Barley	1	0	836	0	51	0	48	0	936	89
	Asparagus	0	137	0	399	0	0	0	0	536	74
	Pasture	0	0	0	0	311	0	29	0	340	91
	Winter Barley	0	40	122	0	0	1002	61	43	1268	79
	Winter Rye	0	0	0	0	62	0	416	0	478	87
	Sugar beets	0	463	0	306	23	0	102	392	1286	30
	Sum	1	2075	1114	725	479	1002	717	688	6801	
Producer's accuracy %		-	67	75	55	65	100	58	57	Overall = 70	

Table 5.5 Error matrix of multi-temporal classification by MLC. Training samples are used separately. Data is matched to the crop calendar.

The overall accuracy of the classification for most crops is higher using merged samples than when using separate samples. The exception is winter barley, which is classified at 14% more accurate using separate samples (Tables 5.5 an 5.6). This fact shows that two or more sub-classes of winter barley fields did exist in the study area. This may be because of different species, cultivation methods, soil types, cultivation direction, or other local parameters of barley fields. Based on these results, it is recommendable to recognize the sub-classes of winter barley and classify them separately. Unfortunately, the small number of winter barley fields (5 sample fields) in the study area does not permit the recognition, classification, and evaluation

of sub-classes separately. However, classification accuracy may increase by classifying winter barley as two or more sub-classes if enough samples are available.

Altogether, it is advisable to merge samples of each class based on the crop types before classification. The overall accuracy of classification is about 14% higher if merged samples are used for training of the classifier. Because of the high difference between overall accuracy of the two tests, Kappa statistics are not necessary for this comparison.

		Reference Data (Pixel)									
	Class names	Others	Potato	Summer Barley	Asparagus	Pasture	Winter Barley	Winter Rye	Sugar beets	Sum	User's accuracy %
Classified Data (Pixel)	Others	-	7	260	5	9	28	39	43	391	-
	Potato	0	1954	0	6	0	0	0	71	2030	96
	Summer Barley	1	0	850	22	25	0	37	0	935	91
	Asparagus	0	0	0	498	0	0	0	0	498	100
	Pasture	0	0	5	0	428	0	20	0	453	95
	Winter Barley	0	0	0	0	1	862	44	19	926	93
	Winter Rye	0	0	0	0	17	48	573	0	638	90
	Sugar beets	0	113	0	195	0	65	4	555	932	60
	Sum	1	2075	1114	725	479	1002	717	688	6801	
Producer's accuracy %		-	94	76	69	89	86	80	81	Overall = 84	

Table 5.6 Error matrix of multi-temporal classification by MLC. Data is matched to the crop calendar and training samples of each class are merged before classification.

5.2.3 Combination of Classification Results

Matching multi-temporal data to the crop calendar is a method that is applied in this study to ML and SVM classifiers. Different data sets are classified for different crops with diverse phenological periods in a classification matched to the crop calendar (Figure 5.5); the classification for one crop is independent from classification for other crops.

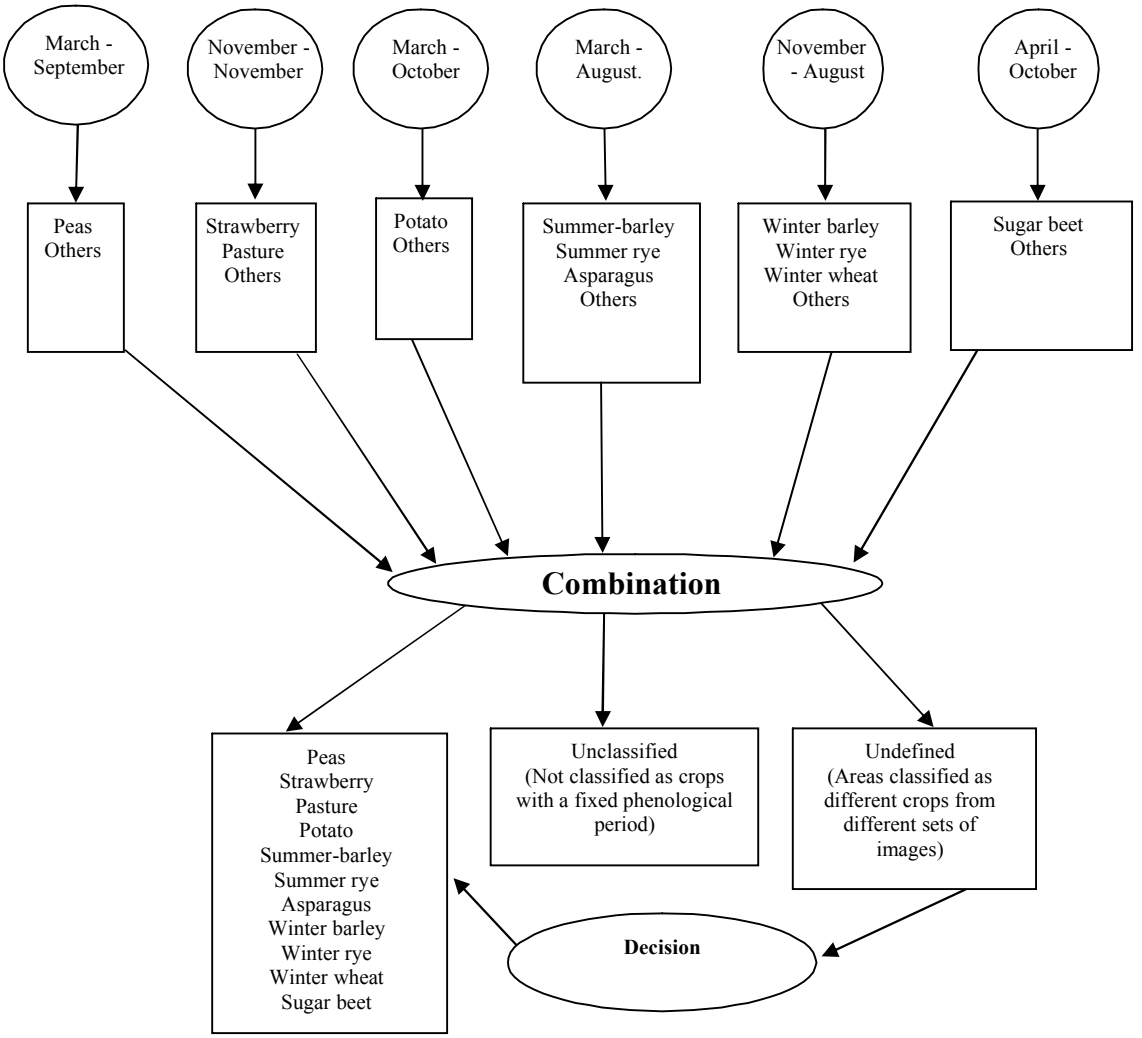

Figure 5.5 A schema of a multi-temporal classification matched to the crop calendar.

Some areas (pixels) may be labeled as more than one crop by classification of different data sets. Since only one of the crops can be cultivated on a field in an agricultural season, classification of one pixel as more than one crop is a conflict that must be solved. Therefore,

the combination of classification results is not a simple spatial arrangement of different classes as a mosaic.

The combination of classification results for different crops is necessary because 1: conflicts must be solved in order to provide a map of classification results, 2: individual classification results confuse an error matrix due to conflict areas that are redundantly present in samples of different crops. Hence, a reliable accuracy assessment is only possible after combination of results. All the error matrices of classifications matched to the crop calendar that are represented in this Chapter are provided after combination of results.

About 12% of control pixels are classified as two or more different crops by MLC matched to the crop calendar. The conflict area for SVM is about 11%. An approach that is used by some authors is decision by chance. Since the conflict pixels are labeled as at least two crops, a decision by chance on average misclassifies at least half of the conflict pixels (about 5-6% of samples). Another approach is to classify conflict pixels using decision parameters of the classification. The decision parameter for MLC is the probability in normal distribution. It must be considered that the number of features affects the maximum likelihood probability. The size of feature space influences Euclidian distances that are used in calculation of probabilities. Hence, maximum likelihood probabilities should be normalized by the number of features in order to allow a reliable comparison of probabilities for different crops that are classified by diverse number of images.

Here, the decision is taken according to the normalized probabilities of a pixel for conflicting classes. A conflict pixel is labeled as the class that has the highest normalized probability for the pixel compared to other classes.

SVM as non-parametric classifier do not calculate a probability for pixels. The distance between conflict pixel vectors and separating hyperplanes of classes in the feature space can be calculated to compare reliability of classification of a pixel as diverse classes. The most misclassification is expected in the marginal area of neighboring classes. Therefore, the larger the distance becomes, the more reliable are the classification results. A conflict pixel is labeled as the class, whose hyperplane in its classification is the furthest one from the pixel. These distances must be normalized similar to the maximum likelihood probabilities.

Results showed that about 0.5% of the control samples are misclassified by the combination rule of MLC whereas 3% of the control samples are misclassified by the combination rule of SVM. It means that about 96% of MLC conflicting pixels and about 70% of SVM conflicting pixels are correctly classified by the combination rules. It indicates that MLC can more effectively solve the conflict problems between independent classification processes.

5.2.4 Multi-Temporal Classification of Calibrated Data

Pixels of a calibrated radar image represent the backscattering coefficient (σ^0) of the corresponding target area. Calibration is especially necessary if radar data of diverse sensors must be compared or processed together. Data of this study is from three swaths of the ENVISAT sensor. Calibration coefficients of the three swaths slightly differ from each other. Hence, the influence of calibration on classification by MLC is tested.

First, we compare calibrated images with amplitude images to explain the changes in results of classification introduced by calibration. Table 5.7 represents the calibration coefficients (k) of the three swaths. Each swath corresponds to a specified range of incident angles (α).

As explained in Chapter 4, the backscattering coefficient (σ^0) is calculated as:

$$\sigma^0 = \frac{DN^2}{K}\sin(\alpha)$$

Hence, the relation $\frac{\sin\alpha}{K}$ defines the conversion from DN^2 to backscattering coefficient. The possible range of values for $\frac{\sin\alpha}{k}$ of three swaths are listed in Table 5.7. The backscattering coefficient is usually given in decibels:

$$\sigma^0_{db} = 10\log_{10}(\sigma^0)$$

Swath	k	Min. α	Max. α	($\sin\alpha / k$) at min. α	($\sin\alpha / k$) at max. α
IS5	949245	35.8	39.4	6.2E-07	6.7E-07
IS6	944449.875	39.1	42.8	6.7E-07	7.2E-07
IS7	1130383.875	42.5	45.2	6.0E-07	6.3E-07

Table 5.7 External calibration constants of ENVISAT swaths IS5, IS6, and IS7 (calibration values may be updated by ESA).

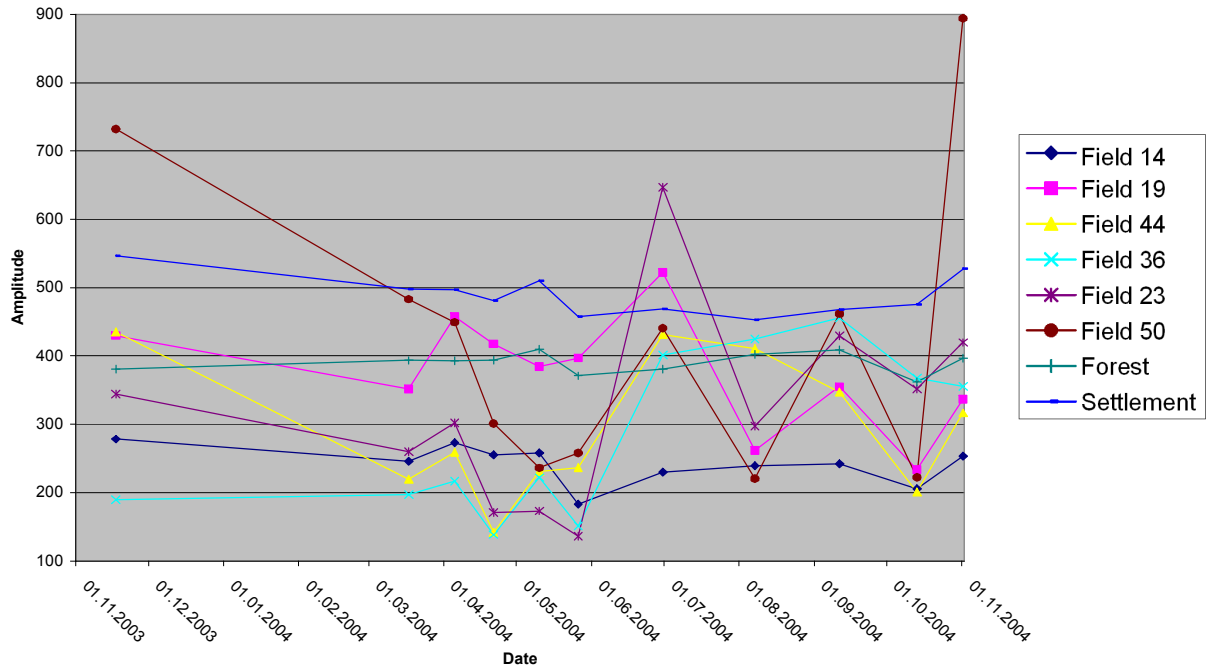

Figure 5.6 Mean amplitude values of VV polarization for some sample areas

The small difference between the values for $\frac{\sin\alpha}{k}$ of the three swaths cause small changes in relations between swaths (Figure 5.8). Plots of amplitude versus backscattering show the almost parallel lines close to each other for swaths IS5, IS6, and IS7. This effect can be seen comparing diagrams of calibrated data (Figures 5.1 and 5.2) with amplitude images (Figures 5.6 and 5.7), too.

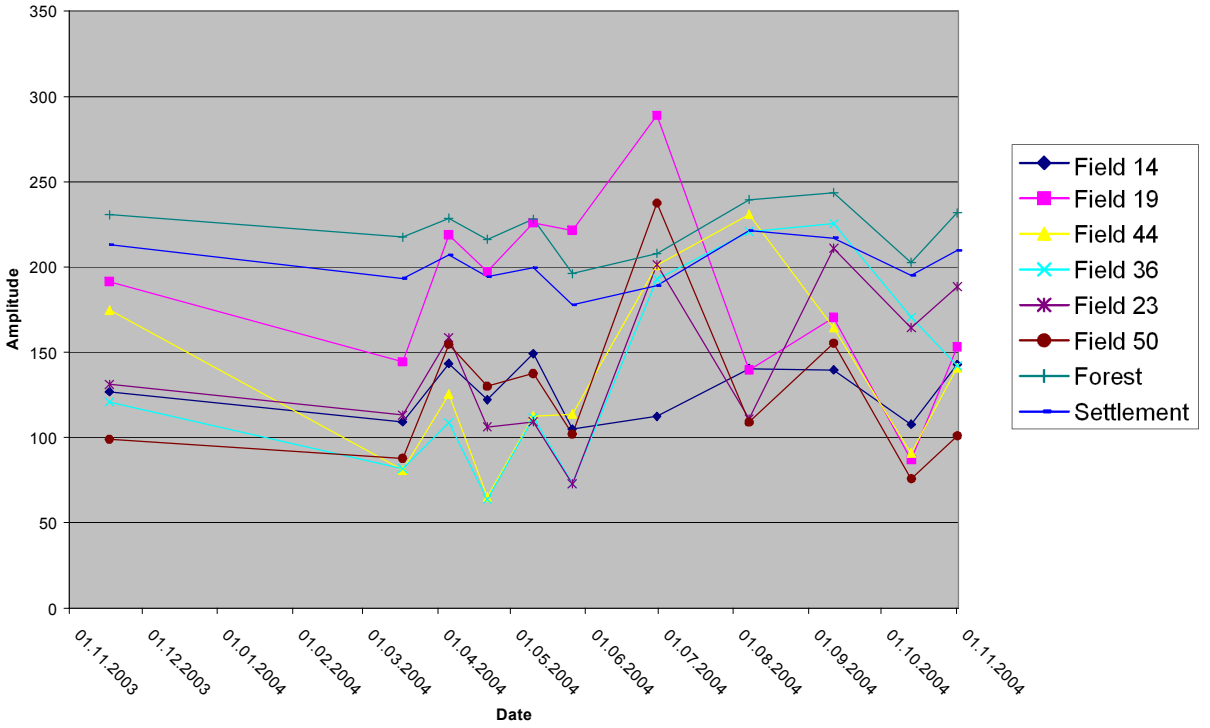

Figure 5.7 Mean amplitude values of VH polarization for some sample areas

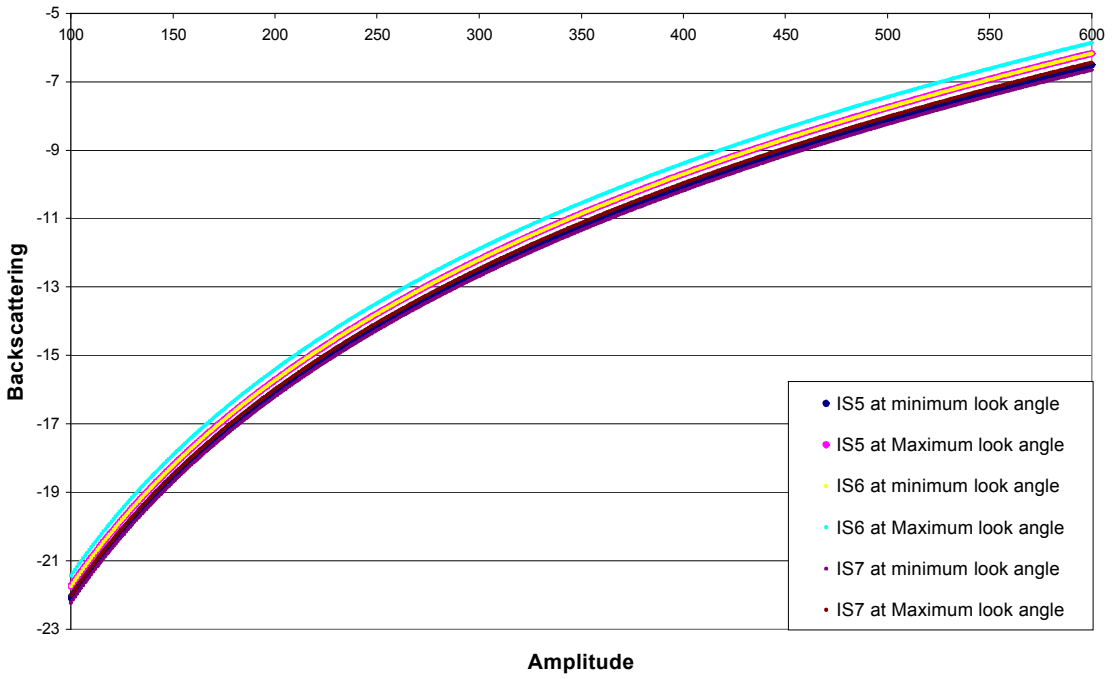

Figure 5.8 Plot of conversion from amplitude to backscattering by calibration of swaths IS5, IS6, and IS7 of ENVISAT data.

Figure 5.8 indicates that for the classification the only important change is the different distribution pattern of the calibrated data. Changes in data distribution primarily affect parametric classifiers such as MLC, but this does not explicitly mean that calibration improves accuracy of classification.

The overall accuracy of classification of calibrated data remains almost equal to the classification of amplitude data (compare Tables 5.6 and 5.8), whereas producer accuracies change diversely. This reflects the impression of calibrated data distribution on classification. The diverse changes of producer accuracies are due to the data distribution pattern of calibrated data which differs from amplitude data.

		Reference Data (Pixel)									
	Class names	Others	Potato	Summer Barley	Asparagus	Pasture	Winter Barley	Winter Rye	Sugar beets	Sum	User's accuracy %
Classified Data (Pixel)	Others	-	0	33	42	6	45	61	17	205	-
	Potato	30	1930	0	0	0	0	6	52	2017	96
	Summer Barley	20	0	1052	0	143	0	113	6	1334	79
	Asparagus	2	0	3	394	1	0	0	0	400	99
	Pasture	3	0	19	3	323	0	8	0	357	91
	Winter Barley	0	0	0	0	0	900	16	2	918	98
	Winter Rye	1	8	3	0	3	45	515	0	575	90
	Sugar beets	26	129	6	286	0	21	1	622	1090	57
	Sum	82	2067	1115	725	476	1012	720	699	6814	
Producer's accuracy %		-	93	94	54	68	89	72	89	Overall = 84	

Table 5.8 Error matrix of multi-temporal classification by MLC. Data is calibrated and matched to the crop calendar.

Overall accuracy is not significantly changed by calibration since accuracy of some classes increase and some classes decrease by calibration. These facts may explain the insignificant difference between overall accuracy of classification using calibrated and amplitude data.

KHAT statistics (Table 5.12) confirm the low confidence level of the difference between classifications of calibrated and amplitude data.

All the classification processes of this study except the classification of the Table 5.8 are based on amplitude data.

5.2.5 Matching to Crop Calendar and Classification by MLC

An error matrix of classification by MLC is provided in Table 5.6 As explained in section 5.2.2 multi-temporal data of the error matrix 5.6 is matched to the crop calendar before classification. i.e. images taken in the phenological period of each crop are stacked and classified for the crop. Hence, each crop is classified via a classification that is independent of classifications for other crops. One multi-temporal data set may be classified for crops having similar growth periods but different multi-temporal data sets for the crops with diverse growth periods.

Another simple approach that is frequently implemented is to classify images of all available dates for all classes in a single classification (Karjalainen 2008). This is multi-temporal classification without matching to the crop calendar. This method has the advantage that only one classification is performed for all classes; no information about crop calendar is required, and no combination after classification is necessary. Table 5.9 represents the error matrix of a classification using multi-temporal data set without matching to the crop calendar by MLC.

Overall accuracy of the classification without matching to the crop calendar at 79% is 5% less than the classification matched to the crop calendar. However, classification for summer barley, pasture, and sugar beet is more accurate without matching to the crop calendar. These classes are partly misclassified as fallow, willow, and rape (represented as others in error matrix) by the classification matched to the crop calendar.

		Reference Data (Pixel)									
	Class names	Others	Potato	Summer Barley	Asparagus	Pasture	Winter Barley	Winter Rye	Sugar beets	Sum	User's accuracy %
Classified Data (Pixel)	Others	-	0	0	0	9	0	0	0	9	-
	Potato	0	1980	0	47	0	0	0	0	2027	98
	Summer Barley	0	0	936	8	7	0	2	0	954	98
	Asparagus	1	0	2	402	0	0	0	0	405	99
	Pasture	0	0	5	0	457	0	20	0	482	95
	Winter Barley	0	0	2	0	1	367	41	16	426	86
	Winter Rye	0	0	56	0	4	9	559	0	629	89
	Sugar beets	0	95	113	268	1	626	95	673	1871	36
	Sum	1	2075	1114	725	479	1002	717	688	6801	
Producer's accuracy %		-	95	84	55	95	37	78	98	Overall accuracy= 79	

Table 5.9 Error matrix of multi-temporal classification by maximum likelihood classifier. Data is not matched to the crop calendar.

Only 9 pixels (of control samples) of the classification without matching to the crop calendar are misclassified as others whereas 391 pixels (mainly from grains and sugar beet control samples) are misclassified as others using data matched to the crop calendar. Fallow, willow, and pasture fields are mainly covered by grass that is somewhat similar to grains. The fields of fallow, willow, and pasture have stable coverage that lasts often longer than grain on the field but grain fields are harvested in summer and may have no vegetation coverage or intermediate plants before and after cultivation period. This important difference between grains and grass fields can be considered in a classification that includes images before and after cultivation period of grains. This condition is fulfilled by the classification without matching to the crop calendar. Therefore, grains especially summer barley are partly misclassified as willow, fallow,

and pasture by the classification matched to the crop calendar, whereas this misclassification does not happen in a classification of data not matched to the crop calendar. A similar condition exists for sugar beet, potato and rape (represented as others in error matrix). Phenological periods of sugar beet, potato, and rape are mainly overlapped and their structure with high water content and extent leaves (compared to grains) is somewhat similar to each other. Backscattering of these fields before and after cultivation period reduces some of their misclassification in a classification without matching to the crop calendar, whereas the classification of data matched to the crop calendar does not consider the data before cultivation and after harvest. Therefore, sugar beet and potato control samples are less accurately classified by classification when matched to the crop calendar.Misclassification between evaluated crops is reduced by matching to the crop calendar so that the overall accuracy is improved with data matched to the crop calendar. Despite more mixture with grass fields (willow, fallow, pasture), winter grain samples are more accurately classified using data matched to the crop calendar because their misclassification as sugar beet is reduced.

All in all, classification for crops using data matched to the crop calendar is more accurate. It is advisable to include an acquisition directly after harvest in multi-temporal classification matched to the crop calendar. Thereby, misclassification of classes having overlapped growth periods may decrease.

Fields may be covered by rests (remaining parts of harvested plants), wild plants, intermediate crops, or nothing after harvest. Hence, dividing into some sub-classes based on the field coverage after harvest is necessary if the data after harvest is included in the classification. Unfortunately, the small sample size of this study does not allow for this investigation.

5.2.6 Classification by Support Vector Machines and Matching to Crop Calendar

Multi-temporal classification by SVM was evaluated for four different kernel types with default parameters of the software ENVI and with Image SVM software. ImageSVM is developed and provided free of charge by “Geomatics Lab of Humboldt University of Berlin” (Schiefer S. et al., 2006). It uses Radial Basis kernel (see Chapter 2) and optimizes the penalty and generalization parameters for each class using a grid search.

Interior accuracy (correctly classified training samples) of classification by four kernel types: linear, polynomial, radial basis function (RBF), and sigmoid using default values of ENVI software was investigated. The values of interior accuracy indicate very poor accuracy of classification. These results indicate that the proper kernel parameters are more important than the kernel type in a SVM classification. To improve accuracy of SVM, kernel parameters, which determine the trade-off between cost of misclassification and fitting on training data, have to be optimized. Any kernel needs at least two parameters (Penalty and generalization parameters (see Chapter 2.3)) that can be set out for each class. An automatic grid search of parameters is a practical alternative for time-consuming manual attempts.

		Reference Data (in Pixel)									
	Class names	Others	Potato	Summer Barley	Asparagus	Pasture	Winter Barley	Winter Rye	Sugar beets	Sum	User's accuracy %
Classified Data (in Pixel)	Others	-	59	441	18	42	14	46	149	770	-
	Potato	0	1849	0	14	0	0	0	58	1921	96
	Summer Barley	0	0	663	6	29	0	75	0	772	86
	Asparagus	9	0	5	681	0	0	0	0	695	98
	Pasture	19	0	6	0	406	0	10	0	441	92
	Winter Barley	0	0	0	0	0	916	53	10	979	94
	Winter Rye	2	1	0	0	2	40	534	4	582	92
	Sugar beets	3	166	0	6	0	32	0	467	674	69
	Sum	33	2075	1114	725	479	1002	717	688	6834	
Producer's accuracy %		-	89	59	94	85	91	74	68	Overall = 807	

Table 5.10 Error matrix of multi-temporal classification by SVM with grid search optimization parameters. Data is matched to the crop calendar and training samples of each class are merged before classification.

Possible combinations of potentially suitable parameters for a kernel are tested to optimize parameters for individual classes based on the binary concept of SVM such the training samples are best classified. Table 5.10 shows error matrix of a classification by SVM with RBF kernel and parameters that are optimized by a grid search for individual classes.

Classification accuracy is obviously improved such that strong overall agreement (Landis et al. 1977) of about 81% is achieved using the RBF kernel with grid search. Almost 100% of training samples area is correctly classified.

		Reference Data (Pixel)									
	Class names	Others	Potato	Summer Barley	Asparagus	Pasture	Winter Barley	Winter Rye	Sugar beets	Sum	User's accuracy %
Classified Data (Pixel)	Others	-	5	166	44	69	17	19	389	709	-
	Potato	0	2021	4	31	0	4	4	4	2067	98
	Summer Barley	7	0	845	36	0	0	0	0	888	95
	Asparagus	4	0	0	610	0	0	0	0	614	99
	Pasture	23	0	6	0	410	0	18	0	457	90
	Winter Barley	0	0	0	0	0	699	17	3	719	97
	Winter Rye	0	1	93	0	0	9	660	0	763	86
	Sugar beets	3	48	0	4	0	273	0	293	620	47
	Sum	37	2075	1114	725	479	1002	717	688	6837	
Producer's accuracy %		-	97	76	84	86	70	92	43	Overall = 81	

Table 5.11 Error matrix of multi-temporal classification by SVM. Data is not matched to the crop calendar.

The overall accuracy of SVM with RBF kernel and grid search is 3% points lower than MLC. Despite the low difference of overall accuracy for SVM and MLC, producer accuracies of individual classes show up to 25% variation between SVM and MLC. Asparagus is classified more accurately by SVM. This may be because of the fact that asparagus fields in different cultivation directions with wide and high (180 x 50cm) cultivation rows affect the distribution of the class data in feature space. MLC is strongly influenced by the distribution of data and performs less accurate than SVM that is not affected by statistical inhomogeneities of asparagus samples. Also winter barley is classified at 5% more accurately by SVM than by MLC. It was discussed in previous sections that winter barley is classified more accurately using separate samples than merged samples because of inhomogeneities in its samples. Similar to asparagus, the inhomogeneities affect statistical data distribution in the feature space. As a result, non-parametric SVM perform more accurately than parametric MLC for classes with internal inhomogeneities in data distribution.

Altogether, MLC is a little more accurate than SVM with data matched to the crop calendar, but some crops are better classified by SVM. KHAT statistics (Table 5.12) confirm this result at a confidence level over 99%.

Another test carried out is the SVM classification without matching to the crop calendar. The overall accuracy of SVM classification without matching to the crop calendar shows no significant difference in comparison with data matched to the crop calendar. In contrast, producer accuracies of classes indicate meaningful differences. Grains (except winter barley), potato, and sugar beet are more accurately classified without matching to the crop calendar. Similarly, we could observe misclassification of these classes as classes fallow, willow, and rape by the MLC classification with data matched to the crop calendar. However, some other misclassifications are prevented by matching to the crop calendar of MLC, which could substitute the misclassification as willow, fallow, and pasture. So MLC on the whole is more accurate with data matched to the crop calendar. In contrast, SVM as non-parametric classifier are less influenced by feature (date) selection (Watanachaturaporn et al. 2004). Although the misclassification of some classes is reduced with SVM classification matched to the crop calendar, overall accuracy does not increase because of low producer accuracy of grains, potato, and sugar beets. All in all, matching to the crop calendar does not improve accuracy of classification by SVM. Inclusion of an acquisition after harvest may increase producer

accuracy of grains, sugar beet, and potato such the overall accuracy increases (as discussed for MLC, too). Kappa statistics (Table 5.12) indicate that matching to the crop calendar does not significantly affect the overall accuracy of classification by SVM.

5.2.7 Confidence of results

Tested methods yield different values of overall accuracy as the evaluation parameter of this study. The method that provides a classification at higher overall accuracy is assumed to be more accurate and more suitable than the other method for multi-temporal crop classification. The more interesting question is if the overall accuracies of two methods are different by chance or the difference reflects the significant different between the methods.

Significance tests of error matrices can be performed by KHAT statistics and presented as a confidence level (see Chapter 4). The confidence level of the difference between two error matrices indicates the probability to get the same result by another test of the methods.

Table 5.12 represents the significance tests of investigated methods. The tests indicate that MLC is more accurate than SVM at higher than 99% confidence level if data is matched to the crop calendar. In contrast, SVM are more accurate than MLC at higher than 99% confidence level if data is not matched to the crop calendar.

Matching to the crop calendar significantly improves accuracy of MLC, whereas SVM are insignificantly (at 40% confidence level) less accurate using data matched to the crop calendar.

These results agree with the theory that parametric classifiers are more affected by feature selection than non-parametric classifiers. Irrelevant data (i.e. images from dates beyond the phenological period) confuse a parametric classifier whereas non-parametric classifiers are less affected by irrelevant data.

Calibration of amplitude images insignificantly affects overall accuracy of MLC at weak confidence level of 91%. This is because of the small differences between calibration coefficients of swaths IS5, IS6, and IS7 of ENVISAT sensor. Therefore, calibration results in a change in data distribution and not in relations between different swaths. This may improve accuracy of some classes and decrease accuracy of some other classes but no exception can be made about a change in overall accuracy.

Comparison	Method	KHAT	Variance (KHAT)	Z	Confidence level %
Matched to the crop calendar	MLC	0.679	2.72301E-05	3.080585	99.79
	SVM	0.656	3.0194E-05		
Not Matched to the crop calendar	MLC	0.624	3.31251E-05	4.520169	99.9994
	SVM	0.660	2.95772E-05		
MLC	Matched to the crop calendar	0.679	2.72301E-05	7.085413	99.99999
	Not Matched to the crop calendar	0.624	3.31251E-05		
SVM	Matched to the crop calendar	0.656	3.0194E-05	0.529223	40.33
	Not Matched to the crop calendar	0.660	2.95772E-05		
Calibration	Calibrated	0.667	2.75788E-05	1.721485	91.48
	Not calibrated	0.679	2.72301E-05		

Table 5.12 Significance tests of implemented methods.

5.3 Summary

Results of the implemented methods are presented and discussed in this Chapter. First, backscattering of crop fields is investigated as a function of surface coverage, moisture, incident angle, and soil. For this investigation, statistics of seven sample areas in the study area are used. Stable areas of settlements, forest, and pastures experience little changes in backscattering in the course of time. In contrast, backscattering of agricultural fields strongly depends on the vegetation coverage and type. In winter, when the fields are free of plants, soil type, soil moisture, and incident angle control the backscattering. Backscattering of fields is

controlled by vegetation coverage in summer. Plants often increase the backscattering of fields, although, some exceptions are observed and discussed.

Multi-temporal classification is investigated together with different speckle filters and data combinations. Speckle suppression and merging similar samples improve accuracy of classification for most crops.

Since all SAR images are from ENVISAT sensor, calibration does not significantly influence classification accuracy of multi-temporal data. Calibration before classification of multi-source SAR data is often necessary. Theoretical discussion and significant tests indicate that calibration does not improve accuracy of classification if data comes from three swaths IS5, IS6, and IS7 of the ENVISAT.

Matching to the crop calendar increases accuracy of MLC whereas SVM overall accuracy is not meaningfully changed due to matching to the crop calendar. However, matching to the crop calendar changes producer's accuracies of SVM classification.

The best overall accuracy is achieved by MLC with despeckled data matched to the crop calendar. However, SVM have the advantage that they are more accurate than MLC without matching to the crop calendar. Hence, SVM classifier is advisable if multi-temporal information on agricultural test fields is lacking.

Chapter 6

6 Conclusions

Multi-temporal classification of ASAR ENVISAT data is implemented for agricultural monitoring. The method uses stacked multi-temporal data for crop classification. The main objective of the study is to investigate methods for multi-temporal classification of SAR data. Some ideas that are considered to strongly influence multi-temporal crop classification are investigated in this study.

The method of multi-temporal crop classification works based on the regular temporal changes of agricultural fields because of cultivation activities and plant growth. This changes radar backscattering and allows the SAR images to be classified for crops.

Classification of calibrated data is investigated in the study. Since all the classified images are from the same sensor and the calibration coefficients of swaths do not significantly alter, no significant improvement in classification accuracy due to calibration is observed.

Furthermore, it is shown that speckle suppression improves classification accuracy and different filters have diverse advantages. Matching to the crop calendar improves accuracy of MLC whereas SVM classification is not significantly improved by matching to the crop

calendar. The result corresponds to the theory that non-parametric classifiers are less influenced by feature selection because the irrelevant data disturb non-parametric classifiers less than parametric classifiers.

Significant tests explicate classification results by KHAT statistics. Implemented methods are compared and it is shown that some methods do not meaningfully differ from each other.

The sample size of the study satisfies the recommended minimum training sample size for evaluated crops but the training sample size of some rare crops (not included in accuracy assessment due to the lack of control samples) is too small. In addition, the training sample size of only a few classes reaches the recommended desirable sample size. Hence, classification accuracy is expected to increase significantly using more training samples.

The available small sample size of most crops is too small to be separated as training and control samples and to satisfy minimum training sample size. Therefore, one sample field per crop could be used as control sample for most crops in order to keep training samples size large enough. One field as the control sample of most crops is smaller than the recommended control sample size at the desired confidence level. Hence, each classification method is repeated three times; each time a new sample field per class is considered as control sample. In this way, the control sample size is enlarged for all evaluated classes such that the minimum control sample size is satisfied for all evaluated classes. The question rises if the confidence level of accuracy by control fields of repeated classifications is the same as the confidence level of accuracy by control fields of a single classification with the same control sample size. This issue must be investigated and recalculation of confidence levels may become necessary. Altogether, providing a larger control sample size is advisable in order to achieve the desired confidence level of accuracy assessment by a single classification.

Considering the spatial resolution of ENVISAT data, the study area is too small to provide enough training and control samples. The small sample size of this study, which satisfies minimum recommendations, covers 14% of agricultural extent of the study area, whereas, less than 10% of study areas are usually sampled by other researchers. It indicates a high density of samples in the study area. This high density of samples increases overall accuracy because of the higher spatial correlation between training and control samples. First, the reported accuracy can only be compared with difficulty to other studies that are usually based on less dense

samples. Second, this sample density cannot be justified for commercial projects in larger areas, whereas the methods may perform less accurate with less sample density. Therefore, investigation of methods in a larger area is recommended so that the desirable sample size covers 5-10% of the study area. This problem is reduced if data with higher spatial resolution are classified. A pixel is often considered as the spatial unit of remote sensing data, hence desirable sample size of data with smaller pixel size (higher spatial resolution) is satisfied by a smaller area.

Higher spatial resolution allows smaller fields to be sampled and classified. Therefore, classification results are valid for small fields as well as large fields. In addition, sample selection becomes more flexible. Thus, classification of high resolution data is recommended for agricultural monitoring.

C-band signal of ENVISAT passes partly through vegetation and hence is often affected by the earth's surface beneath vegetation coverage. Higher frequency signals (e.g., in X-band) are more reflected by vegetation and less affected by earth's surface. Therefore, SAR data of higher frequencies is expected to be more suitable for crop monitoring. However, higher frequencies are more sensitive against atmospheric effects that can affect classification accuracy.

Two classifiers are tested in this study, whereas many other classifiers with different capabilities can be implemented for the introduced methods of this study. Some classifiers such as neural networks are frequently investigated for multi-temporal crop classification by other researchers, but other classifiers need to be investigated.

The method of supervised classification depends strongly on ground truth, which is often the most expensive part of such studies. A model that relates radar backscattering to crop types can be implemented less dependent on training samples. Such methods should consider environmental parameters (Soil, weather, moisture), and additional knowledge (season, plants growing phases, and cultivation consequence). SAR data is especially suitable for this aim, due to the constant acquisition conditions. The antenna of a monostatic sensor transmits always the same amount of energy in controlled direction. Therefore SAR data is (almost) independent from daylight, daytime, variations of natural illumination, and the atmosphere. The most important affecting parameter for SAR data is the land cover. Known mathematical models

such “Markov chain” can be used for instruction of the model that relates the pixel values to land cover.

An important advantage of accuracy assessment is the possibility of comparison between methods. Unfortunately, some issues in the field of remote sensing data classification are not standardized so that comparing methods and data becomes sometimes difficult because of different accuracy assessment methods. One problem is about the data unit. Pixel is often considered as a data unit but some researchers use clusters of pixels or polygons as data unit. In addition, the relation between pixel size and spatial resolution varies for different sensors. Therefore, sample size of different researchers may differ because of selected data unit or sensor, which affects the classification and makes a comparison between different studies difficult. Defining standards for data unit of remote sensing data and clarifying the influence of relation between pixel size and resolution on classification may reduce this problem.

Another problem in the field of accuracy assessment of remote sensing classification is the lack of a standard training sample size. Some experimental recommendations are provided but no global standard training sample size is determined. Hence, comparison of different studies often raises a question about sample size which usually complicates comparison between methods. Spatial statistics especially in the field of accuracy assessment need to be investigated and developed.

References

Alparone L., Baronti S., Carla R., Puglisi C, 1992, “A new adaptive digital filter for SAR images: test of performance for land and crop classification on Montespertoli area” Proceedings of the International Geoscience and Remote Sensing Symposium (/GARSS'92), Houston, TX, May 1992 (Piscataway, NJ: I.E.E.E.), pp. 899-901.

Aizerman M., Braverman E., Rozonoer L., 1964, “Theoretical foundations of the potential function method in pattern recognition learning.”, Automation and Remote Control, 25:821-837.

Anderson T.W., Bahadur R.R., 1966, “Classification into two multivariate normal distributions with different covariance matrices”, Ann. Math. Stat., 33:420-431.

Barrett E.C., Curtis L.F., 1992, "Introduction to environmental remote sensing", Third Edition, ISBN: 0 412 371707.

Bishop C.M., 2007, “Pattern Recognition and Machine Learning”, by Springer. ISBN-IO: 0-387-31073-8, ISBN-13: 978-0387-31073-2

Blaes X., Vanhalle L., Defourny P., 2005, “Efficiency of crop identification based on optical and SAR image time series”, Remote Sensing of Environment, 96, 2005, 352-365.

Ban Y., Howarth P. J., 1999, “Multitemporal ERS-1 SAR data for crop classification: A sequential-masking approach”. Canadian Journal of Remote Sensing, 25(5), 438– 447.

Boerner, W.M., Mott H., Lüneburg E., Livingstone C., Brisco B., Brown R.J., Paterson J.S., 1998 “Polarimetry in Radar Remote Sensing: Basic and Applied Concepts”, Chapter 5 in F.

Boser B.E., Guyon I., Vapnik V.N., 1992, “A training algorithm for optimal margin classifiers.” In Proceedings of the Fifth Annual Workshop of Computational Learning Theory, 5, 144-152, Pittsburgh, ACM.

Bouman B.A.M., Uenk D., 1992, “Crop classification possibilities with radar in ERS-1 and JERS-1 configuration”, Remote Sensing of Environment 40 (1992) (1), pp. 1–13.

Brenning A., Kaden K., Itzerott S., 2006, “Comparing classifiers for crop identification based on multitemporal Landsat TM/ETM data” 2nd Workshop of the EARSeL Special Interest Group on Land Use & Land Cover (Bonn 2006). 27. – 30. September 2006. CD-ROM.

Brisco B., Brown R.J., 1995, “Multidate SAR/TM synergism for crop classification in western Canada”, Photogrammetric Engineering and Remote Sensing 61 (1995) (8), pp. 1009–1014.

Bruzzone L., Marconcini M., Wegmuller U., Wiesmann A., 2004, “An advanced system for the automatic classification of multitemporal SAR images”, Geoscience and Remote Sensing, IEEE Transactions on Volume 42, Issue 6, June 2004 Page(s):1321 – 1334.

Burges C.J.C., 1998, "A Tutorial on Support Vector Machines for Pattern Recognition". Data Mining and Knowledge Discovery 2:121 - 167, 1998.

Camps-Valls G., Gomez-Chova L., Munoz-Mari J., Rojo-Alvarez J.L., Martinez-Ramon M., 2008, “Kernel-Based Framework for Multitemporal and Multisource Remote Sensing Data Classification and Change Detection”, Geoscience and Remote Sensing, IEEE Transactions on Volume 46, Issue 6, June 2008 Page(s):1822 – 1835.

Chen D.M., 2008, “A Standardized Probability Comparison Approach for Evaluating and Combining Pixel-based Classification Procedures”, Photogrammetric Engineering & Remote Sensing, Vol. 74, No. 5, May 2008, pp. 601-610.

Cloude S.R., 1986, ”Group Theory and Polarisation Algebra”, Optic, Vol. 75, No. 1, pp. 26-36.

Cloude S.R, 1992, ”Uniqueness of Target Decomposition Theorems in Radar Polarimetry”, Direct and Inverse Methods in Radar Polarimery, Kluwer Academic Publishers, Netherlands, pp. 267-298.

Cloude S.R., Pottier E., 1995 ”Concept of Polarisation Entropy in Optical Scattering”, Optical Engineering, Vol. 34, No. 6, pp. 1599-1610.

Congalton R. and K. Green. 1999. “Assessing the Accuracy of Remotely Sensed Data: Principles and Practices”. CRC/Lewis Press, Boca Raton, FL. 137 p.

Cortes C., Vapnik V., 1995, “Support-Vector Networks”, Machine Learning, 20, 273-297 (1995)

Courant R., Hilbert D., 1953, “Methods of Mathematical Physics”, Interscience, New York

Del Frate F., Schiavon G., Solimini D., Borgeaud M., Hoekman D.H., Vissers M.A.M., 2003, “On the potential of multi-polarization and multi-temporal C-band SAR data in classifying crops”, Geoscience and Remote Sensing Symposium, 2003. IGARSS '03. Proceedings. 2003 IEEE International, Volume: 4, On page(s): 2195- 2196 vol.4.

Duda R.O., Hart P.E., Stork D.G., 2000 “Pattern Classification”, second edition, by WILLY-INTERSCIENCE, ISBN 0471056693.

Durand J.M., Gimonet B.J., Perbos J.R., 1987, “ S A R data filtering for classification,” IEEE Trans. on Geoscience and Remote Sensing, Vol. GE-25, No. 5, pp. 629-637, 1987.

ESA, 1998, “ENVISAT ASAR Science and Applications”, November 1998, SP1225

ESA, 2002, “ENVISAT ASAR Product Handbook”, ESA August 2002.

Ferrazzoli, P., Guerriero, L., Quesney, A., Taconet, O., Wigneron, J.-P., 1999 “Investigating the capability of C-band radar to monitor wheat characteristics” IEEE Transactions on Geoscience and Remote Sensing 37 (1999) (2), pp. 960–968.

Foody G.M., Mac Culloch M.B., Yates W.B., 1994, “Crop classification from C-band polarimetric radar data”, International Journal of Remote Sensing 15 (1994) (14), pp. 2871–2885.

Frost V.S., Stiles J.A., Shanmugan K.S., and Holtzman J.C., 1982, ”A model for radar mages and its application to adaptive digital filtering of multiplicative noise,” IEEE Trans. Pattern Analysis and Machine Intelligence, vol 4, no. 2, pp. 157-166, March 1982.

Henderson F.M., Lewis A.L., 1998, “Principles & Applications of Imaging Radar”, Third edition, vol. 2, by John Willy & Sons, Inc.

Hochschild V., Weise C., Selsam P., 2005, “Die Aktualisierung der digitalen Grundkarte Landwirtschaft in Thüringen mit Hilfe von Fernerkundungsdaten”, DGPF 3/2005 PP. 201-208.

Hughes G., 1968, “On the mean accuracy of statistical pattern recognizers”, Information Theory, IEEE Transactions on, Publication Date: Jan 1968, Volume: 14, Issue: 1, On page(s): 55- 63.

Karjalainen M., Kaartinen H., Hyyppä J., 2008, “Agricultural Monitoring Using ENVISAT Alternating Polarization SAR Images”, Photogrammetric Engineering & Remote Sensing, Vol.74, No.1, January 2008, pp. 117-126.

Kostinski A.B.**,** Boerner W.M., 1986 ”On the Foundations of Radar Polarimetry”, IEEE Transactions on Antennas and Propagation, Vol. 34, No. 12, pp. 1395-1404.

Jensen J.R., 1996, “Introductory digital image processing”, Second edition, by Prentice-Hall, Inc.

Lee J.S., 1980, “Digital image enhancement and noise filtering by use of local statistics”, IEEE Trans. Pattern Analysis and Machine Intelligence, vol. 2, no. 2, pp.165-168, March 1980.

Lee J.S., 1983, “Digital image smoothing and the sigma filter”, Computer Vision, Graphics, and Image Processing, Volume 24, Issue 2, November 1983, Pages 255-269

Lee J.S., Hoppel K.W., Mango S.A., Miller A.R., 1994 “Intensity and phase statistics of multilook polarimetric and interferometric SAR imagery”, IEE Trans. Geosci. Remote Sensing, vol. 32. pp. 1017-1028, Sept. 1994.

Lopes A., Touzi R. and Nezry E., 1990, "Adaptive speckle filters and Scene heterogeneity", IEEE Transaction on Geoscience and Remote Sensing, Vol. 28, No. 6, pp. 992-1000, Nov. 1990.

Mercer J., 1909, "Functions of positive and negative type and their connection with the theory of integral equations". Philosophical Transactions of the Royal Society A 209: 415–446. doi:10.1098/rsta.1909.0016

Mott, H., 1992 “Antennas for Radar and Communications: A Polarimetric Approach”, John Willey & Sons, New York.

Peak W.H., Oliver T.L., 1971, “The Response of Terrestrial Surfaces at Microwave frequencies”, Ohio state university technical report 2440-7, Columbus, Ohio.

Redslob M., 2000, “Effektive Informationserhebung durch GIS-gestützte Radarfern-erkundung - dargestellt am Beispiel des Niedersächsischen Moorschutzprogramms” A. & C. ROESERATH: Naturschutz und Landschaftsplanung - Moderne Technologien, Methoden

und Verfahrensansätze, Festschrift zum 60. Geburtstag von Prof. Dr. Hartmut Kenneweg.- Mensch & Buch Verlag, Berlin S. 167 – 178.

Reigber A., 2001, "Airborne Polarimetric SAR Tomography", Dissertation, University Stuttgart, Faculty civil engineering and surveying.

Richards J.A., JIA Xiuping, 1999, "Remote Sensing Digital Image Analysis. An Introduction", 3rd revised and enlarged edition by Springer ISBN 3 540 64860 7.

Rosich B., Meadows P., 2004, "Absolute Calibration Of Asar Level 1 Products Generated With Pf-ASAR", REFERENCE: ENVI-CLVL-EOPG-TN-03-0010.

Saich P., Borgeaud M., 1999, "The inter-year stability of ERS agricultural crop signatures" (Flevoland 1993-1996), Geoscience and Remote Sensing Symposium, 1999. IGARSS '99 Proceedings. IEEE 1999 International Volume 4, 28 June-2 July 1999 Page(s):2342 - 2344 vol.4.

Sanchez J.M.L., 1999, "Analysis and Estimation of Biophysical Parameters of Vegetation by Radar Polarimetry", Dissertation, University Valencia.

Sommerfeld A., 1895 "Mathematische Theorie der Beugung", Habilitation, Universität Göttingen.

Schneider D.T., 1994, "Möglichkeiten und Grenzen der spektralen Trennung ackerbaulicher Oberflächentypen – eine Abschätzung anhand spektroskopischer Untersuchungen über die Vegetationsperiode", Mangstl., München, 4. Auflage.

Schotten C.G.J., Van Rooy W.W.L., Janssen L.L.F., 1995, "Assessment of the capabilities of multi-temporal ERS-1 SAR data to discriminate between agricultural crops", International Journal of Remote Sensing 16 (1995) (14), pp. 2619–2637

Seynat C., Hobbs S., 1998, "Crop Parameter Retrieval with Multi-Temporal Coherence Images", Proceedings of the 2nd Intern. Workshop on Retrieval of Bio- & Geo- Physical Parameters from SAR Data for Land Applications. ESA/ESTEC, pp. 191-196, Noordwijk, Oct. 1998.

Story M. and Congalton R., 1986, Accuracy assessment: A user's perspective, Photogrammetric Engineering and Remote Sensing 52 (1986), pp. 397–399.

Swain P.H. and Davis S.M., 1978, "Remote sensing: the quantitative approach", N.Y., McGraw-Hill.

Tavakkoli Sabour S. M., Lohmann P., Soergel U., 2007, "Monitoring Agricultural Activities using Asar ENVISAT Data", esa Envisat Ssymposium. Montreux, 2007, 6S., CD.

Tortora R, 1978, "Anote on sample size estimation for multinomial populations", the American statistician. Vol. 32, No. 3 pp. 100-102.

Touzi R., Lopes A., Bouquet P., 1988 "A statistical and geometrical edge detector for SAR images," IEEE Trans. Geosc-i. Remote Sensing. vol. 26, no. 6, pp. 764-773, Nov. 1988.

Tso B., Mather P.M., 2001, "Classification methods for remotely sensed data", London, New York, Taylor & Francis.

Vapnik V.N. 1979, "Estimation of Dependences Based on Empirical Data [in Russian]". Nauka, Moscow,1979. (English translation: Springer Verlag, New York,1982).

Vapnik V.N., 1982, "Estimation of Dependences Based on Empirical Data", Addendum 1, New York: Springer-Verlag.

Waske B., Schiefer (van der Linden) S., 2006, "Classifying Segmented Multitemporal SAR Data from Agricultural Areas Using Support Vector Machines" Proceedings of the 2nd Workshop of EARSel SIG on Land Use and Land Cover, Bonn, Germany, Pages 48-54

Watanachaturaporn P., Arora M.K., Varshney P.K., 2004, "Evaluation of Factors Affecting Support Vector Machines for Hyperspectral Classification", American Society for Photogrammetry & Remote Sensing (ASPRS) 2004 Annual Conference. May 23-28, 2004, Denver, CO.

Watanachaturaporn P., Arora M.K., Varshney P.K., 2008, "Multisource Classification Using Support Vector Machines: An Impirical Comparison with Decision Tree an neural Network Classifiers", Photogrammetric Engineering and Rempte Sensing, Vol. 74, No. 2, Febraury 2008, pp. 239-246.

Yakam-Simen F., Nezry E., Zagolski F., 1998, "Early estimation of crop surfaces, and agricultural monitoring using RADARSAT data", Proceedings of the ADRO Final Symposium, 9 p., Montréal (Québec, Canada), 13-15 October 1998.

Curriculum vita – Seyed Mohammad Tavakkoli Sabour

Berufs und Ausbildung

Seit July 2008	Wissenschaftlicher Mitarbeiter im Bereich Altlastenuntersuchungen Anhand historischen Luftbilder
Seit September 2004	Promotion am Institut für Photogrammetrie und Geoinformation, Leibniz Universität Hannover
1999 bis 2003	Wissenschaftlicher Mitarbeiter bei "Transport Organisation" und "Wasserressouren Organisation" im Iran im Bereich GIS und Fernerkundung
1998 bis 2001	Masterstudium im Bereich GIS und Fernerkundung
1994 bis 1998	Bachelorstudium im Bereich Physische Geographie
1982 bis 1994	Schulbesuch im Mashad, Iran

Privat

July 2006	Geburt Sohn Ali
April 2003	Heirat mit Lida Arvin
31.12.1975	Geboren in Mashad, Iran

Danksagung

In diesem Kapitel möchte ich mich gern bei einigen Menschen bedanken, durch deren Hilfe diese Arbeit erst möglicht geworden ist.

Mein besonderer Dank richtet sich an:

meinen Doktorvater, Prof. Dr.-Ing. Christian Heipke, welcher meinen Eintritt und meine Promotion am IPI ermöglicht hat. Ich danke ihm für seine Hilfsbereitschaft und seine Zeit und Erfahrung, die er mir zur Verfügung gestellt hat. Des Weiteren habe ich von ihm sehr gute fachliche Hinweise erhalten.

die Korreferenten Prof. Dr.-Ing. Uwe Stilla und Prof. Dr.-Ing. Uwe Sörgel sowie die Korreferentin Prof. Dr.-Ing. Monika Sester, die sich trotz eigener hoher Arbeitsbelastung bereit erklärt haben, die Arbeit zu bewerten. Besonders bedanke ich mich bei Uwe Sörgel der im Laufe der Promotion mich fachlich beraten und motiviert hat. Auch besonderen Dank an Uwe Stilla, der diese Dissertation durch seine konstruktive Kritik und Vorschläge verbessert hat.

meine Kollegen am IPI. Die freundliche Atmosphäre und Zusammenarbeit am IPI bleibt mir als Vorbild für mein Leben, vor allem in der Karriere und Forschung. Ebenfalls, besonderen Dank richte ich an Herrn Dr. Peter Lohmann, der mir fachlich viel geholfen und mir immer wieder neue Wege gezeigt hat. Besonderen Dank richte ich auch an Dipl.-Ing. Ursula Wißmann, die sich um Aufnahme der Daten von Testfelder gekümmert hat. Ohne ihre Hilfe und Erfahrung wäre die Erfassung der Ground Truth nicht in der Qualität erfolgt.

meine Kollegen und Freunde, die Teile oder die gesamte Dissertation Korrektur gelesen haben. Sie sind: Dr.-Ing. Alexander Brzank, Dipl.-Ing. Jan Wegner, Dipl.-Ing. Petra Helmholz, Dipl.-Ing. Mareen Limbach und Peter Walton.

Wissenschaftliche Arbeiten der Fachrichtung Geodäsie und Geoinformatik der Leibniz Universität Hannover

(Eine vollständige Liste der Wiss. Arb. ist beim Geodätischen Institut, Nienburger Str. 1, 30167 Hannover erhältlich.)

Nr. 261	GERKE, Markus:	Automatic Quality Assessment of Road Databases Using Remotely Sensed Imagery. (Diss. 2006)
Nr. 262	KOCH, Andreas	Semantische Integration von zweidimensionalen GIS-Daten und digitalen Geländemodellen. (Diss. 2006)
Nr. 263	Festschrift:	125 Jahre Geodäsie (2006)
Nr. 264	WOLF, Karen Insa:	Kombination globaler Potentialmodelle mit terrestrischen Schweredaten für die Berechnung der zweiten Ableitungen des Gravitationspotentials in Satellitenbahnhöhe (Diss. 2007)
Nr. 265	RAGUSE, Karsten:	Dreidimensionale photogrammetrische Auswertung asynchron aufgenommener Bildsequenzen mittels Punktverfolgungsverfahren (Diss. 2007)
Nr. 266	HAMPE, Mark:	Integration einer multiskaligen Datenbank in eine Webservice-Architektur (Diss. 2007)
Nr. 267	ANDERS, Frauke:	Mustererkennung in Straßennetzwerken - Verfahren zur Interpretation von Vektordaten. (Diss. 2007)
Nr. 268	HESSE, Christian:	Hochauflösende kinematische Objekterfassung mit terrestrischen Laserscannern (Diss. 2007)
Nr. 269	NEUNER, Hans-Berndt:	Zur Modellierung und Analyse instationärer Deformationsprozesse (Diss. 2007)
Nr. 270	WENDT, Axel:	Objektraumbasierte simultane multisensorale Orientierung (Diss. 2007)
Nr. 271	DILßNER, Florian:	Zum Einfluss des Antennenumfeldes auf die hochpräzise GNSS-Positionsbestimmung (Diss. 2007)
Nr. 272	BUTENUTH, Matthias:	Network Snakes (Diss. 2008)
Nr. 273	RAVANBAKHSH, Mehdi:	Road Junction Extraction from High Resolution Aerial Images Assisted by Topographic Database Information (Diss. 2008)
Nr. 274	BRZANK, Alexander:	Bestimmung Digitaler Geländemodelle in Wattgebieten aus Laserscannerdaten (Diss. 2008)
Nr. 275	SCHMIDT, Ralph:	Automatische Bestimmung von Verknüpfungspunkten für HRSC-Bilder der Mars Express-Mission (Diss. 2008)
Nr. 276	HAUNERT, Jan-Henrik:	Aggregation in Map Generalization by Combinatorial Optimization (Diss. 2008)
Nr. 277	NEUMANN, Ingo:	Zur Modellierung eines erweiterten Unsicherheitshaushaltes in Parameterschätzung und Hypothesentests (Diss. 2009)
Nr. 278	WEITKAMP, Alexandra:	Brachflächenrevitalisierung im Rahmen der Flächenkreislaufwirtschaft (Diss. 2009)
Nr. 279	HEUWOLD, Janet:	Automatische auflösungsabhängige Anpassung von Bildanalyse-Objektmodellen am Beispiel Straßen (Diss. 2009)
Nr. 280	KOCH, Christian:	Extraction of Mercury's tidal signal and libration amplitude from synthetic laser altimeter data sets (Diss. 2009)
Nr. 281	GITLEIN, Olga:	Absolutgravimetrische Bestimmung der Fennoskandischen Landhebung mit dem FG5-220 (Diss. 2009)
Nr. 282	ELING, Dirk:	Terrestrisches Laserscanning für die Bauwerksüberwachung (Diss. 2009)
Nr. 283	DOLD, Christoph:	Ebenenbasierte Verfahren für die automatische Registrierung terrestrischer Laserscans (Diss. 2010)
Nr. 284	RIPPERDA, Nora:	Rekonstruktion von Fassadenstrukturen mittels formaler Grammatiken und Reversible Jump Markov Chain Monte Carlo Sampling (Diss. 2010)
Nr. 285	KATTERFELD Christiane:	Interoperables Geodaten-basiertes E-Learning (Diss. 2010)
Nr. 286	JARECKI, Focke:	Spurkreuzungspunktdifferenzen zur Validierung satellitengradiometrischer Messungen (Diss. 2010)
Nr. 287	SCHRAMM, Matthias:	Unüberwachte lineare spektrale Entmischung mit Anwendungen für Baumdichteabschätzungen in semiariden Regionen Afrikas (Diss. 2010)
Nr. 288	ALSAYEL, Mohammed Y.:	Towards Standardizing International Boundary Determination and Quality Consequences on surveying and Mapping (Diss. 2010)
Nr. 289	TAVAKKOLI S., Seyed Mohammad:	Multi-Temporal Classification of Crops Using ENVISAT ASAR Data (Diss. 2011)

Die Arbeiten werden im Rahmen des wissenschaftlichen Schriftenaustausches verteilt und sind nicht im Buchhandel erhältlich. Der Erwerb ist zu einem Stückpreis von € 25,-- bei den herausgebenden Instituten möglich.